Influence of geometric and environmental parameters on air-cooled steam condenser performance

by

R. Joubert

Thesis presented in partial fulfilment of the requirements for the degree of Masters of Engineering (Mechanical) at the University of Stellenbosch

Supervisor: Prof D.G. Kröger

Department of Mechanical Engineering

University of Stellenbosch

South Africa

March 2010

Declaration

I, Retief Joubert, the undersigned, hereby declare that this thesis is my original work. It is being submitted for the Degree of Masters of Engineering (Mechanical) at the University of Stellenbosch. It has not been submitted, in its entirety or in part, for any degree or examination at any other University.

……

Signature of candidate

This …… day of ……

Abstract

Air-cooled steam condensers (ACSCs) are used in the power generation industry to directly condense turbine exhaust steam in areas where cooling water is expensive or unavailable. Large axial flow fans force ambient air through A-frame heat exchanger bundles made up of a number of rows of finned tubes through which the steam is ducted and consequently condensed during the heat transfer process to the air. The heat rejection rate or performance of an ACSC is proportional to the air mass flow rate, determined by fan volumetric performance, and the temperature difference between the finned tubes and the air.

The air flow through a 30 fan ACSC (termed the generic ACSC) operating under windy conditions is solved using the commercial computational fluid dynamics (CFD) code FLUENT and the required data is extracted from the solution to calculate performance trends. It is found that fan performance is reduced due to a combination of factors. The first is additional upstream flow losses caused by separated flow occurring primarily at the leading edge of the ACSC and secondarily at the fan bellmouth inlets. The second factor leading to reduced fan performance is the presence of distorted flow conditions at the fan inlets. Hot plume air recirculation is responsible for decreased ACSC thermal performance due to increased fan inlet air temperatures. It is found that reduced fan performance is the greater contributor to reduced ACSC performance.

The performance effects of varying two geometrical parameters of the generic ACSC, namely the fan platform height and the windwall height, are investigated under windy conditions. It is found that each parameter is linked to a specific mechanism of performance reduction with the fan platform height affecting fan performance and the windwall height affecting recirculation. The respective platform and windwall heights specified for the generic ACSC are found to provide acceptable performance results.

To mitigate wind induced performance reductions a number of modification and additions to the ACSC are investigated. These primarily aim at improving fan performance and included the addition of walkways or skirts, the addition of wind screens beneath the fan platform, removing the bellmouth fan inlets, using different types of fans and increasing fan power. The addition of a periphery walkway and windscreens is considered to be the most practical methods of improving ACSC performance under windy conditions. The generic ACSC is modified to include both modifications and under high wind conditions the performance is found to increase measurably. The modifications also resulted in the ACSC performance being less sensitive to wind direction effects.

Opsomming

Lugverkoelde kondensators word in die kragopwekkings industrie gebruik om turbine uitlaatstoom te kondenseer, veral in gebiede waar verkoelingwater duur of onbeskikbaar is. Aksiaalvloei-waaiers forseer omgewingslug deur A-raam warmteuitruiler bondels wat bestaan uit verskeie rye vinbuise. Die uitlaatstoom vloei in die vinbuise en kondenseer as gevolg van die warmteoordrag na die lug. Die warmteoordragkapasiteit van die lugverkoelde stoom kondensator is eweredig aan die massavloei-tempo van die lug, wat bepaal word deur die waaierwerkverigting, en die temperatuur verskil tussen die vinbuise en die lug.

Die lugvloei deur 'n 30 waaier lugverkoelde stoom kondensator (genoem die generiese lugverkoelde stoom kondensator) onderworpe aan winderige toestande word opgelos deur die gebruik van die kommersiële vloeidinamika-pakket, FLUENT. Die nodige data is onttrek uit die oplossing en werkverrigting neigings is bereken. Dit is gevind dat waaierwerkverigting verminder as gevolg van 'n kombinasie van faktore. Die eerste is bykomende vloeiverliese wat veroorsaak word deur vloeiwegbreking wat plaasvind primêr by die voorste rand van die lugverkoelde stoom kondensator asook by die klokvormige waaier-inlate. 'n Tweede faktor wat lei tot vermindere waaierwerkverigting is die teenwoordigheid van lugvloeiversteurings by die waaier-inlate. Hersirkulering van warm pluim lug is ook verantwoordelik vir verminderde lugverkoelde stoom kondensator werkverrigting. Daar word bevind dat die vermindering in waaierwerkverrigting die grootste bydraende faktor tot vermindere lugverkoelde stoom kondensator werkverrigting is.

Die effek van verandering van twee geometriese lugverkoelde stoom kondensator parameters, naamlik die waaierplatformhoogte en die windwandhoogte is ondersoek onder winderige toestande. Daar word bevind dat elk van die parameters gekoppel is aan 'n spesifieke meganisme van vermindere lugverkoelde stoom kondensator verrigting: Die waaierplatformhoogte beïnvloed waaierverrigting terwyl die windwandhoogte hersirkulering beinvloed. Daar word ook bevind dat die onderskeie waaierplatform- and windwandhoogtes van die generiese lugverkoelde stoom kondensator, van so 'n aard is dat dit aanvaarbare werkverrigting tot gevolg het.

Om verlaging in werksverrigting in winderige toestande te verminder is verskeie modifikasies en byvoegings tot die lugverkoelde stoom kondensator ondersoek wat primêr gemik is op verbetering in waaierwerkverigting. Die ondersoek dek die byvoeging van 'n loopvlak, die byvoeging van windskerms onder die waaierplatform, verwydering van die klokvormige waaier-inlate, die gebruik van verskillende waaiers en die verhoging van waaierdrywing. Daar was besluit dat die byvoeging van 'n loopvlak rondom die rand van die lugverkoelde stoom kondensator en die byvoeging van windskerms die mees praktiese manier was om die lugverkoelde stoom kondensator verigting te verbeter. Die generiese lugverkoelde stoom kondensator was aangepas om beide veranderings in te sluit en meetbare verbetering in werkrigting was verkry. Die veranderings het ook meegebring dat die lugverkoelde stoom kondensator minder sensitief is vir windrigting effekte.

Acknowledgements

I would like to express my sincere gratitude towards Prof. D.G. Kröger for his focus and experience that guided this project. I would also like to thank Mrs Felicity Allwright for her constant smiles, encouragement and logistical support throughout the project.

I also express my thanks to the National Research Foundation and the California Energy Commission for their financial support of the project.

Lastly I'd like to acknowledge the use of the Rhashasta high performance computing facility of the University of Stellenbosch, without which the scope of this project would never have been possible.

Table of contents

List of figures

List of tables

Nomenclature

A	Area, m^2
c_p	Specific heat, J/kgK
d	Diameter, m
g	Gravitational acceleration, m/s^2
H	Height, m
K	Loss coefficient
k	Thermal conductivity, W/mK, or Turbulent kinetic energy, m^2/s^2
m	Mass flow rate, kg/s
N	Rotational speed, rpm
Ny	Characteristic heat transfer parameter, m^{-1}
n	Number
p	Pressure, N/m^2
Q	Heat transfer rate, W
Ry	Characteristic flow parameter, m^{-1}
T	Temperature, K
V	Volumetric flow rate, m^3/s
v	Velocity, m/s
W	Width, m

Greek symbols

β	Volume coefficient of expansion, K^{-1}
Δ	Differential
ε	Turbulent energy dissipation rate, m^2/s^3
μ	Dynamic viscosity, kg/ms

θ	Angle, °
ρ	Density, kg/m^3
σ	Area ratio

Dimensionless groups

Pr	Prandtl number, $\mu c_p/k$

Subscripts

a	Air
b	Beam, or bundle
c	Casing, or contraction
do	Downsteam
dist	Distorted
e	Effective
F	Fan
fr	Frontal
h	Hub
he	Heat exchanger
i	Inlet
id	Ideal
j	Jet
m	Mean
o	Outlet
r	Row
ref	Reference

s	Steam, or static
sc	Screen
t	Tube
ts	Tower support
up	Upstream
v	Vapour
w	Walkway, or wind, or windwall
x	Co-ordinate
y	Co-ordinate
z	Elevation, m
θ	Inclined

1. Introduction

1.1 Background and motivation

The Rankine cycle, shown in figure 1.1 below, is a closed loop thermodynamic cycle in which heat is converted to work. This cycle has been industrialized by the power generation industry to the point where it supplies the majority of the world's electricity.

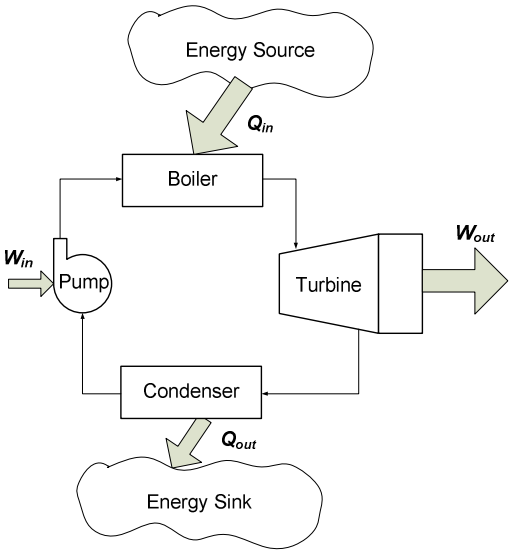

Figure 1. 1: Rankine vapour cycle.

A boiler uses heat, which can be derived from fossil, renewable, solar, or nuclear sources, to generate high pressure vapour that is expanded in a turbine to produce work. The turbine powers a generator that converts mechanical to electrical energy. Waste heat is rejected to the environment in the condenser and the condensate is pumped back to the boiler completing the cycle. Although a variety of process fluids can be selected for the cycle, water is used almost exclusively due to a combination of favourable consideration such as availability, thermodynamic properties, low cost as well as being nontoxic and nonreactive.

The condensation step is commonly accomplished using a surface condenser located at the turbine exhaust which is supplied with cooling water. In once-through cooling the water is extracted from a river, dam or ocean, pumped through the condenser and returned to the source but due to ever increasing environmental considerations this practice is largely obsolete. An alternative solution is indirect cooling where a secondary cooling loop is used to supply the condenser with cooling water that is in turn cooled in a wet cooling tower that relies on heat and mass transfer as cooling mechanisms. According to Kröger (2004) a modern fossil-fuelled wet cooled power plant will require an average of between 1.6 and 2.5 litres of cooling water per kWh(e) of net generation. Additional cooling water is lost to blowdown and drift, i.e. the carryover of water drops entrained in the air stream passing through and out the tower. Considering all the losses, a wet-cooling system of a 600 MW(e) coal-fired plant

operating at 70 percent annual capacity factor could require make-up water in excess of 11 x 10^6 m^3 per year.

In the past, the contribution of water costs to the total busbar energy production cost has generally been small. However, the growing trend of urban and rural development has resulted in the agricultural sector and municipal requirements placing increased pressure on water resources and this has led to dramatic increases in water cost in some areas. However, other and often increasing water usage expenses such as pumping costs, water treatment costs, blowdown disposal costs and environmental study and permit acquisition costs significantly add to the life cycle water usage cost of a power plant. Furthermore current and proposed legislation restricting water usage and specifying conditions of use and disposal could develop into more significant considerations when specifying cooling systems in the future (EPRI, 2005).

The water usage problems associated with wet cooling towers can be addressed by a direct air-cooled configuration that comprises of air-cooled steam condensers (ACSCs) as shown in figure 1.2. It can be seen that the cycle forms a closed loop and as a result there is theoretically no water consumption, however a minor amount of blowdown is required to maintain the quality of the water. Due to low water consumption ACSCs have found extensive application in arid areas.

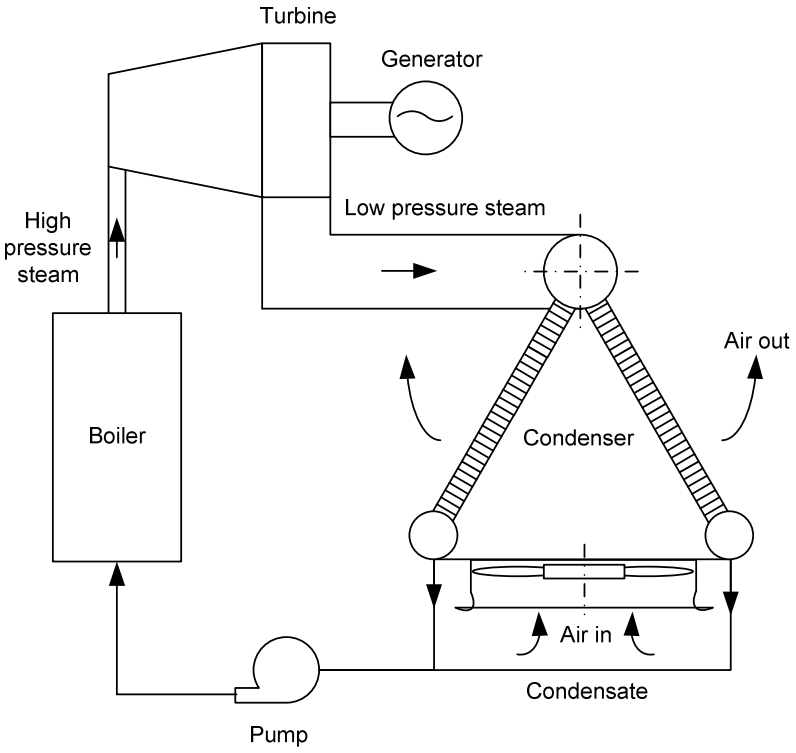

Figure 1. 2: Schematic of direct air-cooled power plant.

In a typical ACSC fan unit, detailed in figure 1.3, turbine exhaust steam is supplied to the heat exchanger bundles via the steam supply duct. The heat exchanger bundles comprises of a

number of finned tubes arranged in bundles due to handling and installation considerations. The tubes are externally finned to provide a larger air side surface area enabling greater heat transfer. The heat exchanger bundles are installed in an A-frame arrangement to reduce the required plant footprint and to effectively remove the condensate at the bottom of the bundles. Fans are used to force cool ambient air over the fins allowing heat transfer from the steam to the air via the tubes. Small amounts of excess steam exiting the condenser are fed to a downstream dephlegmator after which steam extractors vent noncondensable gases that reduce performance, promote metal corrosion and may cause freezing of the condensate in winter. Multiple fan units are arranged as shown in figure 1.4 to form an ACSC.

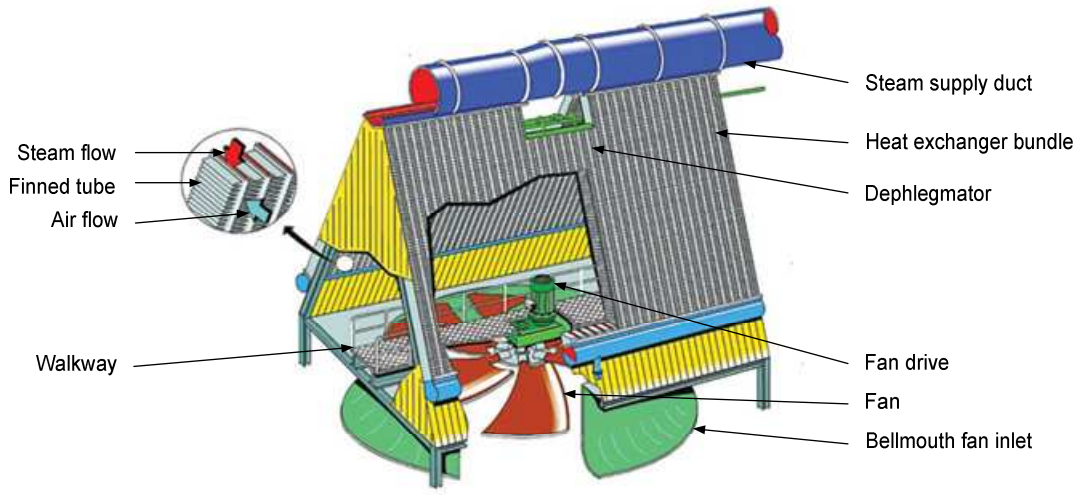

Figure 1. 3: Schematic of an ACSC fan unit (Courtesy of SPX Cooling Technologies Inc.).

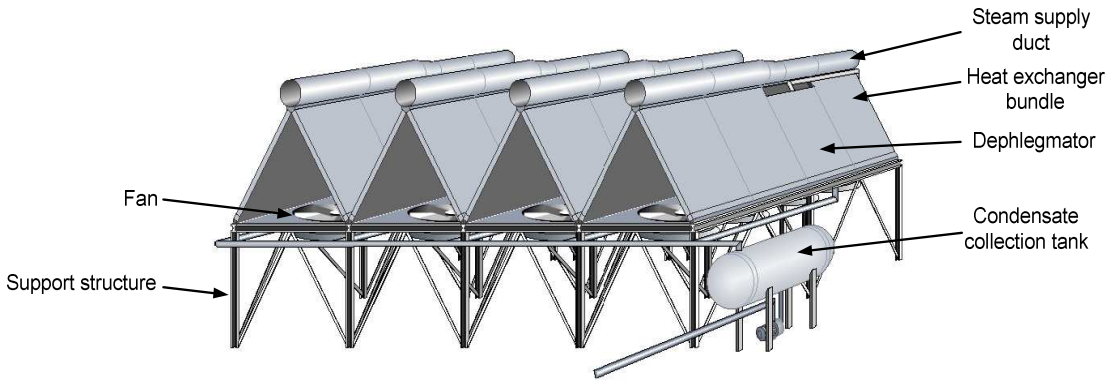

Figure 1. 4: Schematic of an ACSC (Courtesy of GEA).

Many highly efficient gas fired combined cycle power plants (CCPPs) have been built in the U.S.A. and other parts of the world in recent years. Specifying the location of such plants is usually a trade-off between fuel supply- and end user location and often results in plants being constructed in areas with limited and/or highly regulated water resources, resulting in the widespread utilization of ACSCs. A typical example is the ACSC of the 550 MW Astoria

Energy Project CCPP, shown in figure 1.5, which is located in New York City. Although the plant is sited adjacent to the East River it was not permitted to consume or reject any water into the environment. However proximity to an area with high demand for electricity, a nearby local substation for transmission and an existing natural gas pipeline justified the location and as a result an ACSC was specified to meet the cooling requirements. The ACSC consists of 24 low noise fans measuring 11m in diameter. The fan units were pre-assembled in 12 modules, as shown in figure 1.5 (b), nearly 500 km away and barged to the site. This illustrates a further advantage of an ACSC: the modular nature of the fan units can be exploited to shorten construction schedules.

(a) Completed ACSC (b) Two fan ACSC unit during shipping

Figure 1. 5: ACSC of the Astoria Energy Project CCPP in New York (Courtesy of SPX Cooling Technologies Inc.).

Due to limited and/or costly cooling water availability in the U.S.A., ACSCs are increasingly the cooling technology of choice and the total generation capacity of plants using dry cooling exceeds 8 500 MWe (EPRI, 2005). Furthermore industrial water usage in the U.S. requires stringent permits which often translate into a lengthy and expensive acquisition process. This has further forced many utilities and independent power producers to circumvent these issues relying on ACSCs for cooling.

The world's largest ACSC, shown in figure 1.6, became fully operational in 1991 at the 6 x 665 MW(e) Matimba power plant located in the Limpopo province in South Africa. Airflow is supplied by 288 axial flow fans measuring 9.1 m in diameter and each fan is driven by a 270 KW electric motor. To ensure unobstructed airflow and to reduce cross flow at the fan inlets the fans are located on the fan platform 45 m above the ground as shown in figure 1.6 (b).

(a) Arial view of the plant

(b) ACSC fan platform

(c) construction of A-frames.

Figure 1. 6: Matimba power station (Courtesy of Eskom).

As the global adoption of ACSCs speeds up it becomes increasingly important to ensure effective and predictable cooling performance over a wide range of operating conditions.

1.2 Literature study

In an early study, Monroe (1979) identified recirculation of hot plume air as a contributor to reduced air-cooled heat exchanger (ACHE) performance, as shown in figure 1.7. It was recommended that the ACHE inlet approach air velocity should be less than half the velocity through the fan in an effort to minimize upstream system losses.

Van Aarde (1990), who conducted experiments on a full scale ACSC, noticed that the presence of wind led to a considerable reduction in ACSC performance, which was attributed to distorted flow due to separation at the ACSC inlet also shown in figure 1.7.

Goldschagg (1993) found that wind effects lead to ACSC performance reductions at the world's largest ACSC (Matimba power plant, discussed previously). These reductions lead to turbine trips under extremely gusty conditions. Further studies by Goldschagg et al. (1997) showed that modifications of the cladding and windwalls surrounding the ACSC resulted in the

elimination of turbine trips and significant improvements in ACSC performance during windy conditions.

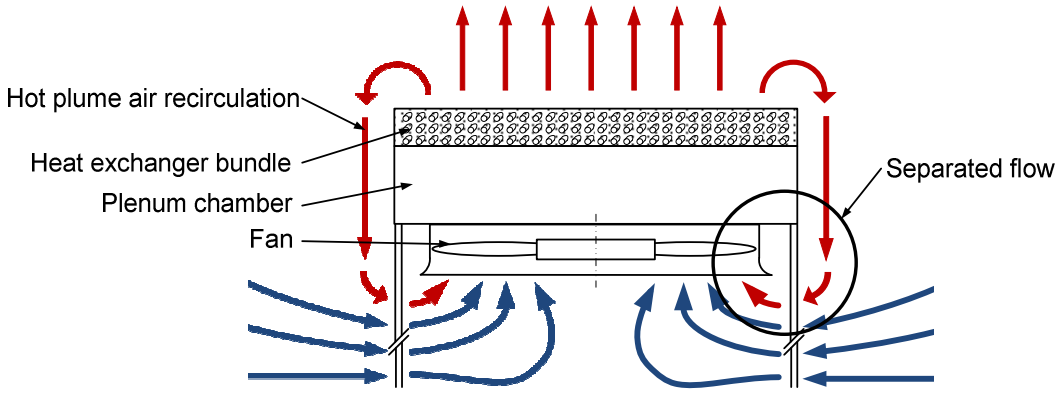

Figure 1. 7: Schematic of phenomena leading to reduced ACHE performance (Hot plume air recirculation and distorted fan inlet air flow conditions due to separation).

The results of an analytical, numerical and experimental investigation of hot plume air recirculation have been reported by Kröger (1989). This study formed the basis of subsequent work by Du Toit and Kröger (1992) from which it was concluded that the analytical model can be used to predict the approximate performance effectiveness of practical mechanical-draft heat exchangers where plume recirculation occurs for no-wind conditions. Du Toit et al. (1993) then expanded this numerical study to include wind effects by modeling the effects of a 2.0 m/s and 5 m/s cross-wind on an essentially two-dimensional ACHE model. It was observed that the performance of the upwind fans along the periphery of the ACHE was the most significantly reduced due to wind effects. Recirculation of plume air was also observed on both the leading and trailing edges of the ACHE.

Salta and Kröger (1995) conducted experimental work to determine fan performance on a simplified scale model of an ACHE. By assuming the flow field, for the case of a sufficiently long ACHE, to be essentially two-dimensional they were able to model up to twelve fan rows. The results of the study were used to formulate correlations for fan performance for single and multi-row ACHE systems as a function of the fan platform height. It was also shown that the addition of a skirt or walkway along the periphery of the ACHE improves the system performance, by mainly improving the performance of the edge fans adjacent to the walkway.

Duvenhage et al. (1996) studied the effect of ACHE platform height on fan performance using numerical models and the same experimental setup of Salta and Kröger (1995). The effect that different inlet shrouds have on fan performance was also examined. The results compare favourably with the correlation of Salta and Kroger (1995) and illustrate the applicability of the numerical approach as an analytical tool for evaluating ACHE performance.

Duvenhage and Kröger (1996) numerically investigated the effects that wind, blowing both perpendicular and parallel to the longitudinal axis of an ACHE, will have on fan performance. According to the study, two contributing factors reduce ACHE: Firstly, the recirculation of hot

air from the plume raises the effective fan inlet air temperature, which reduces the heat transfer of the ACHE. Secondly, fan performance is reduced due to the presence of distorted inlet air flow conditions. This reduces the air mass flow rate, which in turn further reduces the heat transfer of the ACHE.

A numerical study, Meyer (2005) found that flow separation occurring at the fan inlets is responsible for performance reduction of the edge fans in an ACHE, while the inner fans exhibit reduced performance due to cross flow effects. It is also shown that for a two bank ACHE, removal of the fan inlet shroud leads to increases in the performance of the edge fans.

Bredell et al. (2006) performed a numerical study which compares the performance of two different fans in a typical fan row of an ACSC under various degrees of inlet flow distortion. The study utilised a three dimensional model of a row of fan units to model an essentially two dimensional section of an ACSC near the centre. Various mechanisms responsible for the reduction of fan performance were studied and it is shown that different fans vary in their sensitivity to reduced performance.

Maulbetsch and DiFilippo (2007) conducted an experimental study to evaluate the effect that wind has on the performance of large ACSCs at five power plants located in the Western Unites States. The tests were intended to examine the contribution of recirculation of heated plume air and the degradation of fan performance to reduced ACSC performance. The reduced fan performance is the major cause of reduced ACSC performance while wind direction also plays a role in ACSC performance.

In recent numerical work by van Rooyen and Kröger (2008) it was attempted to model a complete 30 fan ACSC system subjected to wind effects. Due to computational limits, all the fan units were not modeled simultaneously and a similar approach to Goldschagg et al. (1997) was followed where the solution of a global flow field is used as an input to a smaller, more detailed flow field of the ACSC. The study found that reduction in fan volumetric effectiveness is the primary contributor to reduced ACSC performance while recirculation played a minor role. The study also reported that some fans experience greater than ideal performance.

Liu et al. (2009) conducted a numerical and experimental investigation into hot air recirculation at a large power plant. The ACSC system and surrounding buildings were modeled in FLUENT and the proximity of the ACSC to the boiler house resulted in wind induced recirculation especially for wind blowing from the direction of the boiler house. Wind speed was also found to play an important role with recirculation effects reducing at very high wind speeds. The trends from the numerical study correlated with the trends from the experimental study obtained by modeling a simplified scale model of the ACSC system in a wind tunnel. It was shown using the numerical model that the detrimental effect of hot air recirculation can be reduced by adding a windwall and increasing the rotational speed of the periphery fans.

Previous experimental and numerical studies confirm the applicability and validity of computational fluid dynamics (CFD) as a tool to investigate the performance of ACHE's under windy conditions. Many of these studies [Du Toit et al (1993); Duvenhage et al. (1996);

Duvenhage and Kröger (1996); Bredell et al. (2006); Meyer (2005); Van Rooyen and Kröger (2008)] simulate the effect of the fan in the flow field using the so-called actuator disk model presented by Thiart and von Backström (1993). In this model the fan blades are not explicitly modeled as three-dimensional rotating volumes but instead the model uses blade element theory to model the thrust and torque exerted by the fan blades on the air. These forces are then introduced as momentum source terms into the Navier-Stokes equations which are solved by the commercial CFD code, FLUENT. This model shows good agreement with experimental data under ideal fan inlet flow conditions but deviates under distorted flow conditions. A further disadvantage is that the model is computationally expensive as compared to built-in FLUENT fan models, which makes it less suitable for models with a large number of fans.

1.3 Problem statement and objective

The main function of a power plant is to efficiently produce electricity, consequently every sub-system and component, bound within a great variety of operating parameters, must ensure that this objective is achieved. This requires that the designers and operators of a plant intimately understand how every component will function across the complete range of possible operating conditions. This knowledge regarding ACSC systems has not as of yet been perfected and reductions in ACSC performance impose limitations on plant output which is highly undesirable from both a plant operation and network stability point of view.

Since the ACSC rejects heat to the atmosphere, the performance of the ACSC is strongly influenced by metrological effects including dry bulb temperature, temperature distribution, and wind speed and direction. It is well established that the heat transfer rate of an ACSC deteriorates under high ambient temperatures and/or windy conditions. Even though ambient conditions, particularly the direction of prevailing winds, were taken into account when specifying the site layout at Matimba (the ACSC is upwind of the turbine and boiler building under prevailing easterly wind), turbine trips occurred due to reduced ACSC performance during periods of westerly winds (Goldschagg, 1993). Turbine trips occur as a result of increased exhaust steam backpressure, caused by reduced ACSC performance, exceeding the design limit of the turbine. Turbine trips are intended to prevent damage to the last stages of the low pressure turbine due to condensate in the steam. These periods of high temperatures and gusty winds often coincide with periods of high demand for electricity (EPRI, 2005). Apart from varying metrological conditions, a number of geometrical parameters of the ACSC system also affect the performance of the ACSC.

The objective of this study is to employ CFD to model performance trends of a generic ACSC subjected to variation of the following parameters, modifications and additions:

- Wind direction
- Wind speed
- Fan platform height
- Wind wall height
- Walkways or skirts

- Screens
- Type of fan inlets
- Type of fan
- Fan power

A better understanding of the performance trend effects of the abovementioned parameters, modifications and additions will permit designers of ACSC to optimise and refine the specifications of such systems. Furthermore the designer will be sensitised to the relative importance of these parameters to system performance. The results can also be applied to existing ACSCs to increase performance and to identify modifications for improved performance.

2. Numerical modeling

CFD is described (Fluent Inc., 2006) as the science of predicting fluid flow, heat transfer, mass transfer, phase change, chemical reaction, mechanical movement, stress or deformation of related solid structures and related phenomena by solving the mathematical equations that govern these processes using a numerical algorithm on a computer. This is achieved by following these steps:

1. Define the modeling goals.

2. Create the model geometry and grid.

3. Set up the solver and physical models.

4. Compute and monitor the solution.

5. Examine and save the results.

6. Consider revisions to the numerical or physical model parameters, if necessary.

This chapter describes the process of deriving a numerical model representative of a generic ACSC and the model's details by examining the first 3 steps.

2.1 Modeling goals and approach

The essence of this study is to model ACSC performance using the CFD code FLUENT. However FLUENT only solves the fluid flow problem and data must then be extracted from the solution to calculate ACSC performance. This calculation requires the air mass flow rate and air inlet temperature for each fan in the ACSC system as input. Thus the goal of the model is to realistically and accurately calculate these two variables and every other modeling decision or assumption must support this goal.

Previous numerical studies used various flow assumptions and novel modeling approaches to reduce the geometrical complexity and size of the problem to accommodate limited computational resources. Van Rooyen (2007) first solved a large global flow field surrounding a simplified multiple fan ACSC and then used the solution as input to several smaller, but more detailed models where each model determined the flow through a particular fan. The results from the second round of simulations were then combined to calculate the system performance. Bredell (2005) used symmetry planes in a similar fashion to the experimental work of Salta and Kröger (1995) to numerically model three fan units that are representative of a long six fan row ACSC. These unavoidable simplifications introduce a number of uncertainties and complications to the modeling process.

This study models the geometrically identical ACSC as examined by Van Rooyen (2007) as a baseline and it is referred to as the generic ACSC throughout this study. The computational resources available to this study allow for the simultaneous solution of the flow through all 30 fans in the generic ACSC. This method is both memory and computational time intensive but these concerns are justified by the added confidence in the modeling process and results

thereof. The generic ACSC is then modified to incorporate the various parameters that are examined in this study and the performance results are determined, presented and discussed.

2.2 Generic model description

Before specifying the geometry of the generic ACSC numerical model the flow through a typical fan unit, as shown in figure 2.1, needs to be examined. The detailed operating and system specifications of an ACSC fan unit are documented in Appendix A.

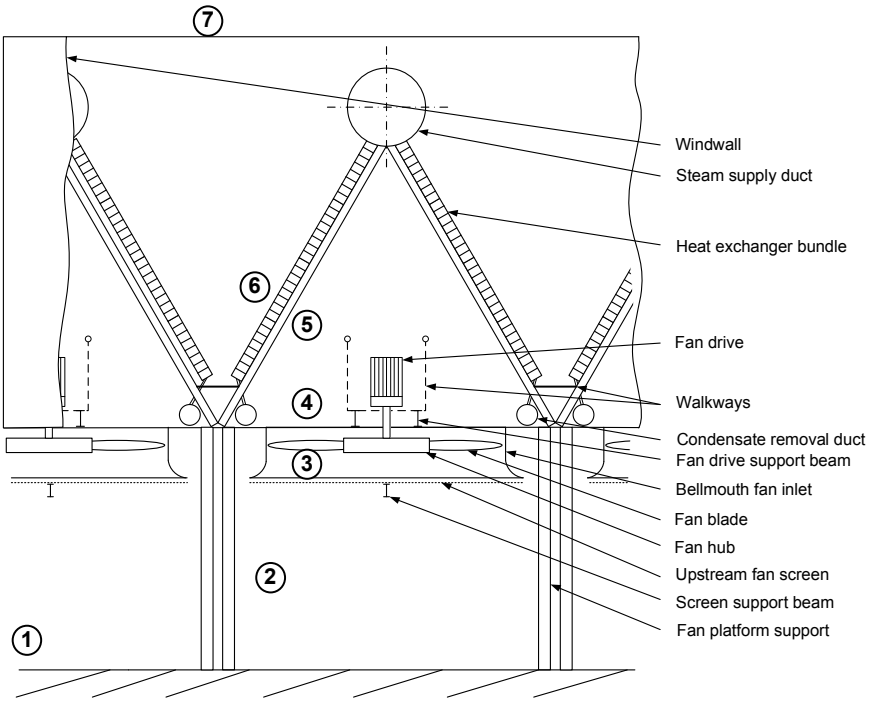

Figure 2. 1: Detailed schematic of an A-frame fan unit.

Stagnant ambient air is drawn from outside the ACSC, 1, past the ACSC support structures to beneath the ACSC at 2. The air passes through the inlet screen, 3, and into the bellmouth inlet. As the air flows through the fan, from 3 to 4, the air experiences a pressure rise as energy is introduced into the airstream and exits the fan into the A-frame plenum chamber. The air is heated as it exits the plenum chamber through the finned tubes bundles, 5 to 6, in which the turbine exhaust steam condenses and is vented into the atmosphere, 7, above the wind wall.

A simplified geometrical representation of the airflow through a generic fan unit must contain all the relevant flow features required to meet the modeling goals. Figure 2.2 shows a schematic of the simplified generic numerical fan unit. It can be seen that many of the physical components are not directly modeled since it will demand considerable computational resources. Furthermore the flow around these components is not the focus of this study. However the effects that these components impart on the airflow are thoroughly documented (Kröger, 2004) and are accounted for in this study as part of the respective fan and heat exchanger models discussed later in this chapter. It can be seen that the A-frame heat exchanger is modeled as a horizontal heat exchanger on top of a rectangular plenum chamber. This simplification, as per Bredell (2005) and Van Rooyen (2007), is made to simplify the

meshing operation and reduce the complexity of the grid and is justified by the fact that the air flow in the plenum chamber is again not the focus of the study.

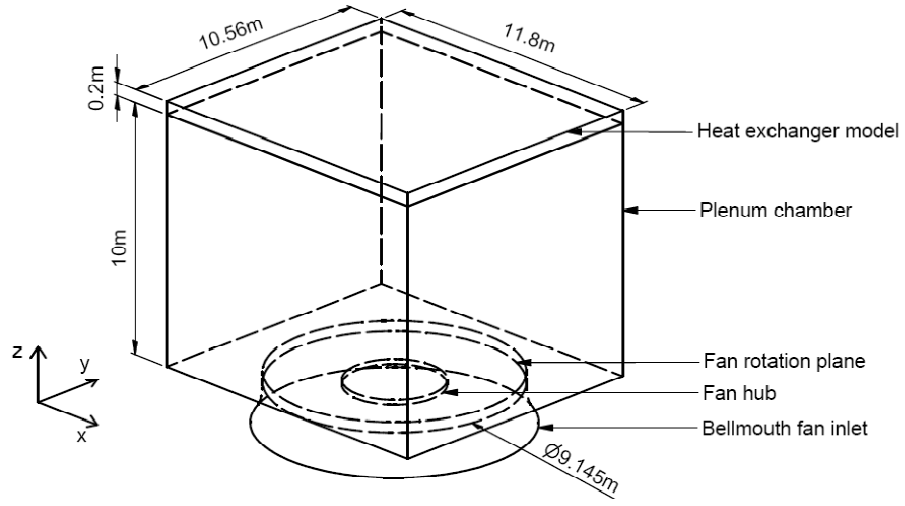

Figure 2. 2: Simplified generic numerical fan unit.

Related studies, as stated previously, employed the actuator disk fan model whereas the current study departs from this approach and utilizes a built-in FLUENT fan model. This method models a fan as an infinitely thin discontinuous pressure rise or jump which is a function of the normal velocity through the fan plane. This choice is motivated by the reduced computational resource requirements of the pressure jump model compared to the actuator disk model and the uncertainties associated with the model. The fan total to static pressure curve for a particular fan, also referred to as the B-fan (d_F = 9.145 m, d_h/d_F = 0.4, N = 125 rpm) used in this study is obtained from Bredell et el. (2005). The definition of the pressure jump fan model requires a static to static pressure curve as derived in Appendix B and requires that the dynamic pressure component ($\rho v_F^2/2$, where v_F is the average axial velocity through the area swept by the fan blades) be added to the fan total to static curve, as shown in figure 2.3. The resultant second order polynomial, in terms of the volumetric air flow rate V_F, is shown in equation (2.1).

$$\Delta p_F = 323.2303 + 0.4938 V_F - 0.001 {V_F}^2 \quad (2.1)$$

FLUENT requires the polynomial to be defined in terms of normal velocity v_F, as per equation (2.2):

$$\Delta p_F = 323.2303 + 27.2461 v_F - 2.6305 {v_F}^2 \quad (2.2)$$

It can be seen in figure 2.3 that the equation (2.2) is limited to a velocity range from 5 m/s to 17 m/s. Below this range the static pressure rise is taken as a constant value. This is done due to the unavailability of test data for the B-fan in the region below 5 m/s; however this approximation of the fan behaviour is an acceptable assumption since only a small percentage of the fans will operate in this velocity range during certain extreme conditions.

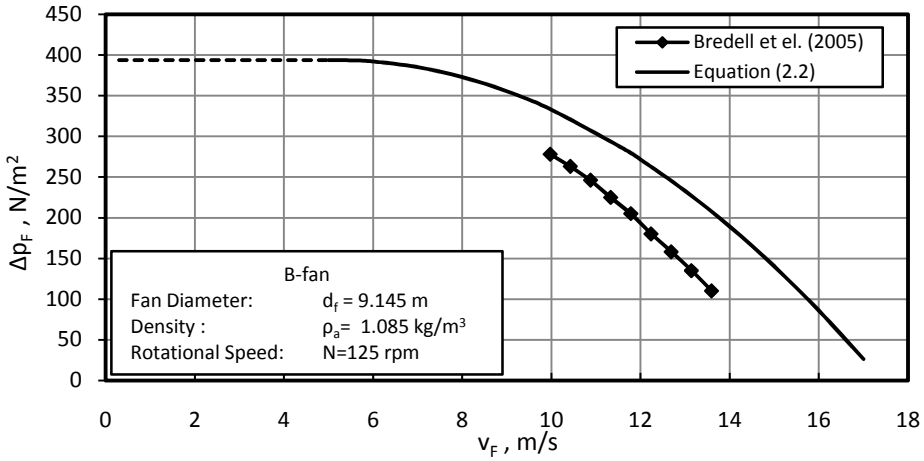

Figure 2. 3: Fan pressure rise curve used in the numerical model.

The heat exchanger model has to simulate two flow phenomena, the first being the system pressure loss caused by the various flow obstructions that have not been modeled directly, i.e. the heat exchanger bundles, supports, screens, walkways and ducts. This is achieved by modeling the heat exchanger as a porous zone in FLUENT that allows the system pressure drop to be introduced as a viscous and an inertial resistance term. These terms are calculated to be 1.897×10^6 and 59.1364 respectively as detailed in Appendix C. To account for the flow straightening effect of the finned tubes the inertial resistance term is defined 10^3 higher in the directions perpendicular to the flow, thus ensuring normal flow at the exit of the heat exchanger model.

Secondly the heat exchanger model must simulate the thermal effect of the heat exchanger bundles, namely the heat transfer from the steam to the air. A user defined function (UDF) was written for FLUENT to calculate the air temperature at the exit of the heat exchanger as detailed in Appendix C.

The fan units shown in figure 2.2 are arranged in a 30 fan array to form the generic ACCS, 5 fans in the x-direction and 6 in the y-direction as shown in figure 2.4. The location and type of boundaries defining the flow domain surrounding the 30 fan unit ACSC is shown in figure 2.5. Effectively all the boundaries, with the ground being the obvious exception, are located 250m away from the nearest ACSC wall and it was found that the simulation results are not influenced by the boundary's location.

The effect of wind direction on ACSC performance is one of the parameters studied and two wind directions are simulated, the first being a "straight" wind in the x-direction, hereafter referred to as the x-wind, and secondly a diagonal "cross" wind in the xy-direction (45° with respect to the x-axis), hereafter referred to as the xy-wind. To this effect the domain boundary normal to the positive x-axis is always a velocity inlet type whereas the domain boundary normal to the positive y-axis is a pressure outlet for an x-wind and a velocity inlet for a xy-wind

as shown in figure 2.5. The pressure outlet boundaries are defined with zero gauge pressure and the ground, ACSC walls, fan inlets and fan hubs are modeled as non-slip walls.

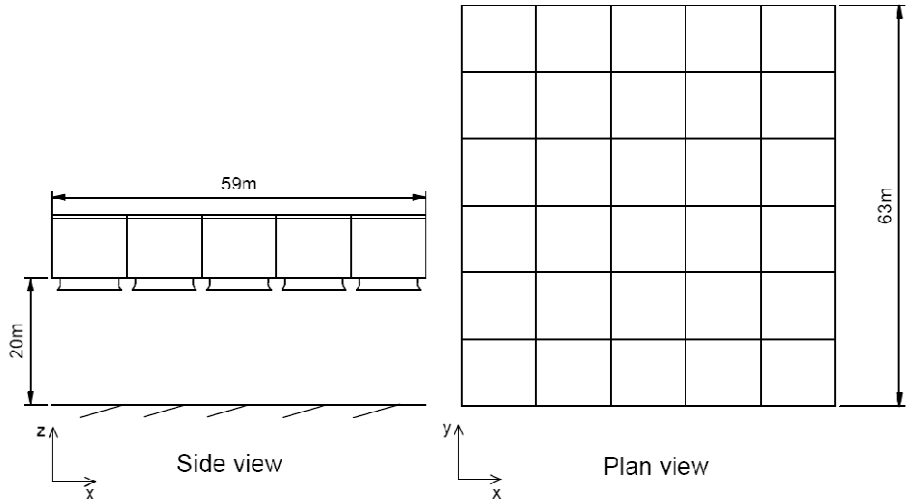

Figure 2. 4: Generic ACSC layout.

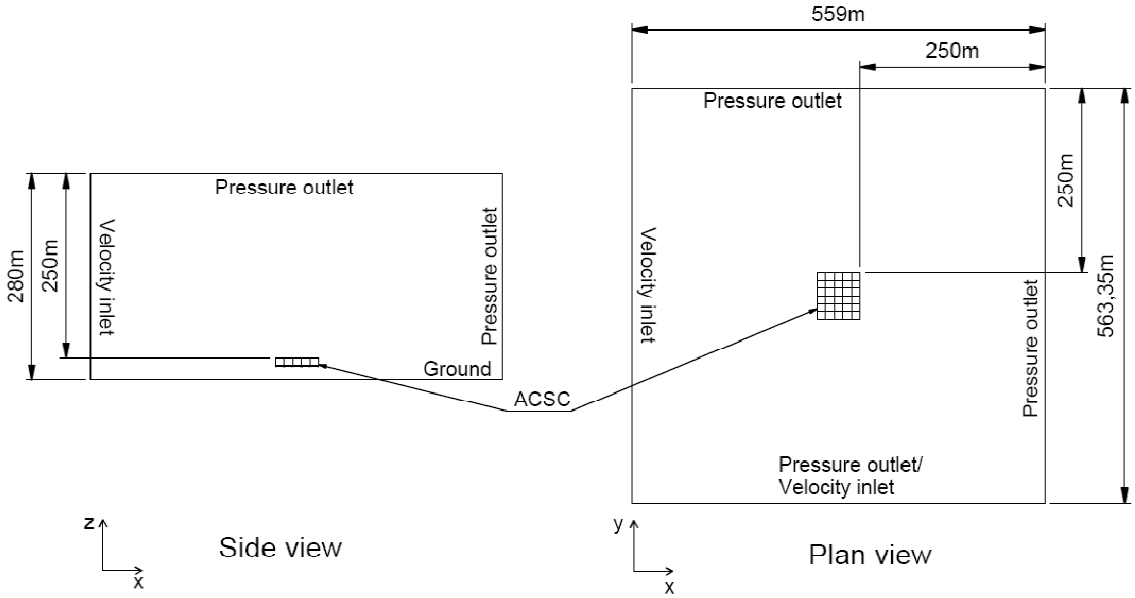

Figure 2. 5: Schematic of the flow field surrounding the ACSC.

Wind effects are modeled as a power-law velocity profile (Van Rooyen and Kröger, 2008) defined on the velocity inlet boundaries as follows:

$$v_w = v_{ref}\left({}^{z}/_{z_{ref}}\right)^{b} \tag{2.3}$$

where b is set to 1/7 and v_{ref} is the reference velocity that occurs at the reference height z_{ref} which is constant at 20m. Three reference wind speeds of 3, 6 and 9 m/s are modeled throughout the study.

The next step after the layout of the CFD model is specified is to generate a mesh or grid which is a collection of points, called nodes, representing the flow field where the equations governing the flow are calculated. It is well established that a CFD solution needs to be grid independent which tends to be achieved with an increasingly finer grid. This however comes at the cost of an increased number of nodes which adds considerable computational time. Furthermore the quality of the grid impacts the accuracy of the solution and as a result both grid generation and the resulting quality of the mesh is an important aspect of any numerical study.

A grid sensitivity study was performed by calculating the air mass flow rate through a single free standing fan unit with varying grid refinements as given in table 2.1 where Case 1 represents a very course grid and Case 4 a very fine grid as indicated by the number of mesh elements. The number of grid elements of the fan face is also presented in table 2.1 as a relative indication of grid refinement.

Table 2. 2: Details of grid sensitivity study performed on a free standing fan unit.

Case	1	2	3	4
Number of total elements	52286	172200	478241	1551770
Number of fan elements	126	341	611	1354
Fan mass flow rate change from average	-0.33 %	0.01 %	-1.78 %	0.21 %

Table 2.1 shows that the changes in air mass flow rate resulting from the grid refinement are very small and no trends are evident. It is therefore concluded that the model, for the purposes of this study, is grid independent.

Considering the flow through the generic 30 fan ACSC in a large flow domain, a grid was generated containing approximately 6.7 million cells with each fan face containing 464 elements. Owing to the simple geometry of the problem a structured conformal mesh is used as shown in figure 2.6.

To further ensure grid independence, the effect of using an adaptive mesh was investigated whereby FLUENT automatically refines the grid in locations with both high velocity and pressure gradients. It was found that the adaptive mesh had no noticeable impact in ACSC performance and the model was therefore considered grid independent.

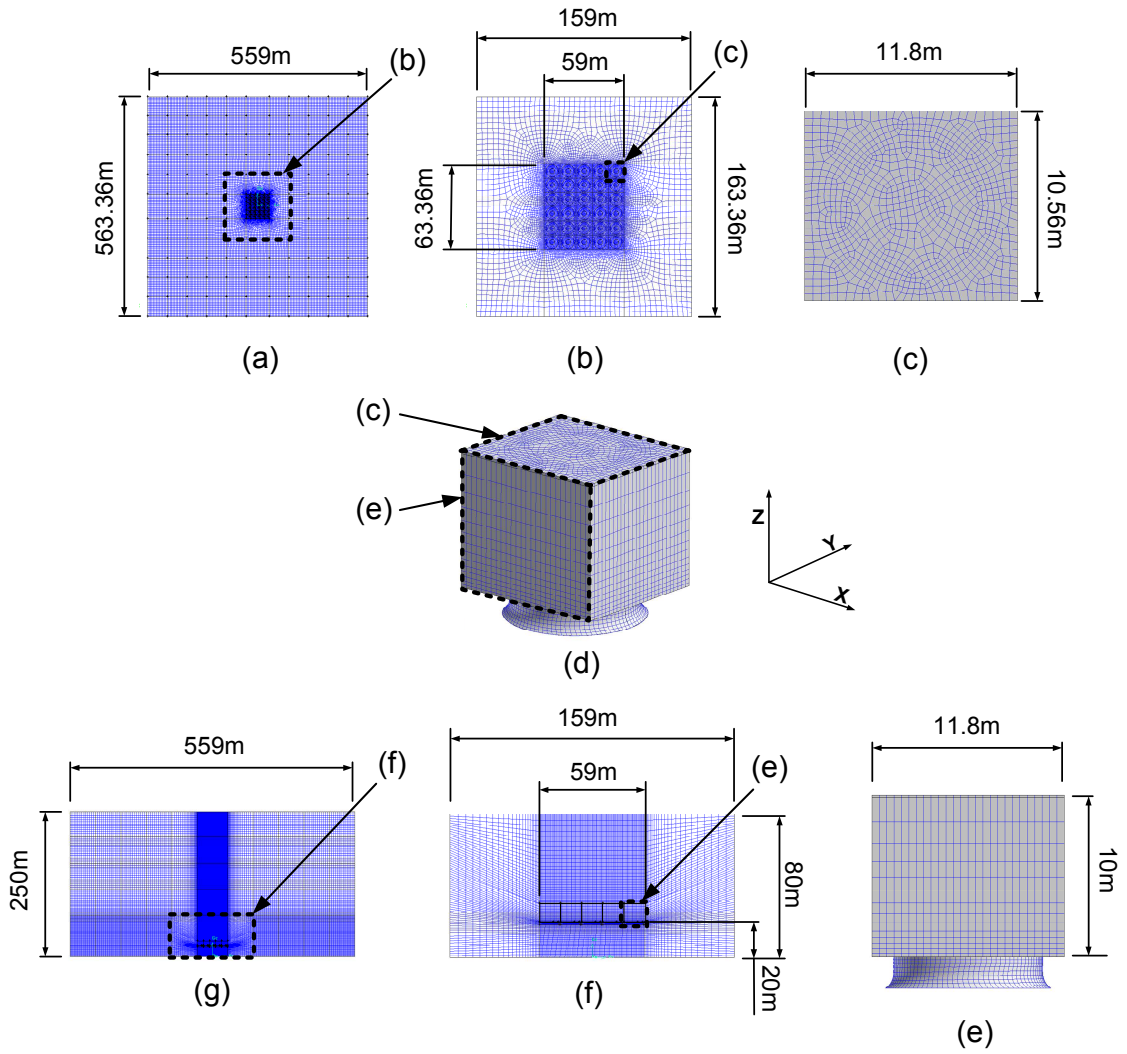

(a) Plan view of flow field mesh
(b) Plan view of flow field mesh in vicinity of ACSC
(c) Plan view of fan unit mesh
(d) Isometric view of fan unit mesh
(e) Side elevation of fan unit mesh
(f) Side elevation of flow field mesh in vicinity of ACSC
(g) Side elevation of flow field mesh

Figure 2. 6: Fan unit and flow field mesh.

2.3 Solution description

There exist, apart from the previously discussed model characteristics, a number of solution specific models and settings inherent to CFD modeling. These are introduced and described in this section.

The pressure-based solver is used to solve the steady state flow, turbulence and energy equations. The SIMPLE segregation algorithm is used for the pressure-velocity coupling method with the default under-relaxation factors. Discretization, which is the mathematical method of replacing differential equations that govern fluid flow with a set of algebraic

equations at each node in the mesh, is accomplished with a first-order upwind scheme for all the flow equations due to its numerical stability and use in previous studies [Bredell et al. (2006); Van Rooyen and Kröger (2008)]. For the case of pressure interpolation the "standard" scheme was used. FLUENT Inc. (2006) provides a detailed explanation of these settings.

Turbulence is modeled using the realizable k-ε model with default settings and standard wall treatment functions. This model is formulated to handle flow subjected to boundary layers with strong adverse pressure gradients, separation and recirculation (Shih et al., 1995) and is deemed the most appropriate for this flow problem.

Buoyancy effects are included with the Boussinesq model that treats density as a constant value in all solved equations except for the buoyancy term in the momentum equation:

$$(\rho - \rho_a)g \approx -\rho_a \beta (T - T_a)g \tag{2.4}$$

where ρ_a is the constant air density of the flow, T_a is the ambient temperature, and β is the expansion coefficient. This approximation is accurate as long as the change in actual densities, which are a function of temperature, is small. FLUENT Inc. (2006) states that the approximation is valid when $\beta(T - T_a) \ll 1$, which is the case for this study.

An essential aspect of any CFD based study is results verification, ideally accomplished by comparing the numerical results with experimental data. Owen (2010) also modeled the generic ACSC studied by Van Rooyen (2007) and the resulting performance trends are in good agreement with the results of both Van Rooyen (2007) and the present study. Owen (2010) also used his model to predict the performance of an actual ACSC and found that the results agree very well with measured data. These results validate the current model as an applicable tool for analysing ACSC performance.

The model can now be solved and the results processed to determine ACSC performance, as shown in the following chapters.

3. Generic ACSC performance

ACSC performance is calculated by extracting and processing the required data from the solution of the numerical model as explained in this section.

3.1 Ideal fan unit flow rate

The flow rate through a single free standing fan unit operating under a no-wind condition needs to be known as it is used as a performance benchmark for the fan units contained in the generic ACSC operating under the influence of various system variables. As per figure 3.1 this is achieved by plotting the effective system resistance of an ACSC fan unit resulting from the various flow obstructions as detailed in Appendix A, against the fan pressure rise presented in Appendix B. The point of intersection is the system operating point, or the ideal fan unit flow rate V_{Fid} which is found to be 636.6 m^3/s. At the specified air density, ρ_a, of 1.0857 kg/m^3, this corresponds to an ideal fan mass flow rate, m_{Fid}, of 691.2 kg/s.

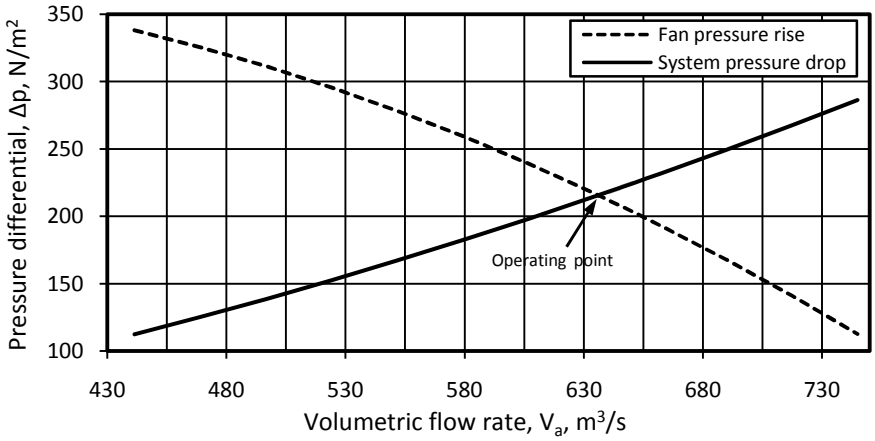

Figure 3. 1: Determining the ideal flow rate of a generic fan unit.

In order to test the validity of the heat exchanger pressure loss model and the pressure jump fan model a single free standing fan unit was modeled in CFD and the mass flow rate was found to be 694.4 kg/s which is in close agreement with the analytical result.

3.2 Definition of performance parameters

The plan view of the 30 fan generic ACSC is shown in figure 3.2 and indicates the wind directions and fan numbers which are labelled using an x,y notation according to the global axis system. The air mass flow rate through each fan, m_{Fxy}, and the average air inlet temperature of each fan, T_{Fxy}, is extracted from the solution of the numerical model and the volumetric flow rate of each fan is calculated as

$$V_{Fxy} = {}^{m_{Fxy}}/_{\rho_a}, \quad m^3/s \tag{3.1}$$

The fan volumetric effectiveness is defined as the ratio of the volumetric flow rate to the ideal volumetric flow rate:

$$Fan_{xy}\ volumetric\ effectiveness = {}^{V_{Fxy}}\!/_{V_{Fid}} \quad (3.2)$$

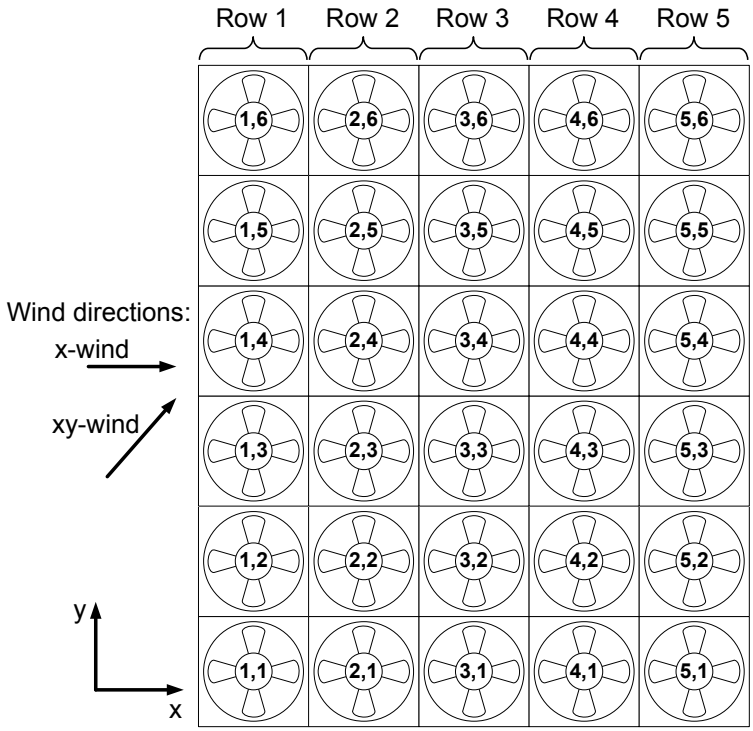

Figure 3. 2: Details of generic ACSC layout.

The system volumetric effectiveness is the ratio of the sum of the volumetric effectiveness of all the fans to the sum of the ideal volumetric flow rates.

$$System\ volumetric\ effectiveness = {}^{\Sigma V_{Fxy}}\!/_{30V_{Fid}} \quad (3.3)$$

Van Rooyen and Kröger (2008) give the total heat transfer of the generic ACSC from the steam to the air during windy conditions as

$$Q = \sum_{x=1}^{5}\sum_{y=1}^{6} m_{Fxy}c_{pa}\left(T_v - T_{Fxy}\right)\left[1 - exp\left(-44.41/{m_{Fxy}}^{0.5443}\right)\right], \quad W \quad (3.4)$$

and under ideal conditions (no wind and no hot air recirculation) for all 30 fans as

$$Q_{id} = 30m_{Fid}c_{pa}(T_v - T_a)[1 - exp(-44.41/{m_{Fid}}^{0.5443})], \quad W \quad (3.5)$$

where T_v is the steam temperature which is 60°C throughout the study. The system thermal effectiveness is the ratio of the numerically calculated heat transfer, as per equation (3.4) to the ideal heat transfer rate, as per equation (3.5):

$$System\ thermal\ effectiveness = {}^{\mathrm{Q}}\!/_{Q_{id}} \quad (3.6)$$

The heat rejected by the ACSC is approximately constant for steady state operation of a power plant and any reduction in performance of the ACSC will result in a rise of the steam temperature, T_v, to ensure constant heat rejection as calculated below

$$Q = Q_{id} = 30 m_{Fid} c_{pa} (T_v - T_a)[1 - exp(-44.41/{m_{Fid}}^{0.5443})]$$

$$= \sum_{x=1}^{5} \sum_{y=1}^{6} m_{Fxy} c_{pa} (T_v - T_{Fxy})[1 - exp(-44.41/{m_{Fid}}^{0.5443})]$$

$$= \sum_{x=1}^{5} \sum_{y=1}^{6} m_{Fxy} c_{pa} T_v [1 - exp(-44.41/{m_{Fid}}^{0.5443})]$$

$$- \sum_{x=1}^{5} \sum_{y=1}^{6} m_{Fxy} c_{pa} T_{Fxy} [1 - exp(-44.41/{m_{Fid}}^{0.5443})], \quad W \qquad (3.7)$$

From which it follows that the steam temperature in K is

$$T_v = \left[Q_{id} + \sum_{x=1}^{5} \sum_{y=1}^{6} m_{Fxy} c_{pa} T_{Fxy} [1 - exp(-44.41/{m_{Fid}}^{0.5443})] \right] /$$

$$\left[\sum_{x=1}^{5} \sum_{y=1}^{6} m_{Fxy} c_{pa} [1 - exp(-44.41/{m_{Fid}}^{0.5443})] \right], \quad K \qquad (3.8)$$

Any rise in steam temperature will then result in higher steam turbine back pressure, p_v. The saturation pressure of the steam corresponding to this temperature is given by Kröger (2004) as

$$p_v = 10^z, \quad N/m^2 \qquad (3.9)$$

where

$$z = 10.79586(1 - 273.16/T_v) + 5.02808\, log_{10}(273.16/T_v)$$

$$+ 1.50474 \times 10^{-4}\left[1 - 10^{-8.29692\{(T_v/273.16)-1\}}\right]$$

$$+ 4.2873 \times 10^{-4}\left[10^{4.76955\{(1-273.16/T_v)\}} - 1\right] + 2.786118312 \qquad (3.10)$$

and T_v is in K.

The mechanisms leading to reduced performance of the generic ACSC are investigated in the next section.

3.3 Mechanisms of reduced ACSC performance

The heat rejected by an ACSC is defined by equation (3.4) and it can be seen that decreases in air mass flow rates and increases in fan inlet temperatures will culminate in a decrease in the heat rejected by the ACSC. For the purposes of this study the remainder of the variables will be assumed as constant. Thus to understand and explore avenues of improving ACSC performance these two variables need to be examined.

3.3.1 Factors affecting air mass flow rate

Axial flow fans, as used in the generic ACSC, are intended to operate with axial flow conditions at the fan inlet, i.e. the flow enters the fan normal to the plane of rotation as shown by the velocity vectors in figure 3.3 (a). Characteristic of such flow is an axi-symmetrical pressure distribution at the fan inlet as shown in figure 3.2 (b). Axial flow conditions result in the fan operating at the designed operating point shown in figure 3.1.

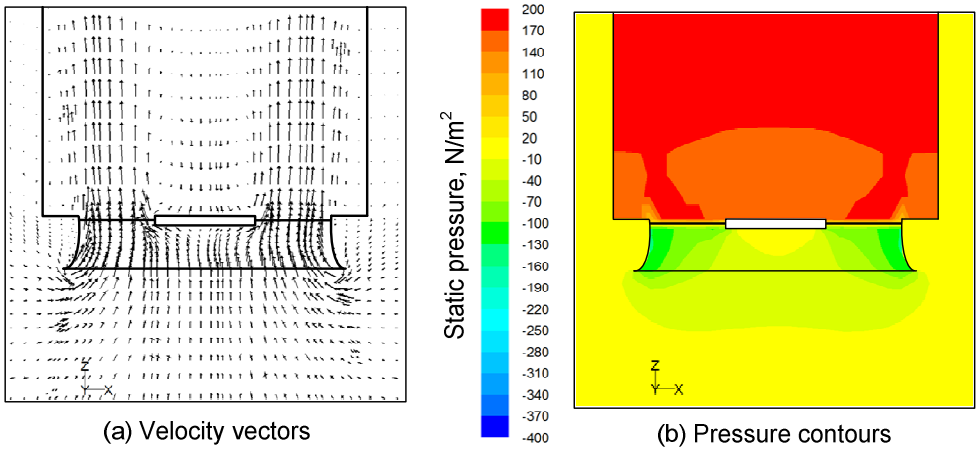

Figure 3. 3: Flow conditions at the fan inlet for a single fan unit, no-wind condition.

With multiple fan units arranged in a matrix, as in the case of the 5x6 arrangement of the generic ACSC, the air for the 12 interior fans is drawn past the periphery fans and cause distorted flow in the form of abnormally high horizontal or cross flow at the fan inlets. The presence of wind significantly increases flow distortion, especially at the upwind periphery and near periphery fans.

Distorted flow conditions underneath the fan platform, be it wind induced or caused by the inherent layout of the ACSC, is observed as two flow phenomena. The first phenomenon is oblique or off axial flow occurring where the flow immediately upstream of the fan deviates from the ideal case of being normal to the fan plane of rotations, and instead the flow is off axial or oblique as shown in figure 3.4 (a). This results in reduced fan performance and hence air mass flow. Stinnes and von Backström (2002) isolated the effect of oblique flow on axial flow fans and found that the decrement in fan static pressure to be equal to the dynamic pressure based on the oblique flow velocity. The pressure jump fan model method utilized in this study calculates the fan pressure rise as a function of the velocity normal to the fan plane as described in section 2. Thus, oblique flow will result in a higher pressure jump affecting a lower mass flow rate as compared to axial flow of the same magnitude.

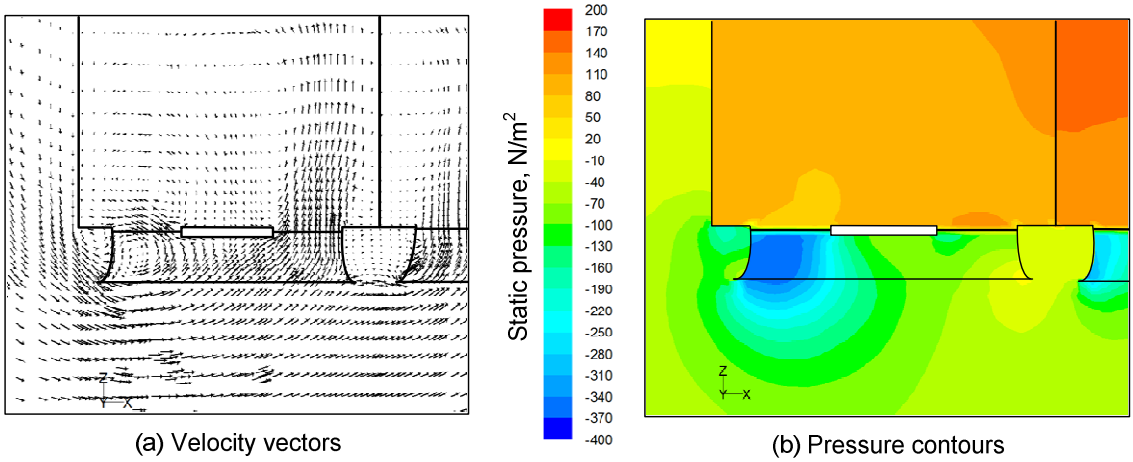

(a) Velocity vectors (b) Pressure contours

Figure 3. 4: Flow conditions at the fan inlet of periphery ACSC fan unit (1,4), v_{ref} = 3m/s x-wind.

The second flow phenomenon associated with distorted flow is the presence of separated flow, identified as areas of low pressure. Flow separation is observed at the upwind edge of the fan platform caused by the wind driven air flow deflecting off the upwind vertical face of the ACSC and flowing down and around the leading edge of the ACSC. This separation creates a large area of low pressure affecting the leading edge fans, as seen on the left hand bellmouth in figure 3.4 (b). Cross flow induced flow separation is also observed at the upwind bellmouth edges, as evident on the right hand bellmouth in figure 3.4 (b). The low pressure areas immediately upstream of the fan caused by flow separation are effectively additional system losses resulting in additional resistances which the fan has to overcome, ultimate resulting in reduced mass flow rate through the fan.

3.3.2 Factors affecting fan inlet temperature

In this study the temperature of the ambient air is a constant value, T_a = 288.75 K, however the fan inlet temperature can increase if hot plume air is drawn down and back into the ACSC as shown schematically in figure 1.7. This effect, known as recirculation, is shown for the generic ACSC in figure 3.5. The fan temperature can also increase under severe flow distortions when backflow occurs through a fan resulting in hot air in the plenum chamber flowing through the fan. This is found to affect a small number of fans under high wind velocities, but does not result in significant temperature increases and can be ignored from a system thermal performance point of view.

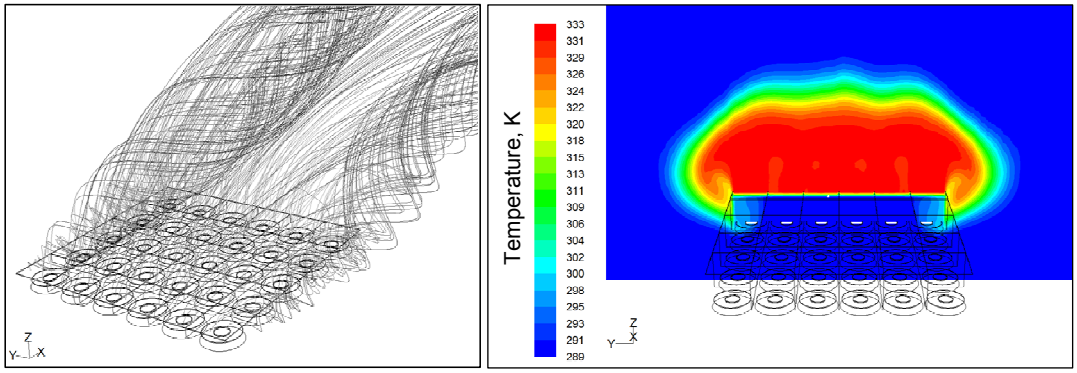

(a) Pathlines showing the plume air being drawn back into the ACSC

(b) Contours of temperatures on section through row 6 showing recirculation effects.

Figure 3. 5: Recirculation effects

3.4 Generic ACSC performance results.

The volumetric effectiveness of the individual fans are given in figure 3.6 for the x-wind case (v_{ref} = 3 m/s, 6 m/s and 9 m/s as per equation (2.3)) and it can be seen that the worst performing fans are the upstream periphery fans, i.e. fans (1,$y_{1\text{-}6}$) with the fans located in the middle of the row, fan (1.3) and (1.4), experiencing the greatest performance reduction of all 30 fans. This indicates the severity of the wind induced leading edge separation and flow distortions affecting the upstream periphery fans. For the rest of the fan rows this trend is reversed with the fans located on the sides of a respective row, e.g. fans (3,1) and (3,6) for the 3rd downstream fan row, performing the worst. When considering fans with a constant y index (effectively moving in the direction of the x-wind down the ACSC) it can be seen that each successive downstream fan performs better than the adjacent upstream fan. A number of fans operate above the ideal flow rate.

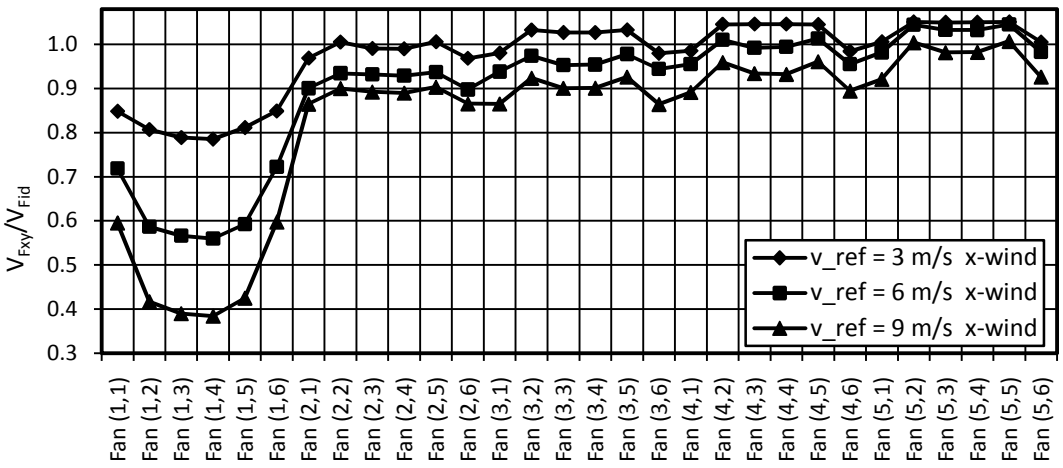

Figure 3. 6: Volumetric effectiveness per fan in generic ACSC for x-wind.

Figure 3.8 shows the performance of the individual fans subjected to a xy-wind (v_{ref} = 3 m/s, 6 m/s and 9 m/s as per equation (2.3)) and it can be seen that as for the case of the x-wind, the

fans located on the upstream periphery of the ACSC, i.e. fans (1,$y_{1\text{-}6}$,) and fans ($x_{2\text{-}5}$,1), are the most sensitive to wind induced performance reduction which again is caused by wind induced leading edge separation and flow distortions affecting the upstream periphery fans. It can be seen that the performance of the interior fans increase as the distance from the upstream edge fans increase. These trends correspond to the pressure contours shown in figure 3.7 (b)

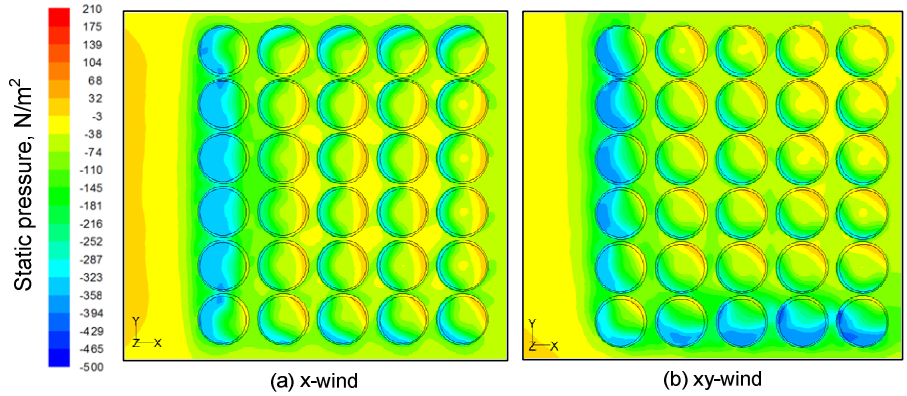

Figure 3. 7: Contours of static pressure in plane of bellmouth inlets showing wind direction effects, v_{ref} = 9 m/s.

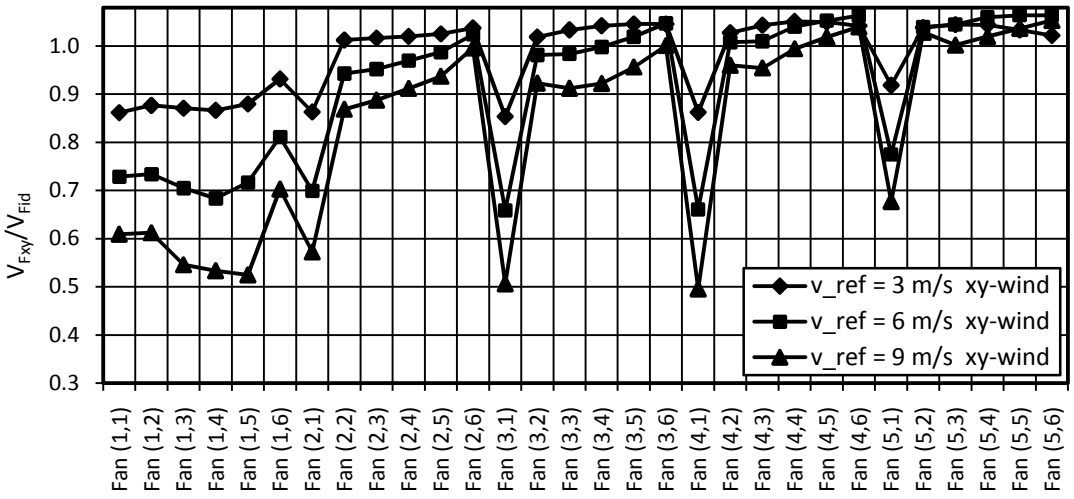

Figure 3. 8: Volumetric effectiveness per fan in generic ACSC for xy-wind.

The system volumetric effectiveness is shown in figure 3.9 and shows a near linear reduction in performance as a function of wind speed and that the x-wind results in greater performance reduction than the xy-wind.

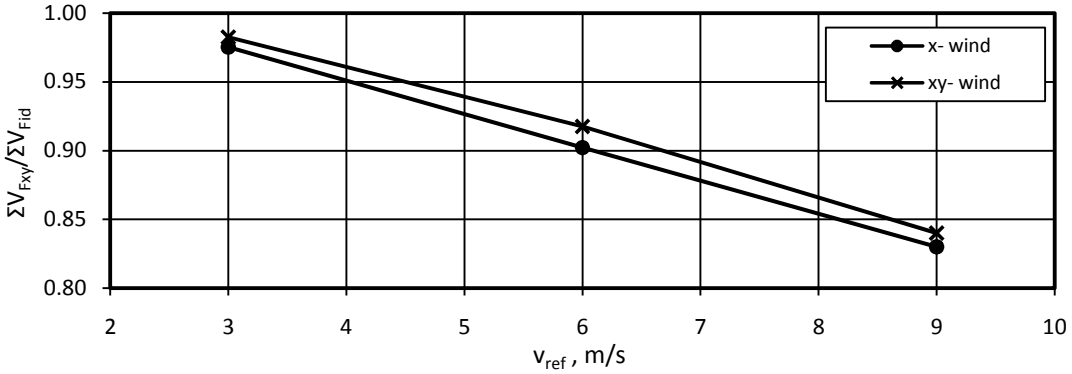

Figure 3. 9: Generic ACSC system volumetric effectiveness as function of wind direction and wind speed.

The system thermal effectiveness is shown in figure 3.10 and the near linear reduction is still present although the gradient for the x-wind is slightly steeper indicating a greater sensitivity to recirculation at high wind velocity. This premise is confirmed by contours of fan temperatures shown in figure 3.11 for v_{ref} = 9m/s, which shows recirculation occurring only for the x-wind case, and not for the xy-wind case. The slightly increased fan inlet temperature shown by some of the upstream fans in figure 3.11 (a) is found to be caused by backflow through the fans caused by the high wind speed and is not the result of recirculation. The thermal effectiveness is also calculated by setting the fan inlet temperature, T_{Fxy} in equation 3.4, equal to the ambient temperature T_a thereby excluding the effects of recirculation, thus the thermal performance is solely a function of reduced volumetric effectiveness. It can be seen that for the xy-wind thermal performance across all wind speeds is not influenced by recirculation. The x-wind is unaffected by recirculation at the lowest wind speed but at increased wind speed recirculation effects becomes more noticeable. It can also be observed that recirculation contributes less to reductions in thermal performance as compared to the effect of reduced fan performance.

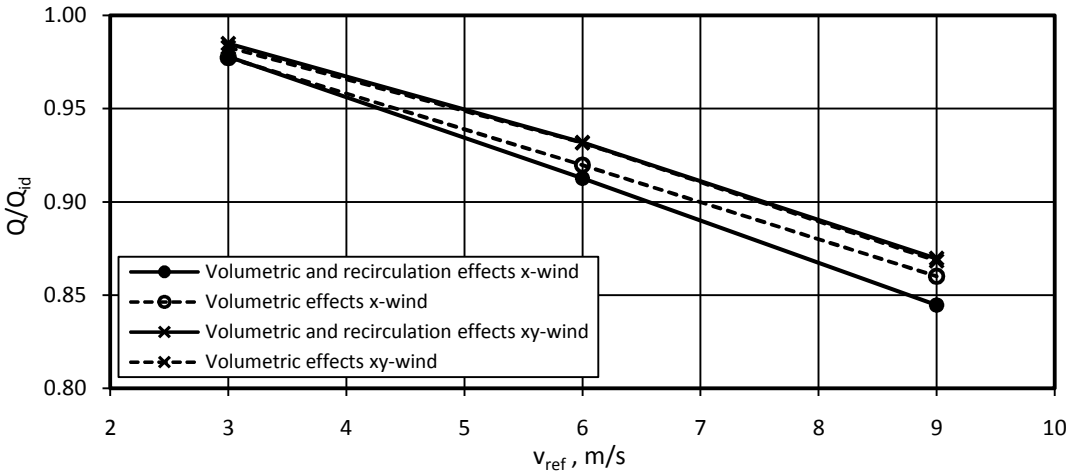

Figure 3. 10: Generic ACSC system thermal effectiveness as function of wind direction and wind speed.

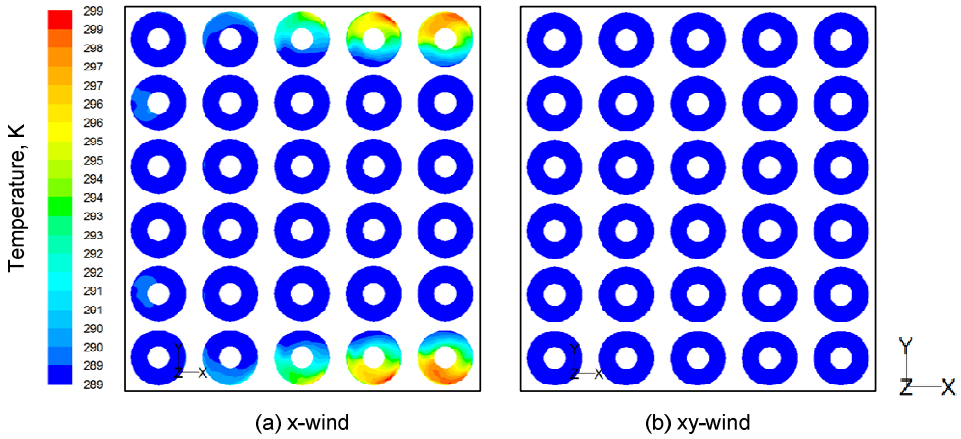

Figure 3. 11: Contours of fan temperatures showing wind direction effects, v_{ref} = 9 m/s.

The steam temperature and turbine back pressure is shown in figure 3.12 and reflects the trends discussed so far.

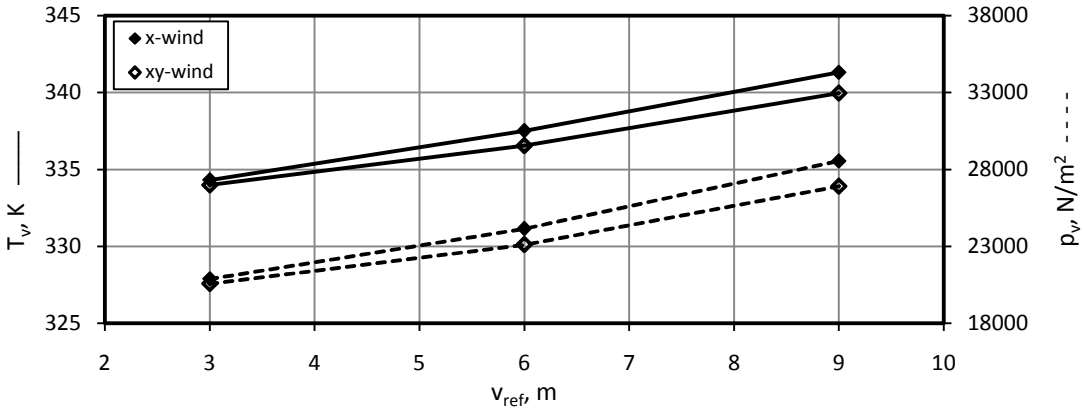

Figure 3. 12: Generic ACSC steam temperature and turbine back pressure as function of wind direction and wind speed.

A comparison of the results to those obtained by Van Rooyen (2007) is presented in Appendix D. In sections to follow, trend that various system parameters have on ACSC performance are examined by modifying the generic ACSC accordingly and calculating the performance parameters as described in this section.

4. Effect of platform height variation

To determine the effect of platform height variation (H_i as shown in figure 4.1) on ACSC performance the generic ACSC is modeled with a platform height of 10, 15, 20 and 25 m. The windwall height is kept constant at 10m and the three reference wind speeds (v_{ref} = 3 m/s, 6 m/s and 9 m/s as per equation (2.3)), in both the x- and xy-wind direction are modeled.

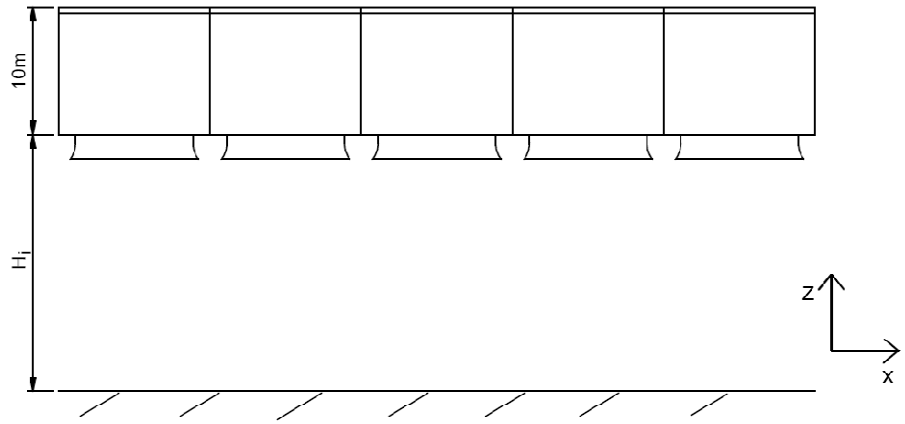

Figure 4. 1: ACSC platform height, H_i, variation.

The system performance results are shown in figures 4.2 and 4.3 where the detrimental effect of reduced platform height for both wind directions is clearly visible. This stems from the fact the as the platform height decreases the effective open area at the edge of the ACSC also decreases. This requires that for a comparative air mass flow rate through the ACSC the average horizontal velocity beneath the leading edge of the ACSC has to increase. As discussed in section 3.3 increases in velocity are observed as low pressure areas as shown in figure 4.4 from where it can be seen that for a low platform height (H_i = 10m) the low pressure area has spread to the second row of fans whereas at higher platform heights (H_i = 20m) the low pressure area is considerably smaller and less severe.

In figure 4.2 it can be seen that the system volumetric effectiveness is reduced to a greater degree by the x-wind direction compared to the xy-wind direction. This is expected since, for the case of the xy-wind, the effective open area at the upwind edge of the ACSC is greater, which in effect reduces the average horizontal velocity into the ACSC which in turn leads to smaller low pressure areas underneath the ACSC. The difference in performance between the two wind directions increases as the platform height decreases. In figure 4.3 it can be seen that the system thermal effectiveness follows the same trend as stated above.

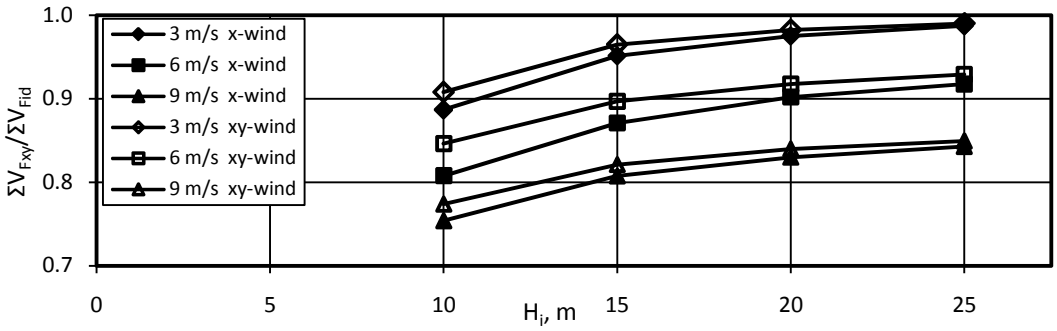

Figure 4. 2: System volumetric effectiveness as a function of platform height, wind direction and wind speed.

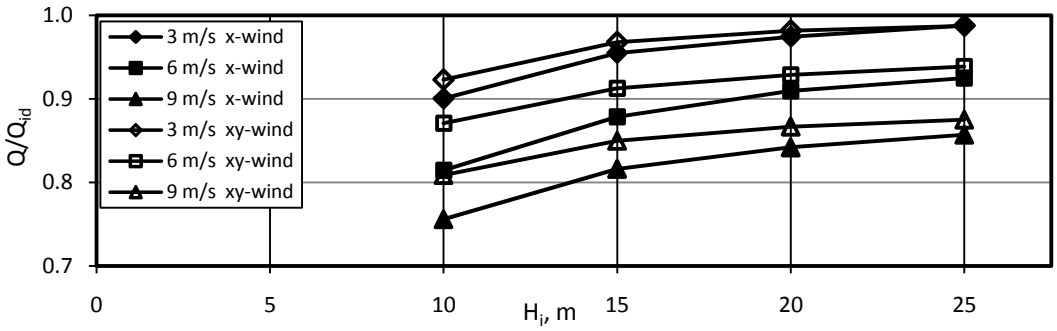

Figure 4. 3: System thermal effectiveness as a function of platform height, wind direction and wind speed.

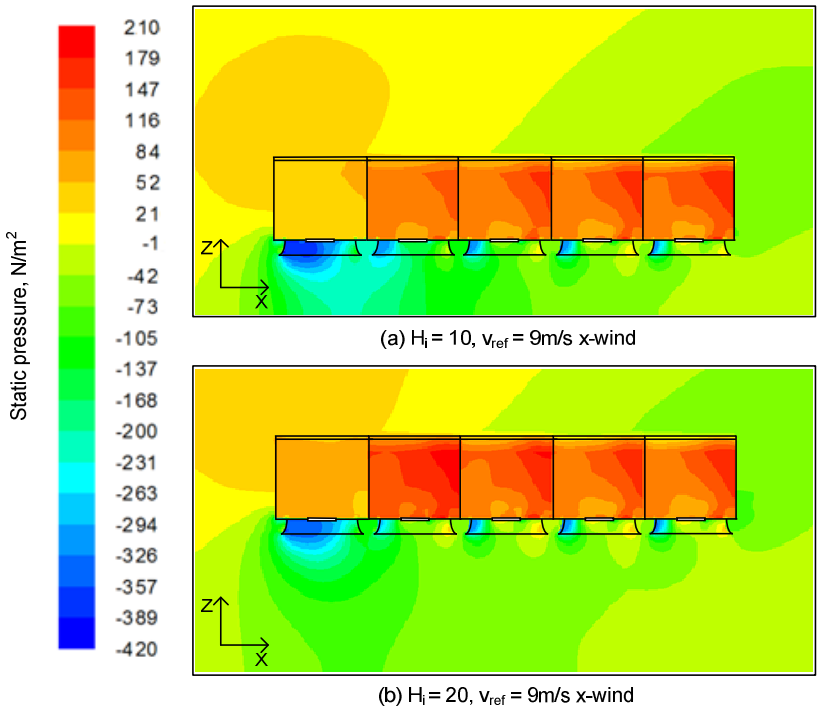

Figure 4. 4: Contours of static pressure on section through fan ($x_{1\text{-}5}$,4) showing platform height effects.

The steam temperature and turbine back pressure are shown in figure 4.5 and reflect the trends discussed so far.

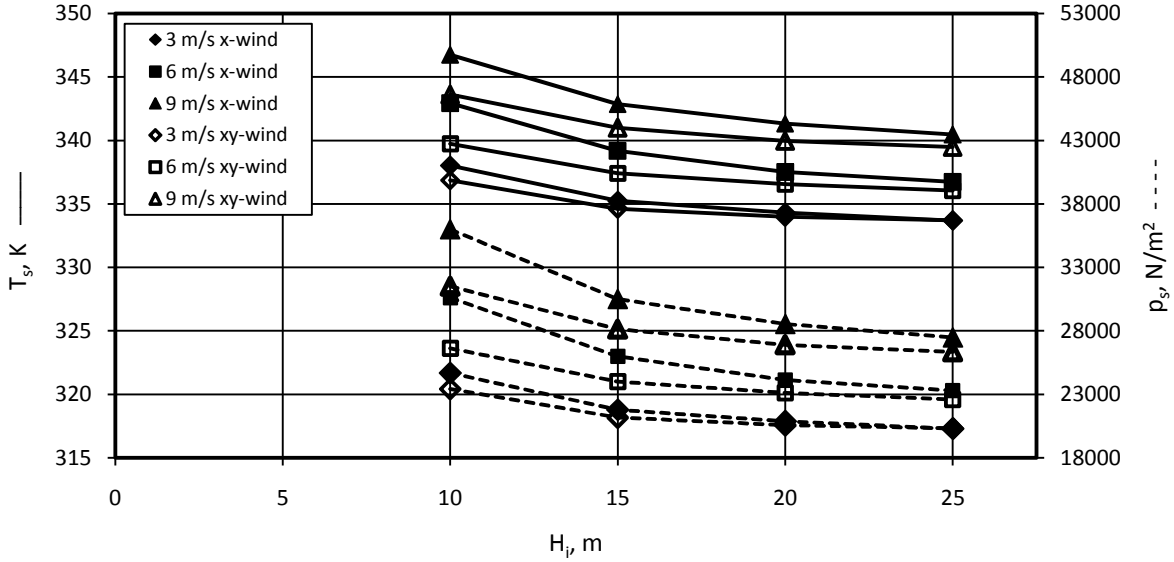

Figure 4. 5: Steam temperature and steam pressure as functions of platform height, wind direction and wind speed.

From this section it is concluded that the generic ACSC platform height specification of H_i = 20m is an acceptable value and although a higher fan platform (H_i = 25m) will result in slightly improved performance an in-depth study will be required to determine if the added expense of a higher fan platform is justified by the additional performance.

5. Effect of windwall height variation

The effect of windwall height variation, H_w, on ACSC performance is modeled by adjusting the height of the rectangular plenum chamber of the generic ACSC as shown in figure 5.1. Windwall heights of 2.5, 5, 7.5 and 10 m are modeled with a constant platform height of 20m for three reference wind speeds (v_{ref} = 3 m/s, 6 m/s and 9 m/s as per equation (2.3)) for both the x- and xy-wind direction. The results are shown in figures 5.2 and 5.3.

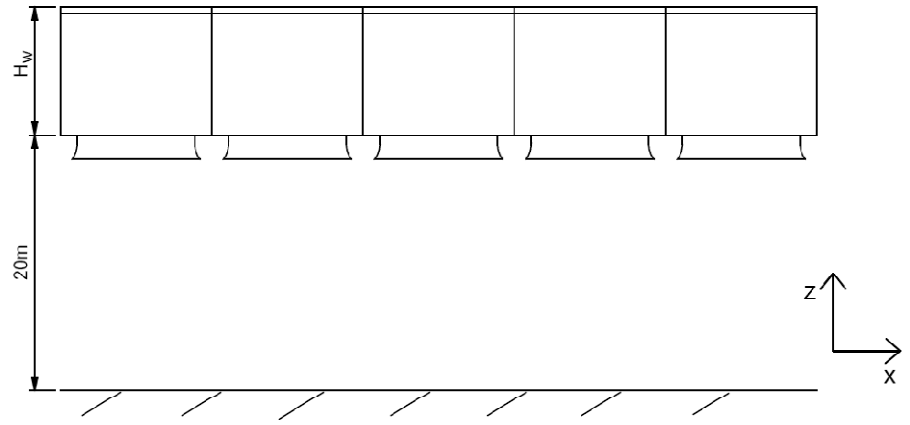

Figure 5. 1: ACSC windwall height, H_w, variation.

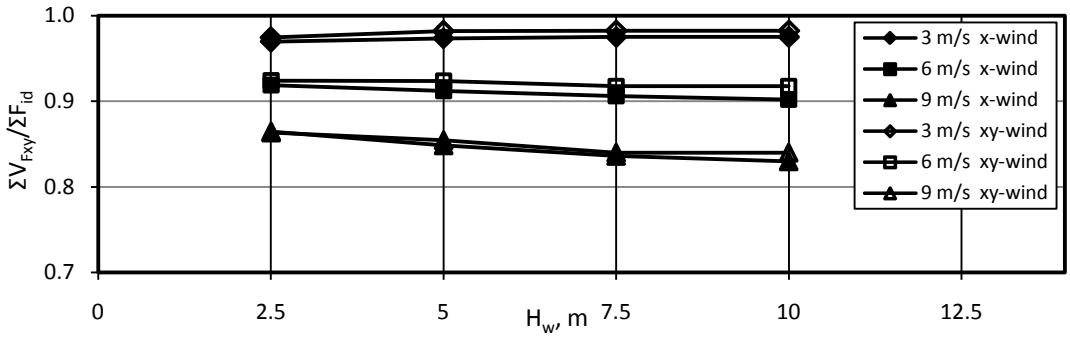

Figure 5. 2: System volumetric effectiveness as function of windwall height, wind direction and wind speed.

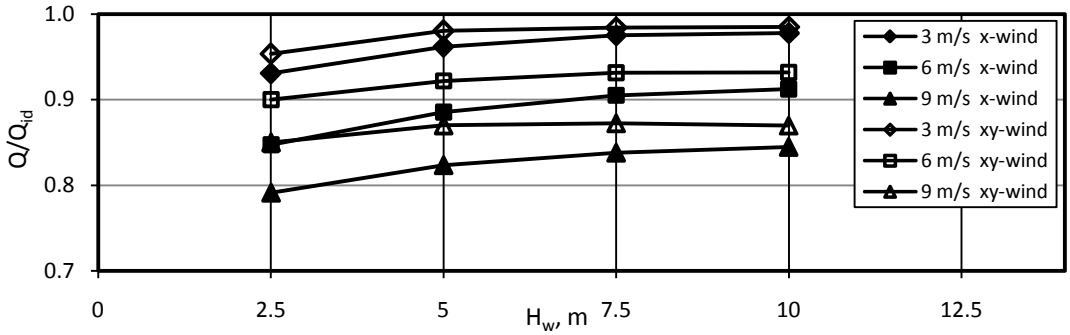

Figure 5. 3: System thermal effectiveness as function of windwall height, wind direction and wind speed.

From figure 5.2 it can be seen that a decrease in windwall height has negligible effect on the volumetric effectiveness of the system, regardless of wind direction. At high wind speed (v_{ref} = 9m/s) and low windwall height (H_w = 2.5 and 5m) the volumetric effectiveness improves slightly which is attributed to the fact that the ACSC frontal area decreases with a decrease in windwall height and as a result the ACSC is more streamlined causing less flow obstruction as compared to higher wind wall heights which in turn results in less flow distortion at the inlets of the periphery fans.

Figure 5.3 shows that reducing the windwall height reduces the thermal performance of the ACSC. The thermal performance is a function of air mass flow rate and fan inlet temperature as detailed in section 3.3, however figure 5.2 shows that the changes in volumetric effectiveness, and hence the air mass flow rate, are too small to account for the change in thermal effectiveness. Therefore an increase in fan inlet temperature, caused by hot plume air recirculation, is responsible for reduced thermal performance.

Contours of fan inlet temperature are plotted in figures 5.4 (a) and (b) and show that for a high windwall height (H_w = 10 m) and wind speed (v_{ref} = 9m/s) recirculation is only slightly noticeable for the x-wind on the fans located on the sides towards the rear of the ACSC and there is no recirculation for the xy-wind. However figures 5.4 (c) and (d) show that for the lowest windwall height (H_w = 2.5 m) and high wind speed (v_{ref} = 9m/s) recirculation is clearly visible. For the xy-wind recirculation is evident for the fans on the wind facing edges. These observations are to be expected as windwalls are used primarily to reduce recirculation effects which are seen to be more pronounced in the x-wind direction especially at higher wind speeds.

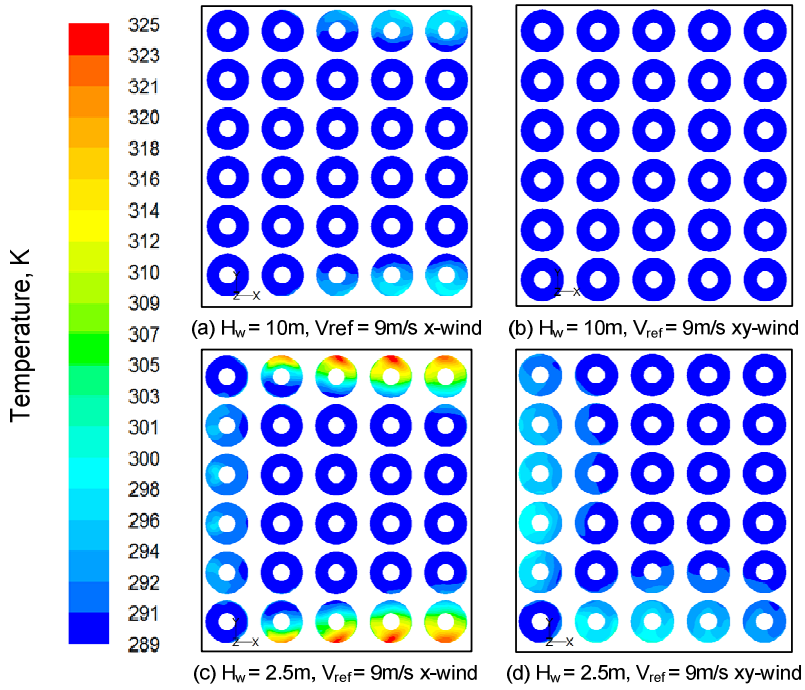

Figure 5. 4: Contours of fan temperature showing windwall height effects.

Figure 5.5 shows pathlines of the flow exiting the top of the ACSC and it can be seen how the hot plume air forms into two large vortexes. The warm buoyant plume air acts as a flow obstacle to the wind which has to flow around the plume and the ACSC causing the vortexes, a small portion of which is sucked down and into the ACSC by the downwind fans resulting in the raised fan inlet temperatures shown in Figure 5.4.

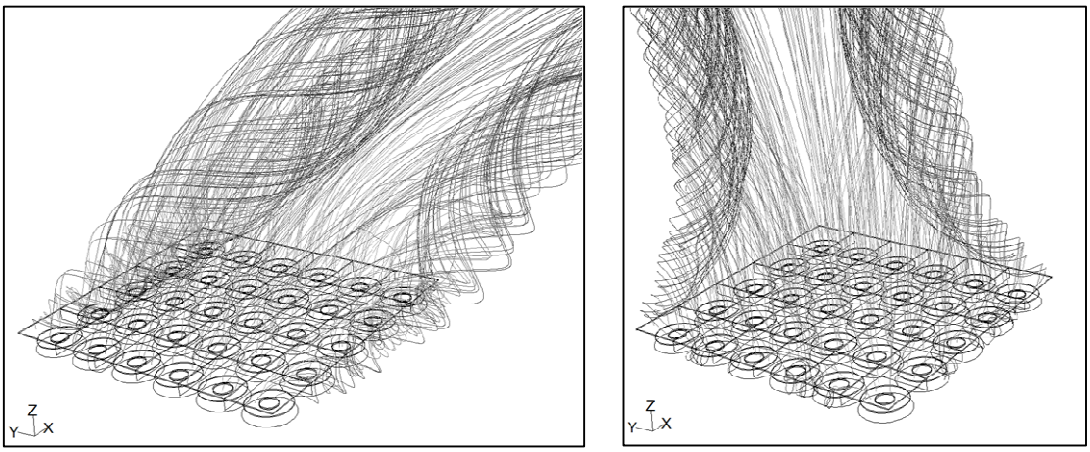

(a) W_w=2.5m, V_{ref}=9m/s x-axis (b) W_w=2.5m, V_{ref}=9m/s xy-axis

Figure 5. 5: Pathlines showing recirculation effects at low windwall height for x- and xy wind.

Figure 5.6 shows steam temperature and pressure and reflects the decrease in thermal performance caused by the recirculation effect.

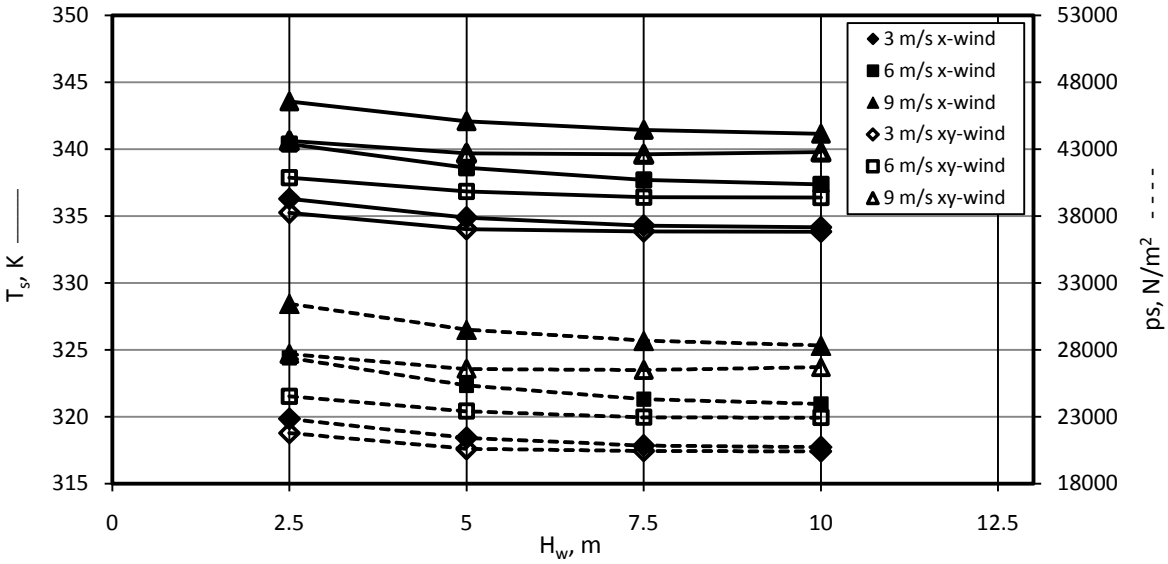

Figure 5. 6: Steam temperature and steam pressure as functions of windwall height, wind direction and wind speed.

From this sections it is concluded that the generic ACSC windwall height specification of H_w = 10m is an acceptable value however for ACSCs sited at locations not exposed to excessively

windy conditions a lower windwall height of 7.5m could also be appropriate, however a life cycle cost analysis should be used to calculate the final height.

6. Effect of walkways

As discussed in section 3.3.4 ACSC fan performance is reduced by the presence of off axial flow conditions at the fan inlets as shown in figure 6.1 (a) and by the presence of additional flow losses resulting from flow separation at the leading edge of the ACSC and the bellmouth inlets, observed as areas of low pressure (figure 6.1 (c)). These flow phenomena are apparent mainly at the periphery fans and are most severe at the upwind sides of an ACSC operating under windy conditions as indicated by figure 3.6 and 3.8.

Salta and Kröger (1995) experimentally showed that the addition of an external walkway or skirt improves the performance of the fans in the proximity of the walkway. The presence of the walkway improves fan performance by addressing both flow phenomena leading to reduced fan performance. Firstly, the flow has to pass around the walkway and back towards the ACSC as shown in figure 6.1 (b). This results in near horizontal flow at the leading bellmouth edge as opposed to the generic case (figure 6.1 (a)) where the flow at the bellmouth edge is angled downwards at the bellmouth edge as the air deflects down the leading vertical face of the ASCS. This improvement leads to better axial flow conditions at the fan face and ultimately improved fan performance.

A second benefit of the walkway is that the area of separation, although still present and starting from the leading edge of the walkway as shown in figure 6.1 (d), is moved away from the bellmouth and hence covers a smaller area of the fan inlet. This mitigates fan performance degradation resulting from additional losses in the bellmouth inlet.

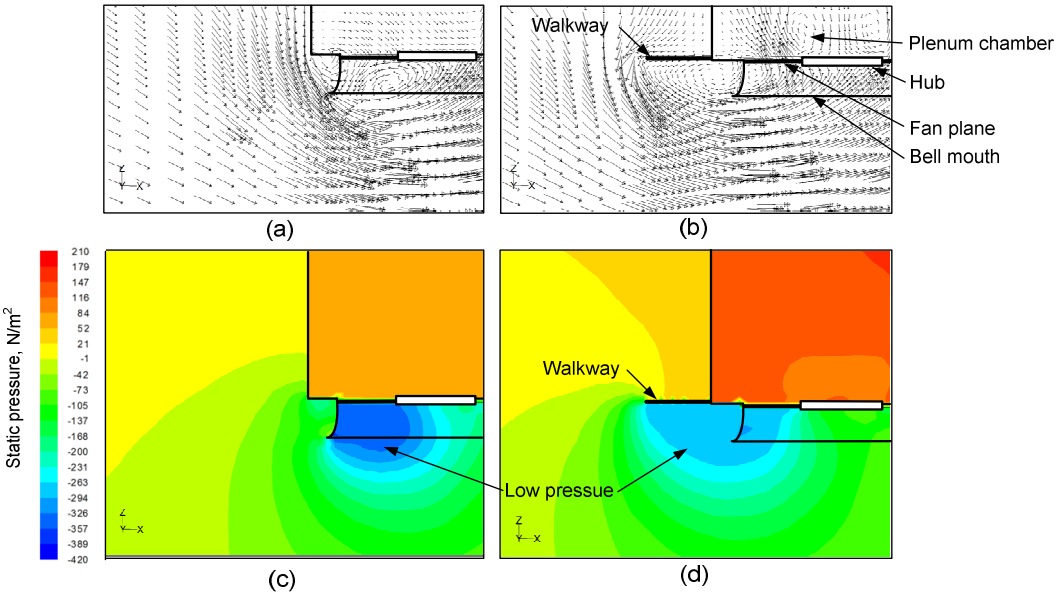

Figure 6. 1: Section through typical upwind periphery fan unit showing flow distortion effects with and without a walkway, v_{ref} = 6m/s, x-wind.

Walkway effects on the generic ACSC are studied by adding a walkway of width W_w as shown in figure 6.2. The walkways are located according to two cases, the first case being on only the up- and downstream edges of the ACSC as shown in figure 6.3 and referred to as the UD case.

For the second case the walkways are located around the periphery of the ACSC and referred to as the P case. Walkway widths of 1.2, 1.7, 2.2, 3, 4, 6 and 8 m are modeled with a constant platform height of 20 m and wind wall height of 10m for three reference wind speeds (v_{ref} = 3 m/s, 6 m/s and 9 m/s as per equation (2.3)) for both the x- and xy-wind direction.

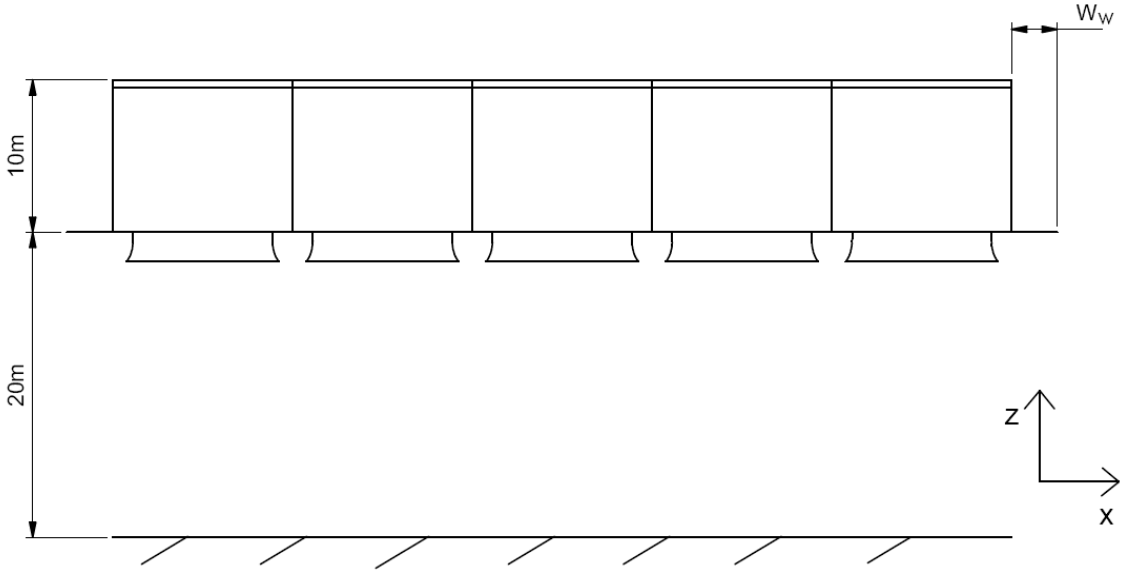

Figure 6. 2: ACSC with walkway, W_w.

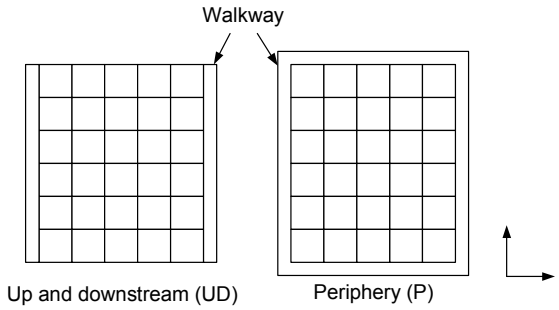

Figure 6. 3: Plan view of the location of the up- and downstream and periphery walkways.

The ACCS system volumetric effectiveness results are shown in figure 6.4 as a function of W_w and the performance increase across all combinations of variables is clearly visible. The gradient of the lines of the various cases indicates the change of performance per change in walkway width and is the steepest at the smallest walkway width, flattens as the walkway width increases and approaches zero at low wind speeds (v_{ref} = 3 m/s) at large values of W_w. This suggests that the greatest performance gain per unit walkway width is achieved with a narrow walkway and the performance increase per increase in walkway width decreases up to a point where a wider walkway has no effect on volumetric effectiveness, however this point is wind speed dependent.

In terms of walkway location figure 6.4 shows that the P case (dotted lines) performs better than the UD case (solid lines) regardless of wind speed or direction. When considering the interaction between wind direction (filled markers for x-wind and unfilled markers for xy-wind) and walkway location it can be seen that the UD case generally performs better under x-wind than xy-wind direction, which is the worse performing configuration for W_w greater than 1.7m. By comparing Figure 6.5 (a) and (b) to (c) and (d) respectively it can be seen that the UD configuration only benefits the fans located next to the upstream walkway while the low pressure areas for the rest of the fans remain unchanged from the no walkway cases for a given wind direction.

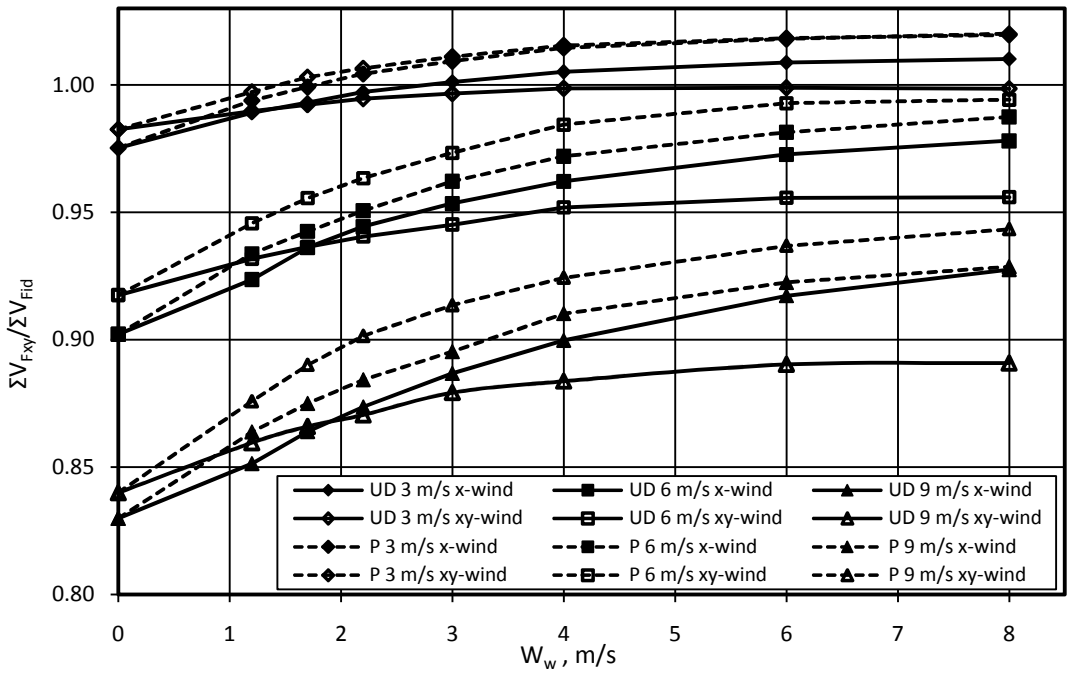

Figure 6. 4: System volumetric effectiveness as a function of walkway width, walkway location, wind direction and wind speed.

For the P case the performance is generally better under an xy-wind than x-wind direction, however it must be noted that the generic ACSC without walkways (figure 6.4, W_w = 0m) is less suseptable to decreases in performance caused by an xy-wind as compared to a x-wind. It can be seen that this inherent performance difference is near constant when comparing wind direction effects for P cases, except for v_{ref}= 3m/s cases where the wind direction no longer impacts performance for walkway widths greater than 3m. By comparing Figure 6.5 (a) and (b) to (e) and (f) respectively it can be seen that the P configuration reduces the low pressure areas of all the fans subjected to separated flow conditions for both wind directions.

The effect of walkways on system thermal effectiveness is shown in figure 6.6 and exhibits the same trends as volumetric effectiveness of figure 6.4. The steam temperature and turbine back pressure is presented in Appendix E.

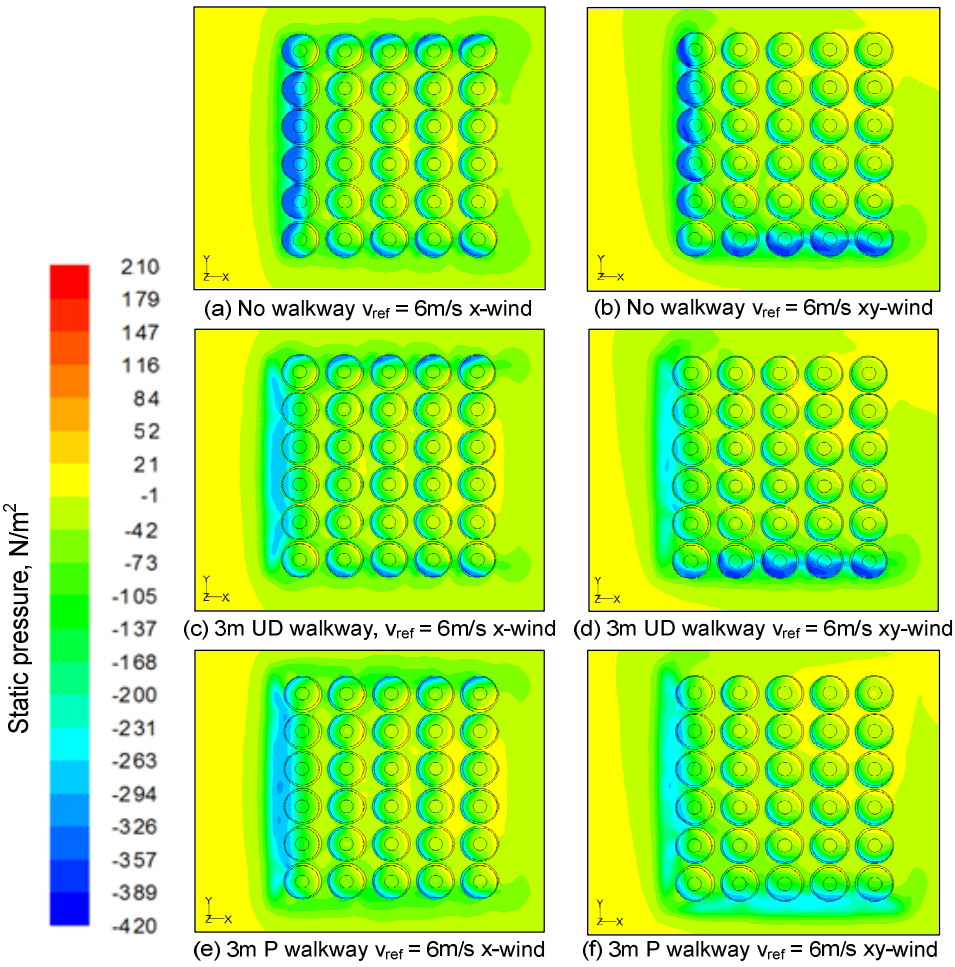

Figure 6. 5: Contours of static pressure in plane of bellmouth inlets showing walkway location and wind direction effects, v_{ref} = 6 m/s.

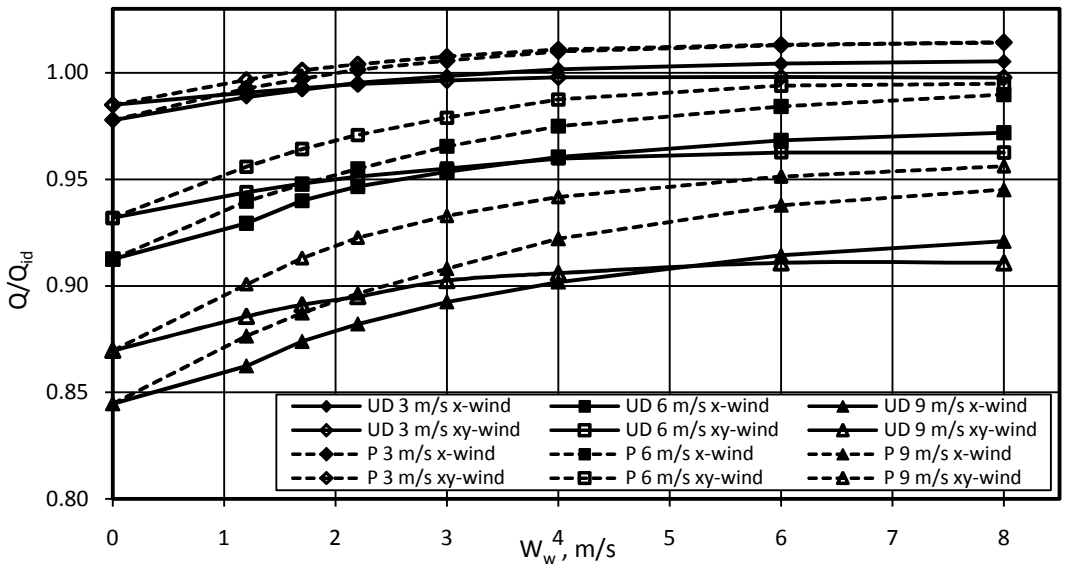

Figure 6. 6: System thermal effectiveness as a function of walkway width, walkway location, wind direction and wind speed.

7. Effect of windscreens

As discussed in section 3.3 the horizontal component of the airflow underneath the ACSC leads to reduced fan and consequently ACSC performance. However the energy available in the wind, that is the origin of the reduced fan performance, can theoretically be harnessed to improve fan performance. An idealized example illustrating the concept would be to place the axis of the fans parallel to the wind direction (analogous to the setup of a wind turbine used to generating electricity) with the upstream face of the fan facing the wind. This arrangement would offset a part of the energy required by the fan with the dynamic energy already present in the wind. Such a setup is by no means practical in the context of an ACSC but illustrates the concept that wind effects should not be dismissed as only being detrimental to fan performance. Therefore the challenge is to formulate methods of exploiting the energy content of wind in ways that enhance fan performance.

Such a method is the addition of windscreens underneath the fan platform of the generic ACSC and has been implemented at a number of operational ACSCs (Maulbetsch and DiFilippo, 2007). The locations of the screens are shown in figure 7.1 with the relevant dimensions. The screens are located parallel to the x-axis along the middle of the ACSC and parallel with the y-axis between the third and fourth fan row. The 20m height beneath the fan platform is divided into four equal panels allowing screens with different loss coefficients to be specified for each panel.

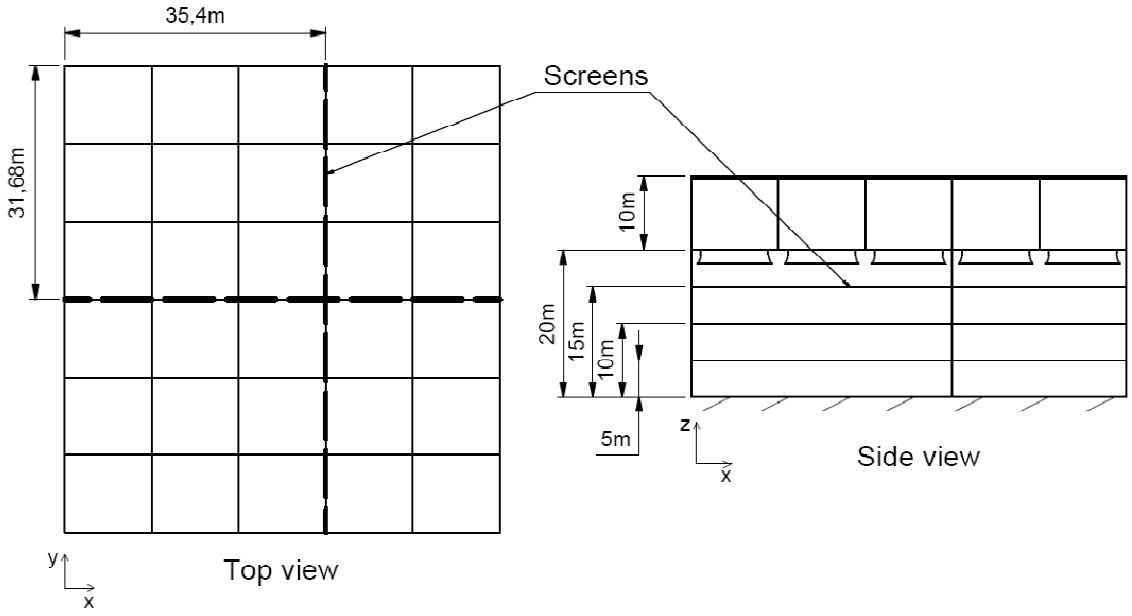

Figure 7. 1: ACSC with windscreens.

The screens act as a flow resistance blocking the air flow and create a stagnation effect under the ACSC, observed as increased static pressure as shown in figure 7.2, by converting the kinetic energy of the flow to potential energy which in turn reduces the fans energy requirements.

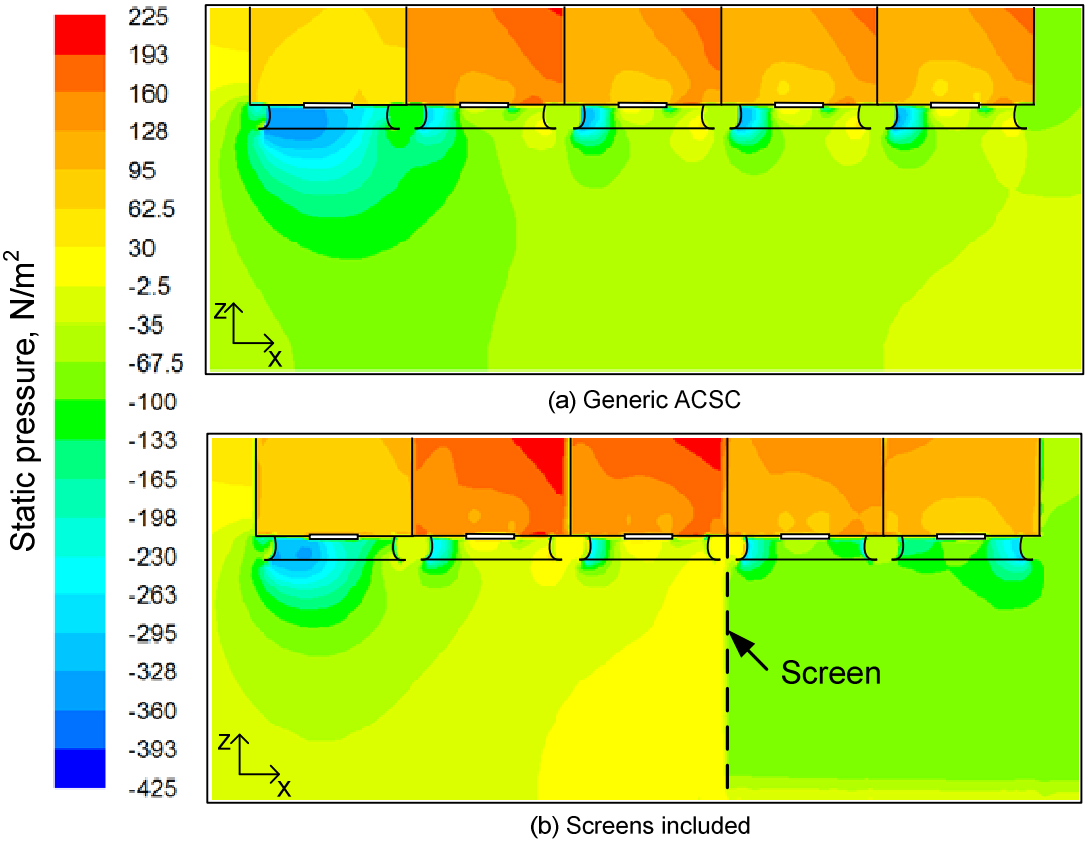

Figure 7. 2: Contours of static pressure on section through fan ($x_{1\text{-}5}$,4) showing the effect of screens for screen configuration Case A, v_{ref} = 9 m/s x-wind.

The screens can also be configured in such a way that the flow is deflected into the fan inlets. This is accomplished by specifying screens with higher flow resistance, or denser screens, towards the ground and screens with less flow resistance towards the fan platform causing the flow to deflect upwards into the fan inlets as shown by the velocity vectors in figure 7.3 below.

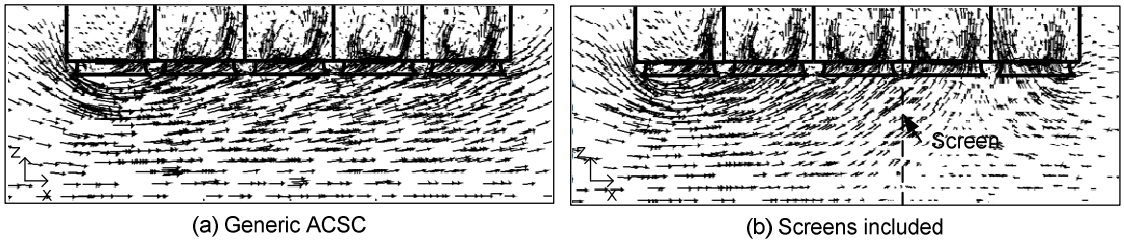

Figure 7. 3: Velocity vectors on section through fan ($x_{1\text{-}5}$,4) showing the effect of screens for screen configuration Case A, v_{ref} = 9 m/s x-wind.

Three different types of screens are utilized in this study as detailed in table 7.1 alongside the respective screen loss coefficients K_{sc} as a function of Ry (defined by equation (A.5)). The closed screen does not allow the passage of flow and is consequently modeled as a wall. With three types of screens that can be specified on four different panels a large number of possible screen combinations exist but as stated previously the general approach is to locate denser

screens towards the ground and the screens with less flow resistance towards the fan platform and with this in mind the initial screen combinations are shown in figure 7.4. The screens are modeled with three reference wind speeds (v_{ref} = 3 m/s, 6 m/s and 9 m/s as per equation (2.3)) for both the x- and xy-wind direction.

Table 7.1: Screen details.

Name	Loss coefficient, K_{sc}
55 % Closed	$0.501Ry^{0.132}$
65 % Closed	$4.501Ry^{0.015}$
Closed (Wall)	∞

Panel height	Case A	Case B	Case C
20m	55% Closed	65% Closed	55% Closed
15m	65% Closed	65% Closed	65% Closed
10m	65% Closed	Closed	Closed
5m	Closed	Closed	Closed

Figure 7. 4: First set of screen combinations.

The volumetric effectiveness, as shown in figure 7.5, clearly shows the improvements affected by the addition of screens, especially at high wind speeds and shows that the benefits are more pronounced for the x-wind cases. Case A is seen to be the best screen configuration for both wind directions with Case B and Case C showing near identical performance. It can therefore be concluded that the difference between the 55% closed screen and the 65% closed screen is negligible from a flow effect point of view.

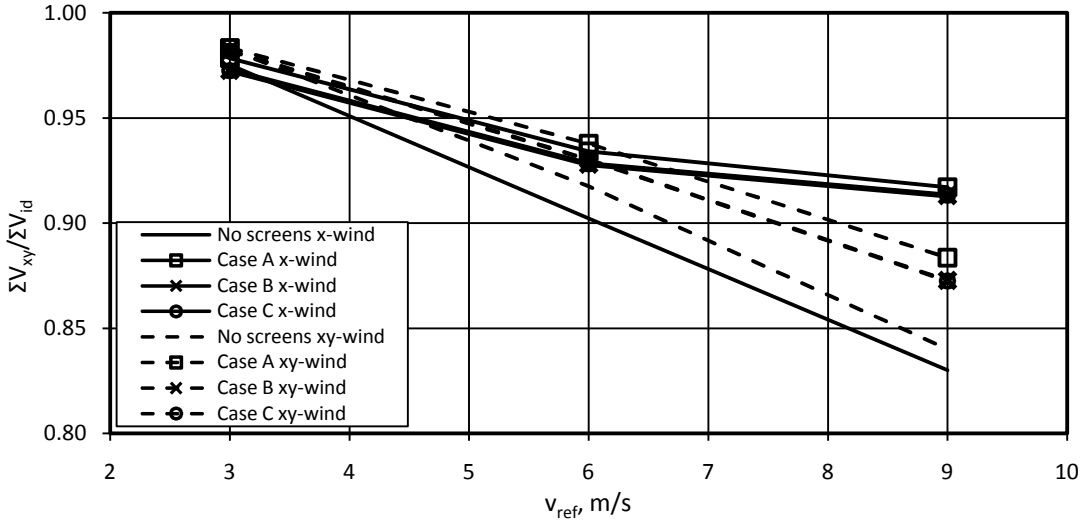

Figure 7. 5: System volumetric effectiveness as a function of screen configuration (1st set), wind direction and wind speed.

Figure 7.6 compares the individual fan performance of Case A with the generic ACSC (no screen) with v_{ref} = 9 m/s for both wind directions. For the x-wind case the volumetric effectiveness of the first three fan rows, i.e. the fans located upwind of the screen in the y-direction, show improvements from the generic case as expected. Although the performance of the fourth fan row (the first fan row downstream of the screens) is lower than the third row it is still improved from the generic case and only the middle four fans in the last fan row do not show improvements over the generic case. This is attributed to the fact that due to the screens blocking the airflow from the upwind side of the ACSC that normally feeds into these fans, air has to be drawn from the downwind side of the ACSC as shown in the vector plots of figure 7.3 (b) which sections fan (5,4). This results in the same separation losses for these fans normally associated with the upwind fans but to a lesser degree as indicated by the contours of pressure at the bellmouth inlets shown in figure 7.7 (c) as well as from the pressure contours of figure 7.2 (b).

For the case of the xy-wind the benefit of adding screens are most visible for the nine fans upwind of the screens located in the corner of the ACSC facing the wind, however the fans on the diagonally opposite corner of the ACSC show marked reductions in volumetric effectiveness (fans (4,y_{5-6}) and fans (5,y_{4-6})) compared to the generic case. As in the case of the x-wind this is again caused by separation at the ACSC inlet and distorted flow conditions at the bellmouth inlets as air has to be draw in from the sides of the ACSC but in the case of the xy-wind more fans are affected as indicated by figure 7.7 (d).

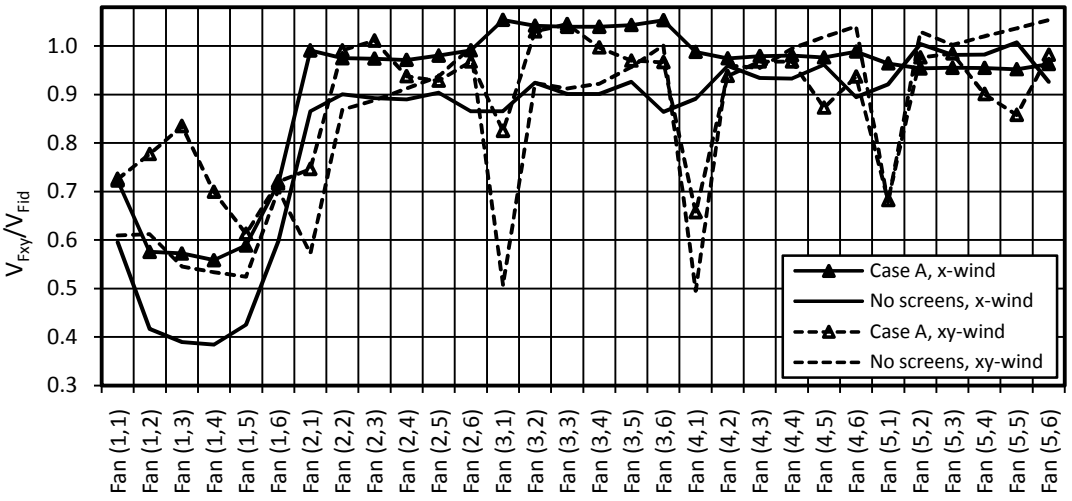

Figure 7. 6: Individual fan volumetric effectiveness with (as per Case A) and without screens for v_{ref} = 9m/s and both wind directions.

The system thermal effectiveness shown in figure 7.8 indicates that the performance increases are less wind direction dependant compared to the volumetric effectiveness due to increased levels of hot plume air recirculation mitigating the benefits of increased fan performance achieved for the x-wind case.

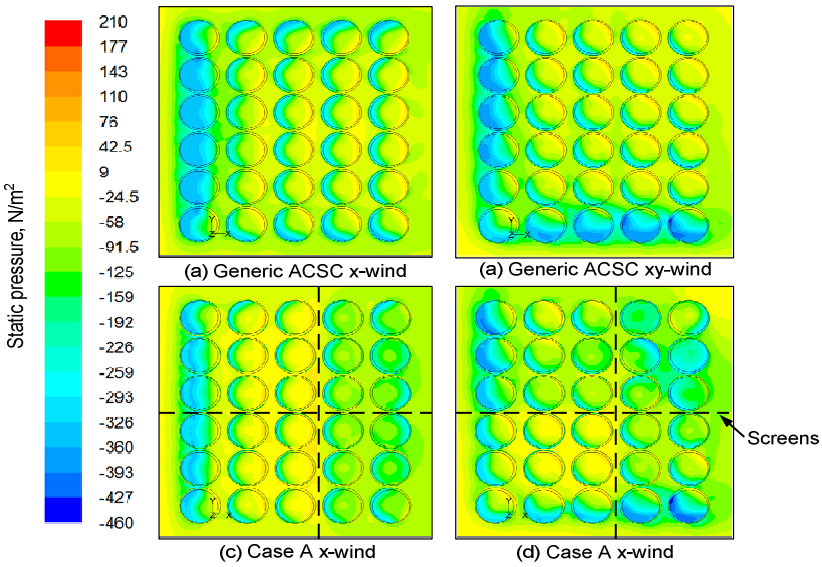

Figure 7. 7: Contours of static pressure in plane of bellmouth inlets showing screen and wind direction effects, v_{ref} = 9 m/s.

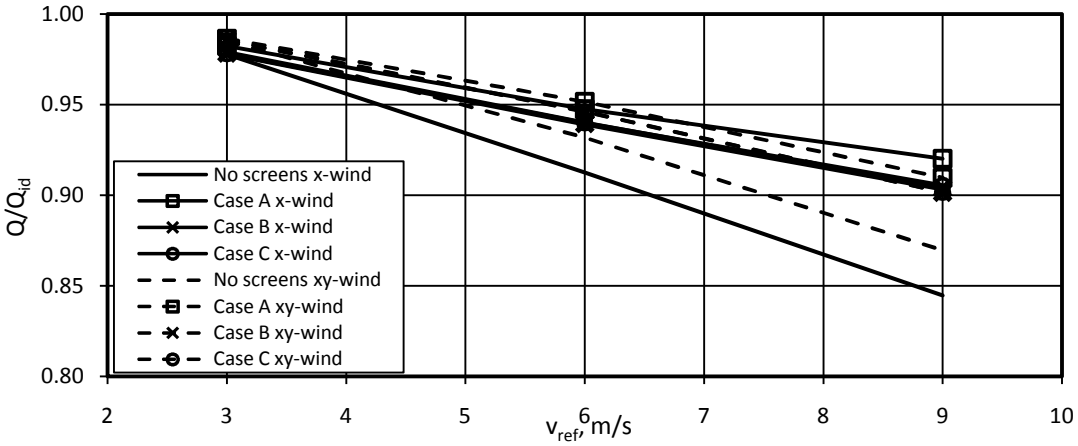

Figure 7. 8: System thermal effectiveness as a function of screen configuration (1st set), wind direction and wind speed.

As Case A presents the best screen configuration it is used as a benchmark for a second series of screen configurations obtained by sequentially removing the screen from the topmost panel as detailed in figure 7.9. The system volumetric effectiveness's for the resulting combinations are given in figure 7.10 for the x-wind. Case A is seen to still be the best performing screen combination, however the difference in performance between Case A and the next best performing combination, which is both Case D and Case E, is very slight and considering that both Case D and E require 25% less screen material than Case A might culminate in these configurations being more cost effective. Continuing with this analysis it can be seen that the screen configurations that specify screens for only the bottom two panels (Case F and G) still perform well compared to the previously discussed combinations with Case G showing superior performance at higher wind velocities compared to Case F. Again Case F and G might provide a better return in investment considering the reduced size of the screens.

Case H shows the least, but still noteworthy, improvement in system volumetric effectiveness. These trends are found to be similar for the system thermal effectiveness as well as for the xy-wind and are therefore not shown here.

Panel height	Case A	Case D	Case E	Case F	Case G	Case H
20m	55% Closed	Open	Open	Open	Open	Open
15m	65% Closed	65% Closed	65% Closed	Open	Open	Open
10m	65% Closed	65% Closed	Closed	65% Closed	Closed	Open
5m	Closed	Closed	Closed	Closed	Closed	Closed

Figure 7. 9: Second set of screen combinations.

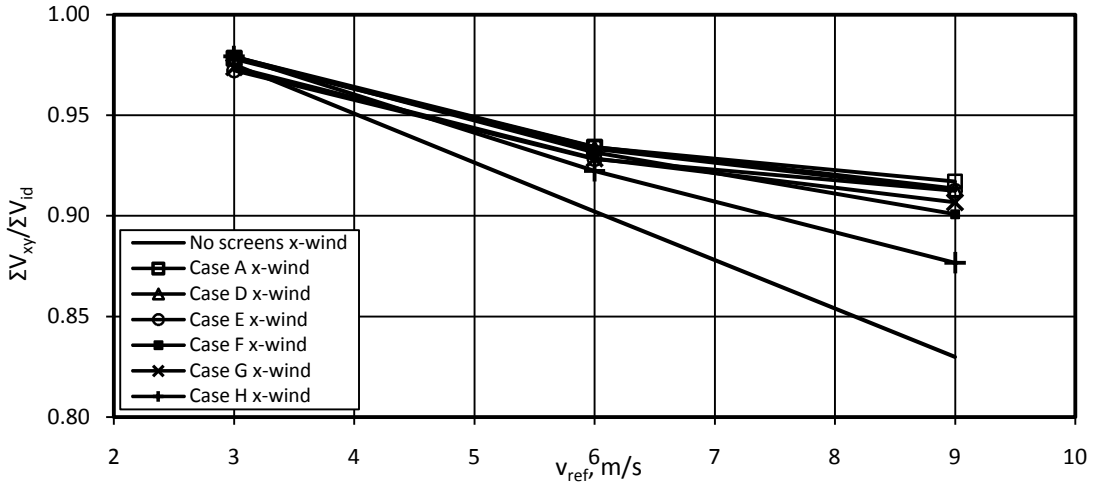

Figure 7. 10: System volumetric effectiveness as a function of screen configuration (2nd set) and wind direction.

A third series of configurations are examined by again using Case A as a starting point and modifying the screens as shown in figure 7.11:

Panel height	Case A	Case I	Case J
20m	55% Closed	55% Closed	55% Closed
15m	65% Closed	65% Closed	55% Closed
10m	65% Closed	65% Closed	55% Closed
5m	Closed	65% Closed	55% Closed

Figure 7. 11: Third set of screen combinations.

The thermal effectiveness for the screen configurations of figure 7.11 are shown in figure 7.12 and it can be seen that Case I slightly outperforms Case A for v_{ref}= 9 m/s for an x-wind but figure 7.13 shows that when the effects of recirculation are excluded and only fan

performance improvements are considered, Case A still presents the best case. For the xy-wind it is found that both the volumetric and thermal effectiveness are similar for Case A and Case I.

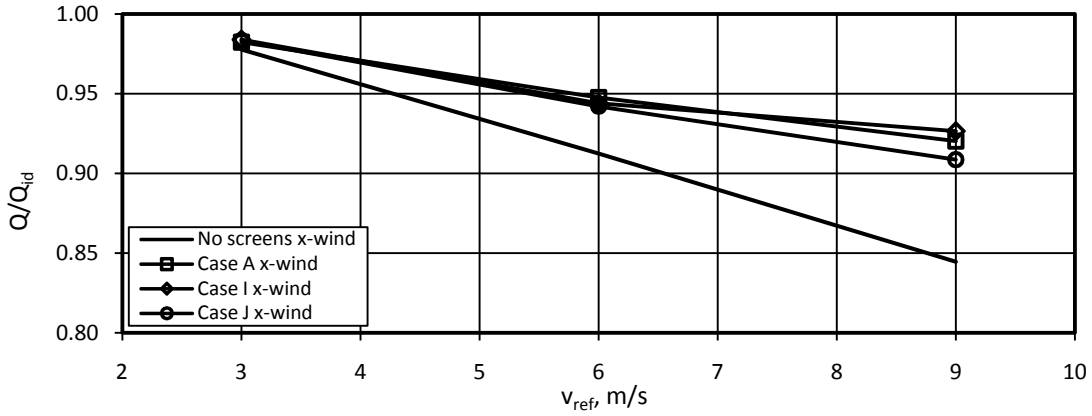

Figure 7. 12: System thermal effectiveness as a function of screen configuration (3rd set) and wind direction.

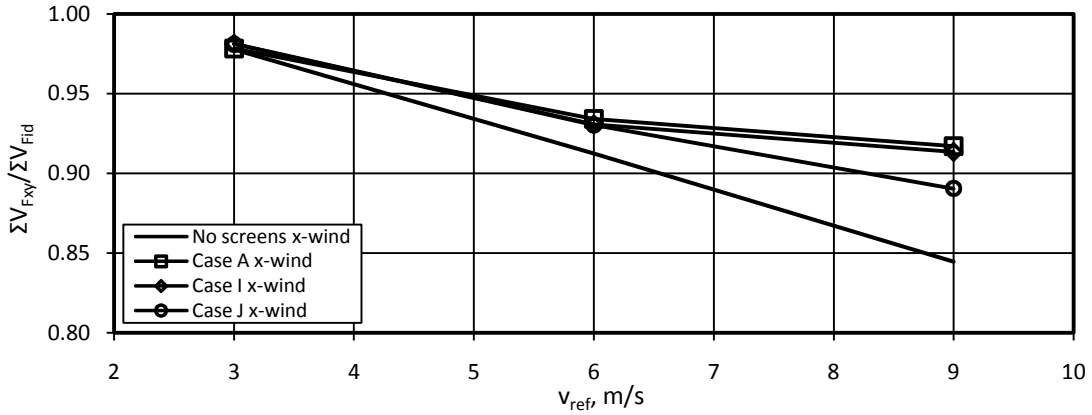

Figure 7. 13: System volumetric effectiveness as a function of screen configuration (3rd set) and wind direction.

The examination of screen effects on ACSC performance is expanded by considering the effect of screen location. This is accomplished by moving the screens that are parallel to the y-axis, which up to this point have been located between the third and fourth fan rows as per figure 7.1, to new positions as shown in figure 7.14 below. The screens parallel to the x-axis remain in the middle of the ACSC and the new screen locations are modeled with three reference wind speeds (v_{ref} = 3 m/s, 6 m/s and 9 m/s as per equation (2.3)) for only the x-wind.

Instead of modeling the whole spectrum of configurations examined thus far only two screen configurations are selected and specified at the new locations. The first is the configuration given by Case A in figure 7.4 since it shows the best volumetric improvements of all the configurations. The second is Case G (figure 7.9) since it is considered to be a good trade-off between cost and improved performance and from a practical point of view Case G is an attractive configuration in that it can be constructed from any solid material and should essentially be maintenance free as opposed to installing screens which are subject to aging,

fouling and tearing that could affect the resistance of the screen over time and hence the performance of the ACSC.

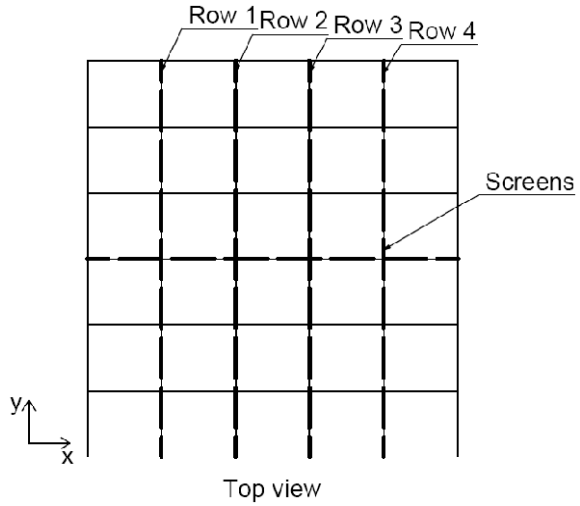

Figure 7. 14: Locations of screens as part of location effect study.

The thermal effectiveness for the various screen locations are shown in figure 7.15 and shows that the screens are most effective when located towards the rear of the ACSC with the screen located at Row 4 showing the greatest performance improvements. Figure 7.16 (a) shows the contours of pressure under the ACSC for this case. The screens located towards the front of the ACSC are seen to reduce performance as it is found that the screens block the airflow to the downstream fans leading to a large low pressure zone underneath the ACSC as shown in figure 7.16 (b).

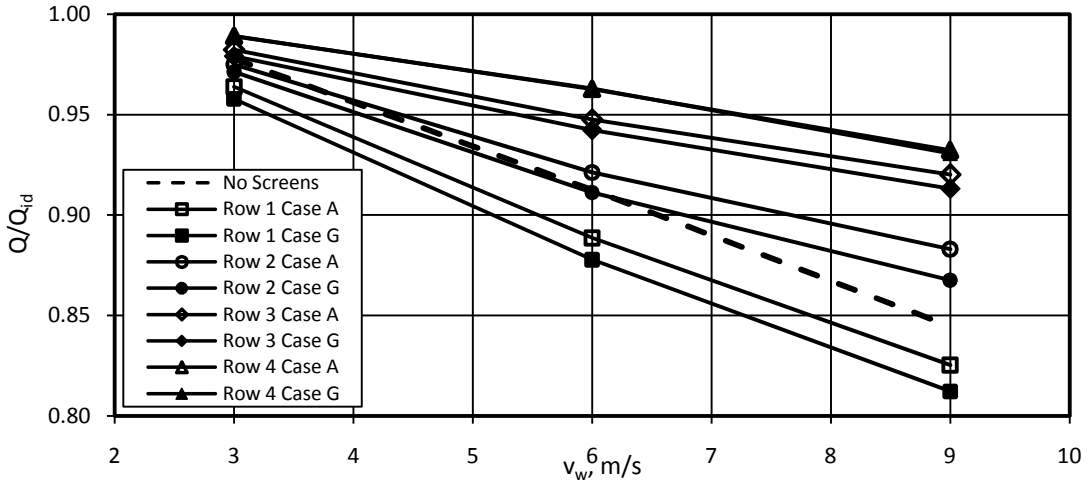

Figure 7. 15: System thermal effectiveness as a function screen configuration, screen location and wind speed.

With the screens located in row 4 it can be seen from figure 7.15 that the screen configuration does not affect the system performance with both cases having identical performance however Case A results in better performance for the other locations. Lastly it should be noted

that although the screens located at row 4 result in considerable system performance improvements, especially at high wind speed, should the wind direction reverse and blow in the negative x-direction the situation will be exactly that of row 1 which will then result in reduced performance. Thus it is recommended that the screens should be located in such a way as to minimise performance fluctuation resulting from wind direction changes.

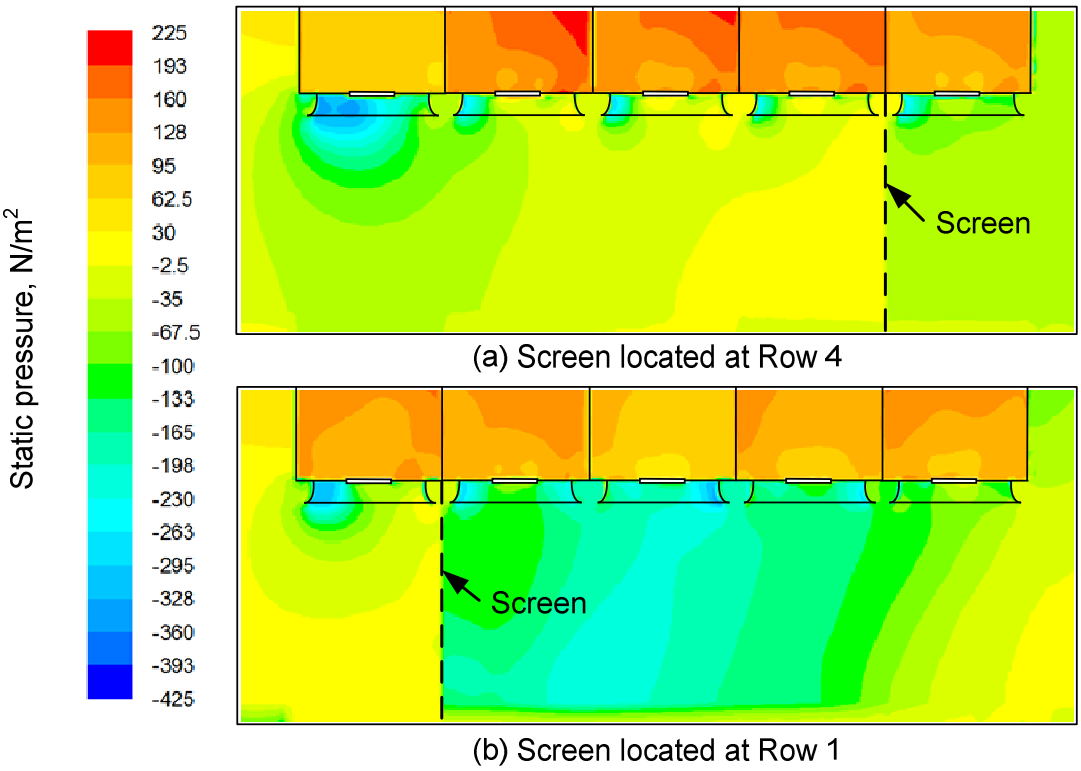

Figure 7. 16: Contours of pressure on section through fan ($x_{1\text{-}5}$,4) showing the effect of screen location for Case A, v_{ref} = 9m/s x-wind.

8. Effect of bellmouth fan inlets

The results and discussion presented in this report thus far identified separation at the bellmouth fan inlet as a major contributor to reduced fan performance and consequently ACSC performance. In the numerical study on the effect of inlet flow distortions on forced draught air-cooled heat exchanger performance Meyer (2005) suggests that the presence of the bellmouths at the periphery fans lead to separation and recirculation in the bellmouth and shows that removing the bellmouth fan inlet of the periphery fans improve system performance.

This section explores this concept by modelling the generic ACSC with the bellmouths removed from the periphery fans as well as having the bellmouths removed from all the fans. Figure 8.1 details the geometry of the numerical fan unit with and without the bellmouth fan inlet and shows the dimension of the fan casing that remains after the bellmouth has been removed.

A theoretical analysis of an ACSC with the bellmouth fan inlet removed requires the addition of a further inlet loss to the effective system resistance and this was found by Duvenhage et al. (1996) to result in a 5% reduction in fan static pressure. However it was found in the current work that adjusting the system resistance with an inlet shroud loss coefficient, K_{Fsi} = 0.9 as suggested by Kröger (2004), resulted in unrealistically high reduction in fan performance since the numerical model accounts for the additional losses as it incorporates the presence of increased flow distortion at the fan inlet resulting from the removal of the bellmouth. Thus including a loss coefficient on top of the actual flow losses present in the model is doubling the effect of removing the bellmouth. Thus the generic ACSC is modelled by simply removing the bellmouth inlets without adjusting either the fan pressure or system resistance. The modified ACSC is modeled with three reference wind speeds (v_{ref} = 3 m/s, 6 m/s and 9 m/s as per equation (2.3)) for both the x- and xy-wind direction.

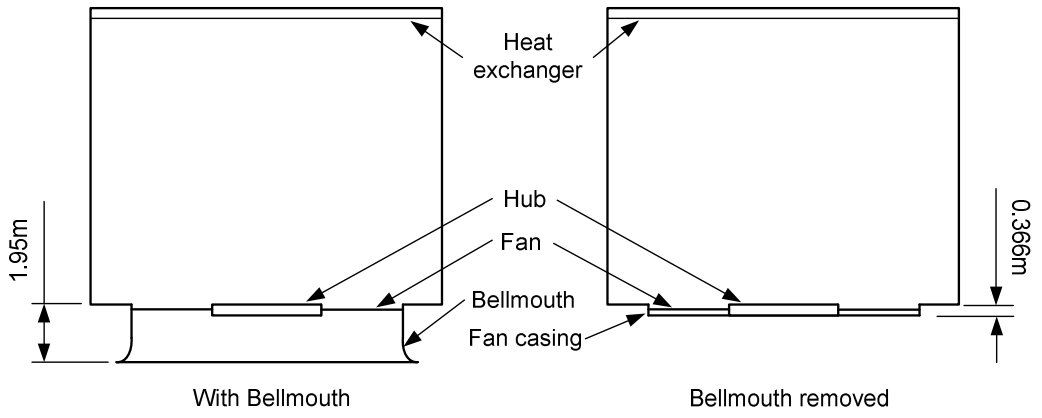

Figure 8. 1: Details of the numerical fan unit with and without a bellmouth fan inlet.

The system thermal effectiveness is shown in figure 8.2 and figure 8.3 for the x- and xy-wind respectively and shows the trends to be similar for both wind directions. It can be seen that removing the bellmouths for the periphery fans does not lead to increased system performance as found by Meyer (2005). Possible reasons for the difference in the results could

stem from the fact that Meyer (2005) used the actuator disk model to model the fans, that only a two fans were modeled representing a four fan row located in the middle of a long ACSC instead of modeling a complete ACSC and perhaps most importantly that Meyer (2005) did not include wind effects. The reduction in performance caused by removing the periphery bellmouths is very slight and at high wind speeds the performance is nearly identical to the generic ACSC. Removing all the bellmouth inlets result in reduced system performance which is slightly more pronounced at low wind speeds.

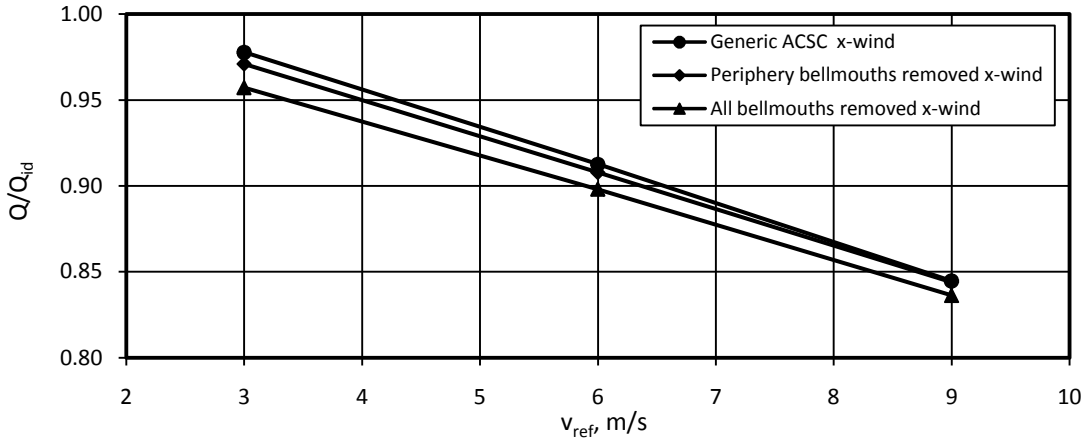

Figure 8. 2: System thermal effectiveness as a function of bellmouth configuration and wind speed, x-wind.

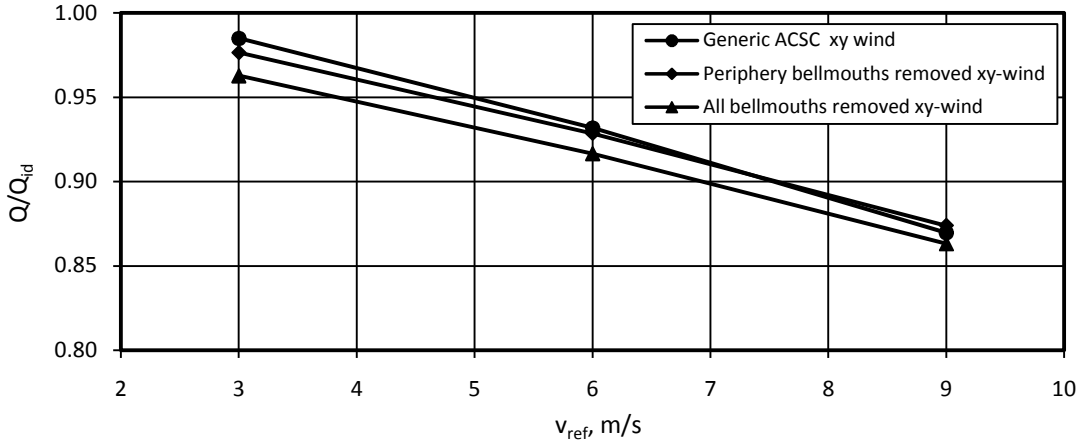

Figure 8. 3: System thermal effectiveness as a function of bellmouth configuration and wind speed, xy-wind.

Figure 8.4 presents the individual fan volumetric effectiveness for the v_{ref} = 9/ms x-wind and it can be seen that the upstream periphery fans benefit the most from the removal of the bellmouths with the periphery bellmouth removed case experiencing the greatest performance improvement for these fans. Figure 8.5 shows contours of static pressure on a section view of the ACSC parallel to the x-wind through fan (1,4) and it can be seen that removing the bellmouth from the leading edge fan moves the area of separation from the bellmouth edge to the upstream edge of the ACCS and results in a smaller and less severe low

pressure area under the leading edge fan resulting in reduced flow losses and increased fan performance. It is also found that for the case of removing the bellmouth from only the periphery fan that the remaining downstream bellmouths block the flow benefitting the fan upstream with the removed bellmouth. This explains the difference in fan performance of the first row of fans (figure 8.4) between the two modified cases.

This situation is reversed for the second fan row where the fans for the case where the periphery bellmouths are removed exhibit the worst performance followed by the case where all the bellmouths are removed and the generic case shows the best performance for this row. Comparing figure 8.5 (a) and (b) it can seen that the separation at the bellmouth of the second fan row is more pronounced for the case where the periphery bellmouths are removed which explains the reduced performance. The increased separation is caused by the flow having to flow down and around the bellmouth in (b) whereas the upstream bellmouth present in (a) results in better aligned flow for the second bellmouth. In effect what is gained in performance on the first fan row is lost again on the second when comparing these two cases, resulting in similar system performance.

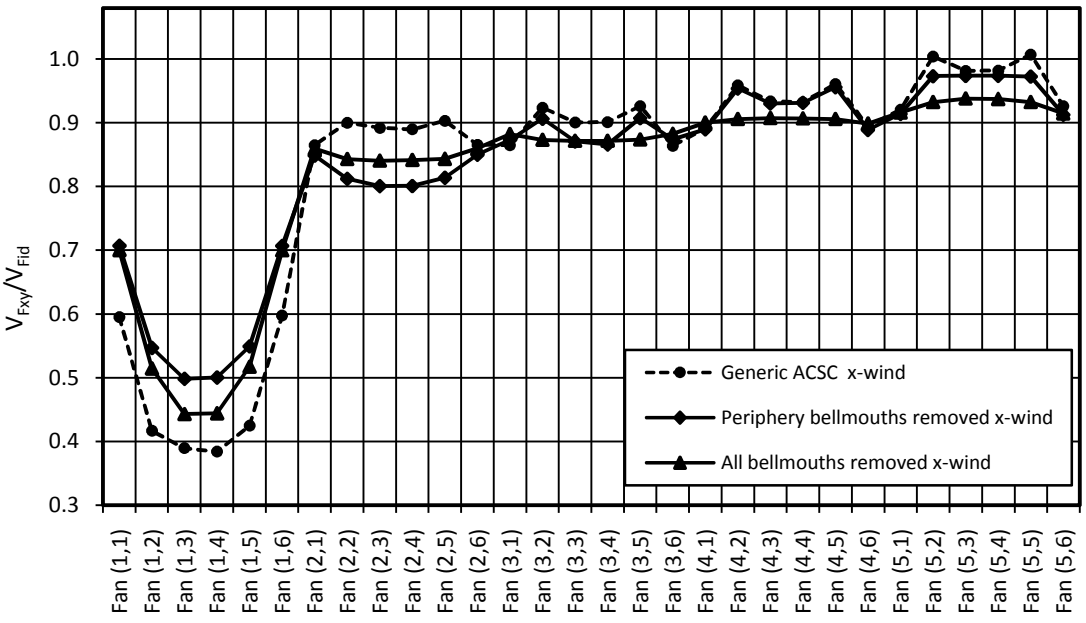

Figure 8. 4: Individual fan volumetric effectiveness for various bellmouth configurations, v_{ref} = 9m/s x-wind.

It can be seen in figure 8.5 (c) that removing all the bellmouth inlets rid the fans of the low pressure areas caused by separation at the fan inlets, with the upstream periphery fan being the obvious exception due to the separation at the leading edge of the ACSC. However as seen in figure 8.1 the absence of the separation zones does not translate to improved fan performance as the off axial flow conditions at the fan face, as shown for fan (4,4) and (4.5) in figure 8.6, impede fan performance as described in section 3.3.4. This observation emphasises

the contribution of off-axial flow conditions at the fan inlets to reduced fan performance and demonstrates the flow straightening benefit of the bellmouth inlet.

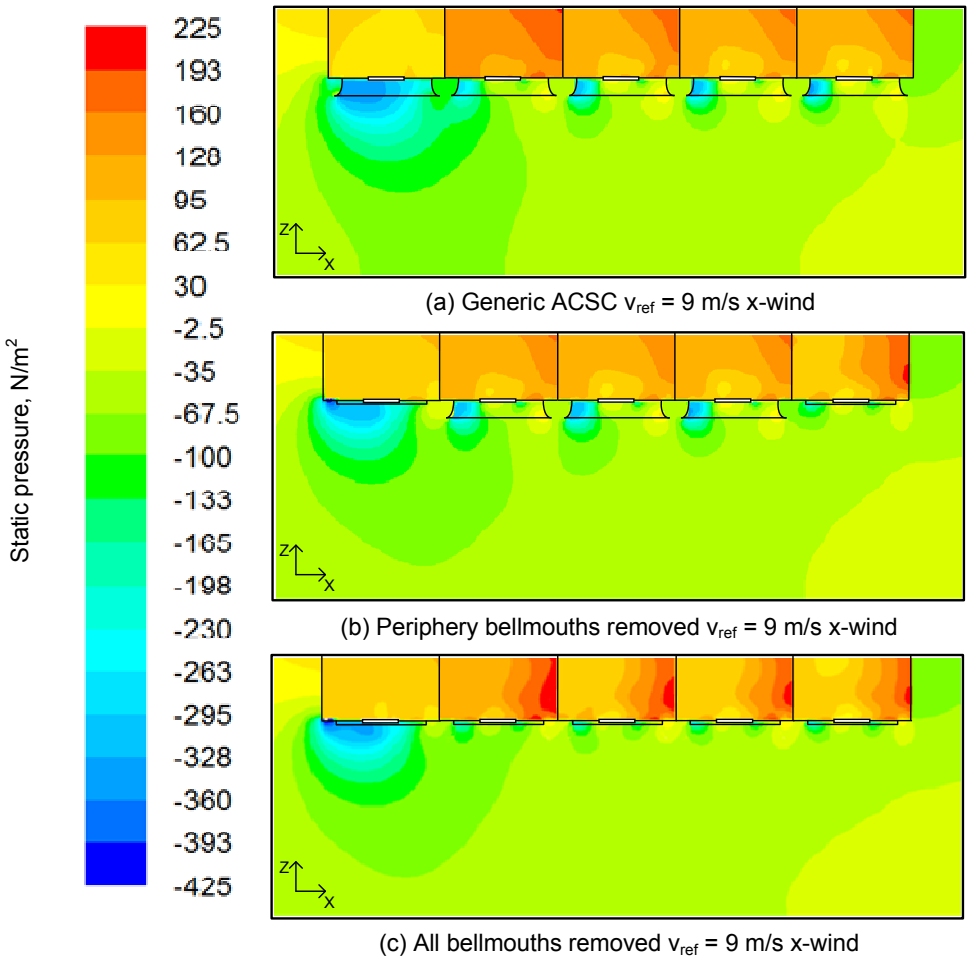

(a) Generic ACSC v_{ref} = 9 m/s x-wind

(b) Periphery bellmouths removed v_{ref} = 9 m/s x-wind

(c) All bellmouths removed v_{ref} = 9 m/s x-wind

Figure 8. 5: Contours of pressure on section through fan ($x_{1\text{-}5}$,4) for the various bellmouth inlet configurations.

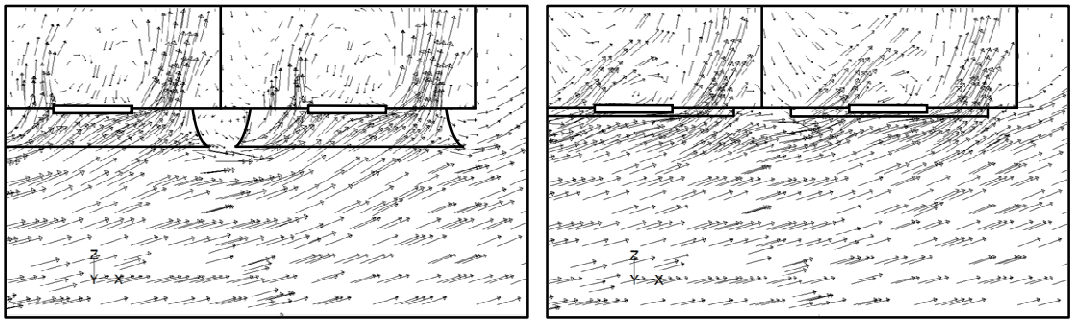

(a) Generic ACSC v_{ref} = 9 m/s x-wind

(b) All bellmouths removed v_{ref} = 9 m/s x-wind

Figure 8. 6: Velocity vectors through fan (4,4) and fan (5,4) with and without bellmouths.

9. Effect of fan type

In previous studies it was noted that the type of fan utilized in an ACSC operating under non-ideal conditions affects the system performance with certain fans being less sensitive to distorted flow conditions than others (Duvenhage et al. (1996), Bredell et al. (2006)). Figure 9.1 shows the fan curves for two arbitrary fans which intersect the effective system resistance curve at the same point, which represents the operating point under ideal conditions, V_{id}. This implies that both the fans will have the same flow rate under ideal flow conditions. Additional flow losses will result in a shift in the system resistance curve by δp_i which is assumed to be constant for the purposes of this simplified discussion. The fans will then operate at the intersection with the new system resistance curve at volumetric flow rates V_1 and V_2 for the respective fans and it can be seen that the changes in volumetric flow rate, δV_1 and δV_2, is determined by the gradient of the fan curve. With a steeper curve Fan 2 experiences a smaller performance reduction than Fan 1 when operating under non-ideal conditions and is therefore better suited to ACSC applications where distorted flow conditions are expected.

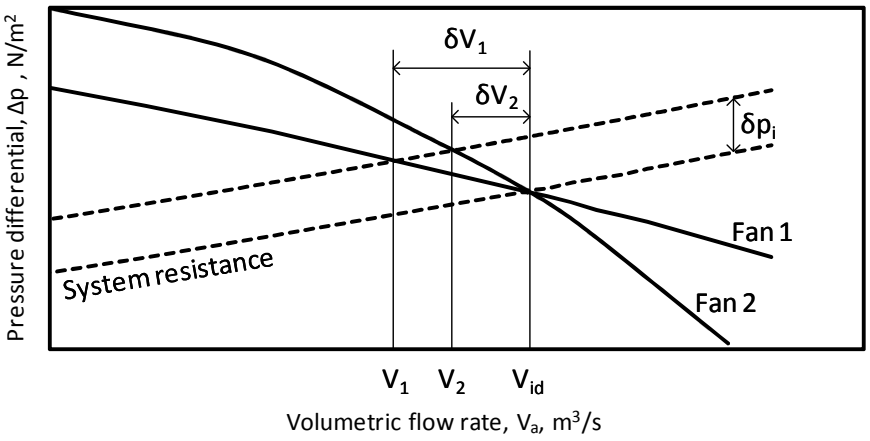

Figure 9. 1: Effect of inlet flow distortion on the volumetric flow rates of two arbitrary fans.

To examine the effect of different types of fans on ACSC performance the generic ACSC is modeled, in addition to the B-fan, with two types of fans called the L-fan and N-fan as described in table 9.1 and shown schematically in figure 9.2. The various fan total to static pressure curves are given in figure 9.3. and it can be seen that the L-fan has the steepest curve at flow rates less than the ideal flow rate (i.e. the point of intersection) whilst the B-fan has the steepest curve at flow rates higher than the operating point. The N-fan has the flattest curve for the complete range of flow rates.

Table 9. 1: Fan information of B-, L- and N-fans.

	B-fan	L-fan	N-fan
Diameter, d_F	9.145m	9.145m	9.145m
Number of blades, n_{FB}	8	8	8
Hub-tip ratio, d_h/d_F	0.4	0.153	0.153
Rotational speed, N	125 rpm	125 rpm	125 rpm

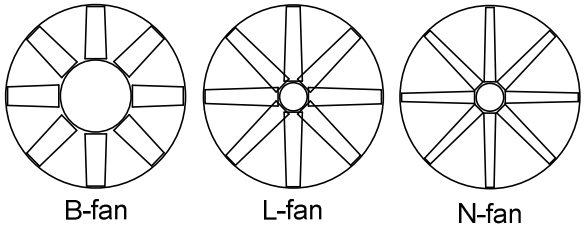

Figure 9. 2: Schematic of B-, L- and N-fans.

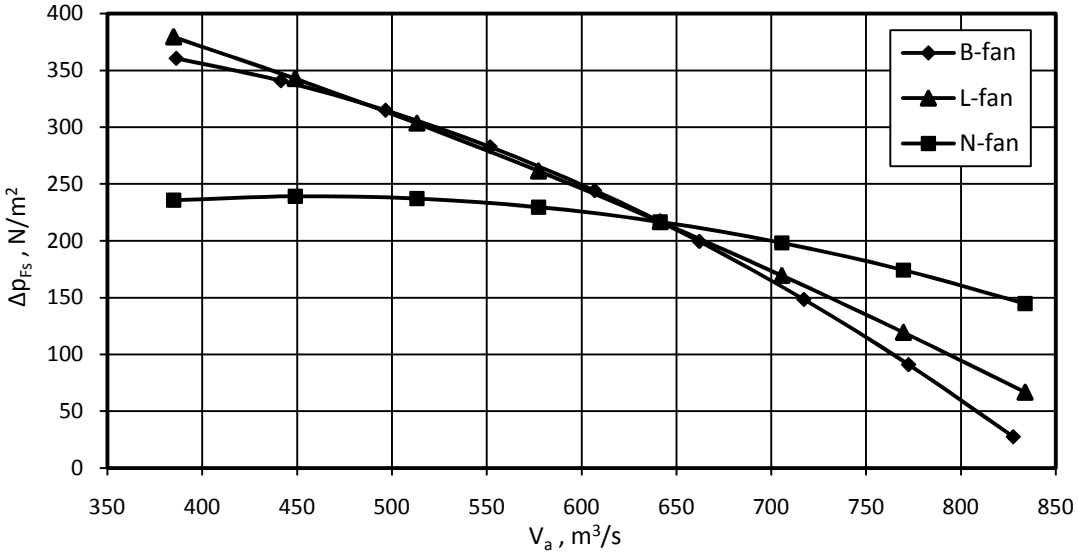

Figure 9. 3: Static pressure curves of B-, L- and N-fans.

The generic ACSC with the different types of fans is modeled with three reference wind speeds (v_{ref} = 3 m/s, 6 m/s and 9 m/s as per equation (2.3)) for both the x- and xy-wind direction. The system volumetric effectiveness is shown in figures 9.4 and 9.5 for the x- and xy-wind respectively and it can be seen that regardless of wind direction the L-fan performs the best, followed by the B-fan, while the N-fan shows the worst performance. Owing to the slight difference in fan curve gradient the performance of the B- and L-fan is relatively close, however the N-fan shows considerably reduced performance due to its flat fan curve.

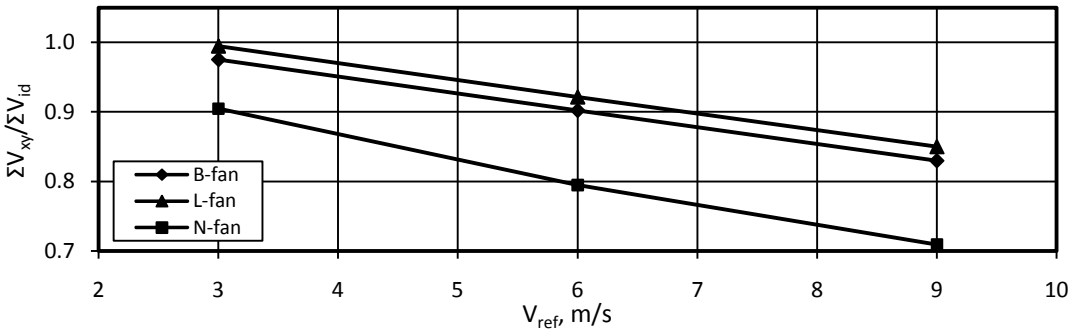

Figure 9. 4: System volumetric effectiveness as function of fan type and wind speed, x-wind.

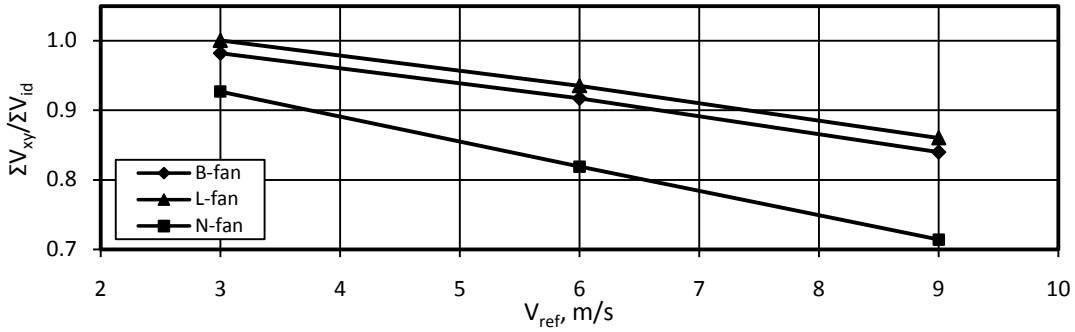

Figure 9. 5: System volumetric effectiveness as function of fan type and wind speed, xy-wind.

The system thermal effectiveness is shown in figures 9.6 and 9.7 and follows the same trends as the volumetric effectiveness.

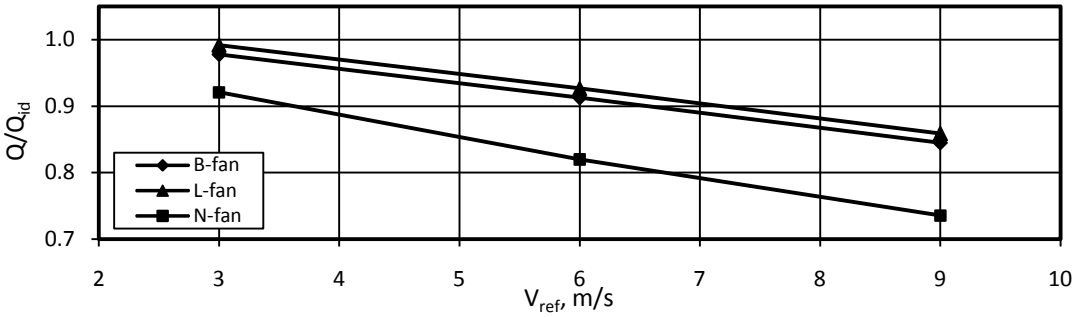

Figure 9. 6: System thermal effectiveness as function of fan type and wind speed, x-wind.

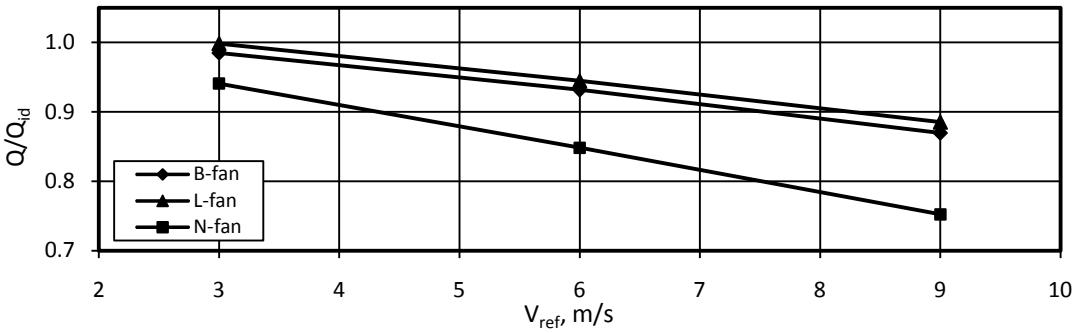

Figure 9. 7: System thermal effectiveness as function of fan type and wind speed, xy-wind.

It must be kept in mind that when specifying a fan for use in an ACSC the steepness of the fan pressure curve is by no means the only consideration and other factors, for example fan power requirements, must also be taken into account.

10. Effect of fan power variation.

It is suggested by Liu et al. (2009) that increasing the rotational speed of the periphery fans improves the performance of the ACSC by mitigating performance reductions resulting from hot air recirculation. In the study the increase in rotational speed is modeled as increased inlet and exit velocities since neither the fans nor the internal flow in the ACSC is modeled. The increased exit velocity at the top of the ACSC results in an increased jetting effect where the flow has more momentum and is less susceptible to directional changes and as expected this results in less plume air being drawn back into the ACSC.

This concept has further merit during periods of high wind where supplying additional power to the fans, resulting in increased rotational speed as per the study by Liu et al. (2009), would result in increased air mass flow rates and increased ACSC performance that could reduce the danger of turbine trips.

To study the effect of increased fan power on ACSC performance the power of the fans in the generic ACSC is increased by 5%, 10% and 20% by using the fan laws to adjust the B-fan static pressure curve, resulting in fan rotational speeds of 127, 129 and 132.8 rpm respectively. The ACSC is modeled with three reference wind speeds (v_{ref} = 3 m/s, 6 m/s and 9 m/s as per equation (2.3)) for both the x- and xy-wind direction. Furthermore the power increases are applied in two cases, to just the 18 periphery and also to all 30 fans. The system performance results are calculated using the unadjusted ideal mass flow rate as given in section 3.1.

It can be seen in figures 10.1 and 10.2 that the increase in fan power results in the expected increase in system volumetric effectiveness for both wind directions with the relative increases being constant across the range of wind speeds and power increase configurations, i.e. the curves are all parallel to one another. It is found that the difference between increasing the power to all or just the periphery fans is proportional to the number of fans with adjusted performance, i.e. 30 vs 18 fans. It was also found that the increased flow rates from the additional power does not significantly affect the performance of the non-adjusted fans.

Figures 10.3 and 10.4 shows the system thermal effectiveness and the same trends as for the volumetric effectiveness can be seen and this indicates that recirculation effects are not influenced by fan power increases as found by Liu et al. (2009). Figure 10.5 compares the fan inlet temperature for the generic, 10% and 20% fan power increase for the periphery fans and it can be seen that the temperature distribution is nearly identical, confirming that recirculation has neither in- nor decreased by increasing the fan power. Figures 10.6 and 10.7 shows the steam pressure as a function of fan power increase for the two cases examined and exhibits the same trends discussed thus far.

Figure 10.3 can also be used to gain a better appreciation of the sensitivity of the ACSC to wind induced performance reductions where the generic ACSC thermal effectiveness is reduced from 0.978 to 0.845 across the range of the reference velocities studied which do not even represent extremely windy conditions. This 0.133 reduction can be put in context by the fact that a 20% fan power increase for all the fans results in the best thermal performance increase of only 0.045 which occurs at the v_{ref} = 3m/s wind speed.

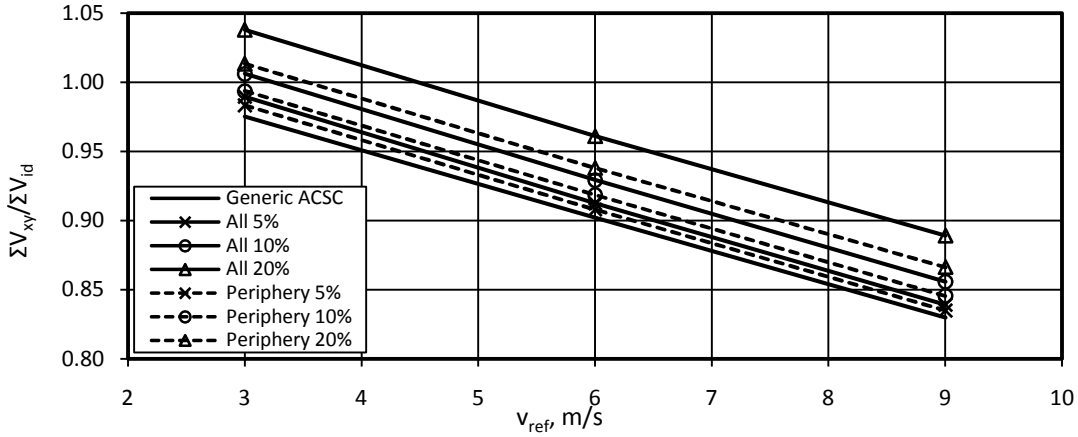

Figure 10. 1: System volumetric effectiveness as function of fan power increase and wind speed, x-wind.

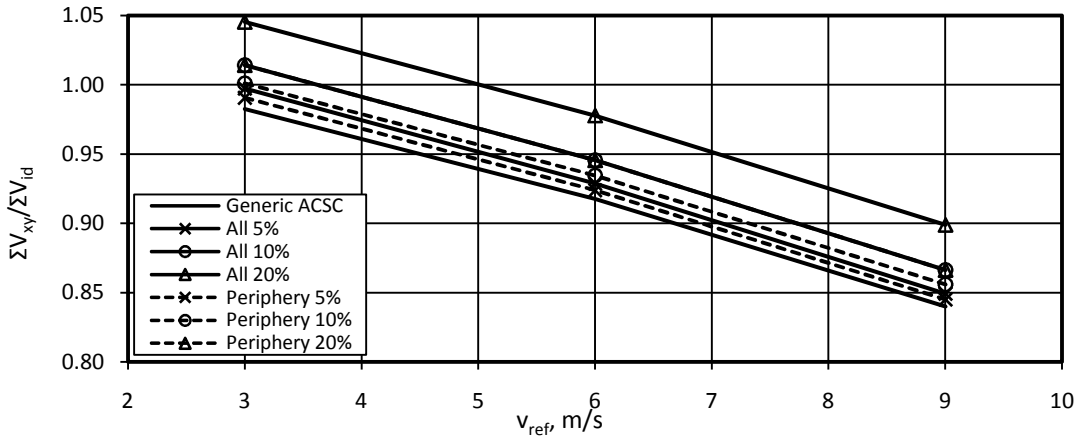

Figure 10. 2: System volumetric effectiveness as function of fan power increase and wind speed, xy-wind.

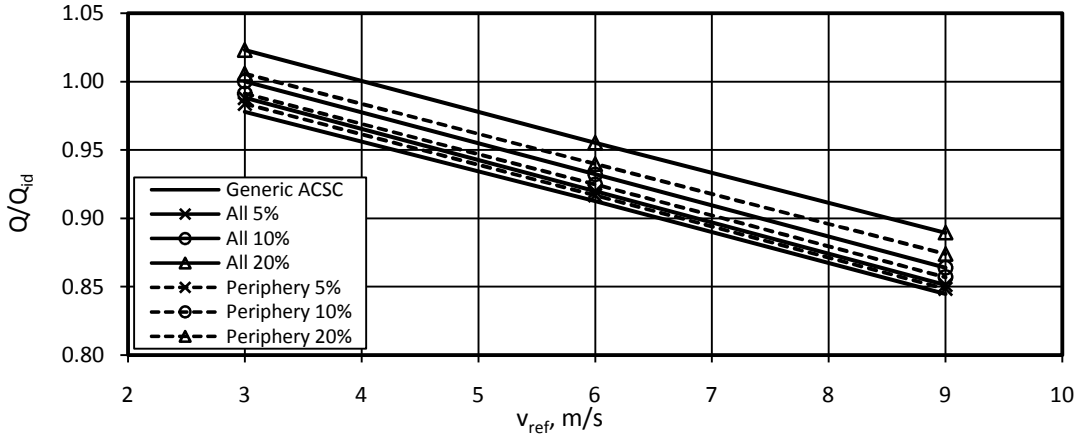

Figure 10. 3: System thermal effectiveness as function of fan power increase and wind speed, x-wind.

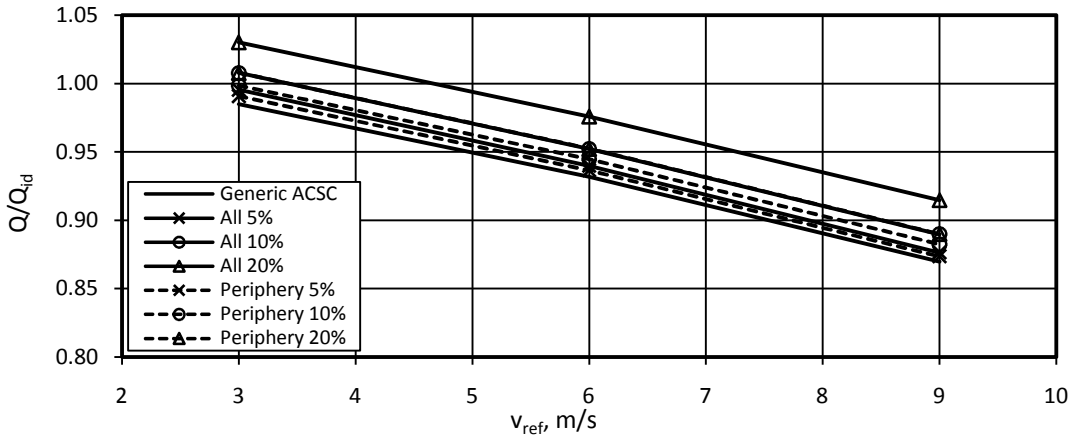

Figure 10. 4: System thermal effectiveness as function of fan power increase and wind speed, xy-wind.

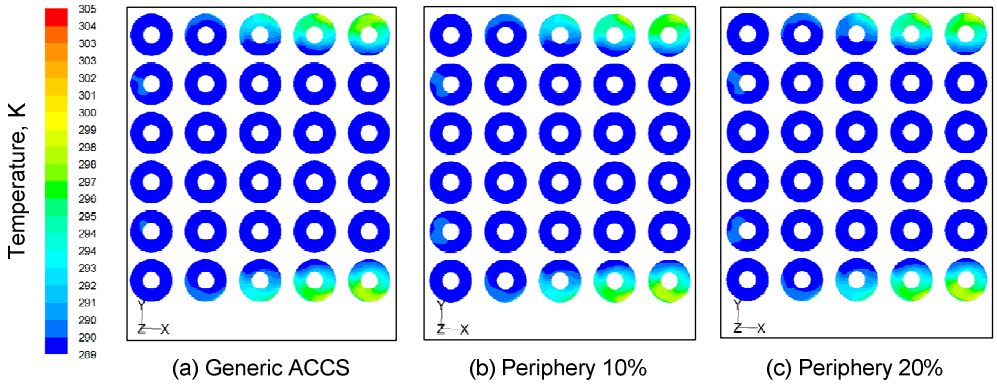

Figure 10. 5: Contours of fan temperature for various cases of fan power increases, v_{ref} = 9m/s x-wind.

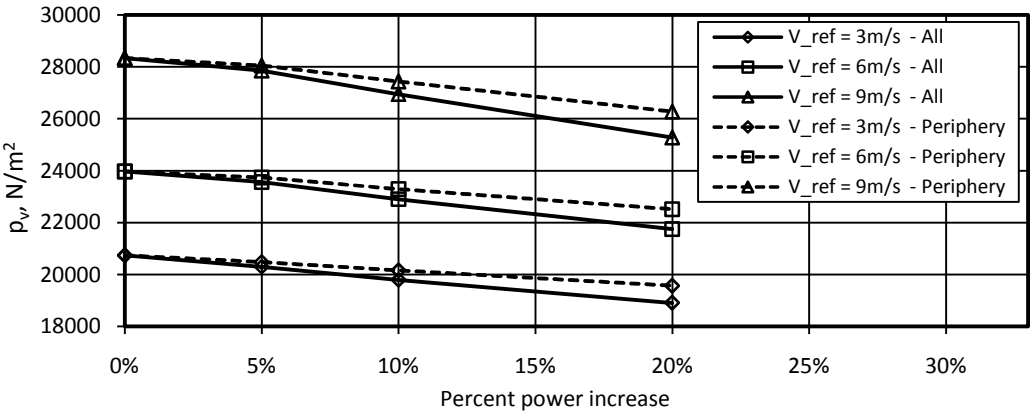

Figure 10. 6: Steam pressure as function of various cases of fan power increases and wind speed, x-wind.

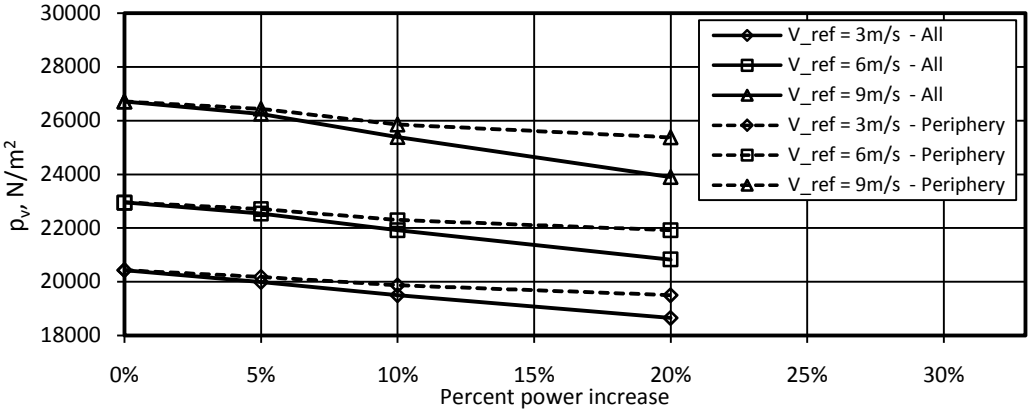

Figure 10. 7: Steam pressure as functions of various cases of fan power increases and wind speed, xy-wind..

Although turbine performance will increase due to the reduced backpressure most of the additional power generated will be required by the fans. In a well designed ACSC the net increase in plant output will be negligible (Owen, 2010).

11. Effect of wind direction.

The effect of wind direction on ACSC performance has thus far been examined throughout the study by modeling two wind directions, namely the x-wind and xy-wind as shown in figure 3.2 and it was found that the x-wind direction results in greater reduction in ACSC performance. The study into wind direction effects is expanded in this section by modeling the generic ACSC with an extended and refined range of wind directions as shown in figure 11.1, where it can be seen that the wind direction is adjusted in 15° increments in an anti-clockwise direction starting from the x-wind at 0°. Consequently the xy-wind represents the 45° wind. Due to symmetry only winds in the first quadrant needs to be examined and the standard three reference wind speeds are modeled (v_{ref} = 3 m/s, 6 m/s and 9 m/s as per equation (2.3)).

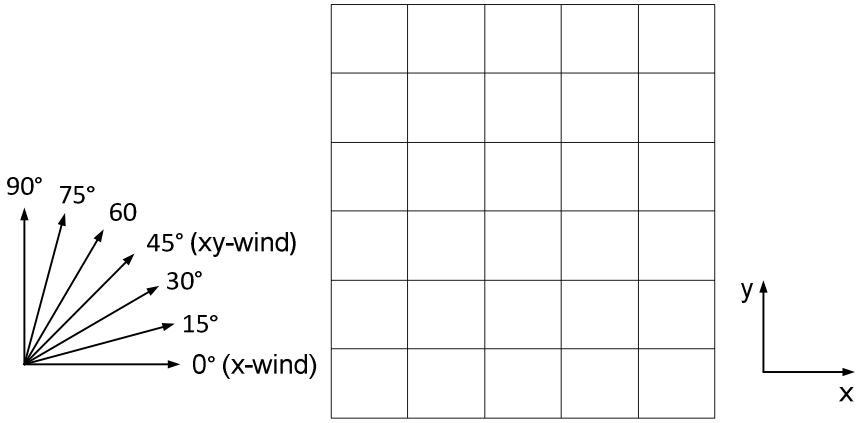

Figure 11. 1: Top view of the generic ACSC with details of wind directions.

The system volumetric effectiveness is shown in figure 11.2 and indicates that the performance gradually improves from the lowest effectiveness at 0° to the highest effectiveness at 90°. This improvement is attributed to the number of upwind periphery fans, for the 0° wind there are 6 upwind fans which have been show in section 3.3 to experience considerable reductions in performance. For the 90° wind there are only 5 upwind fans subjected to similar flow conditions resulting in the slightly better effectiveness. The effect of wind direction on volumetric effectiveness is minor for the low wind speed case (v_{ref} = 3m/s).

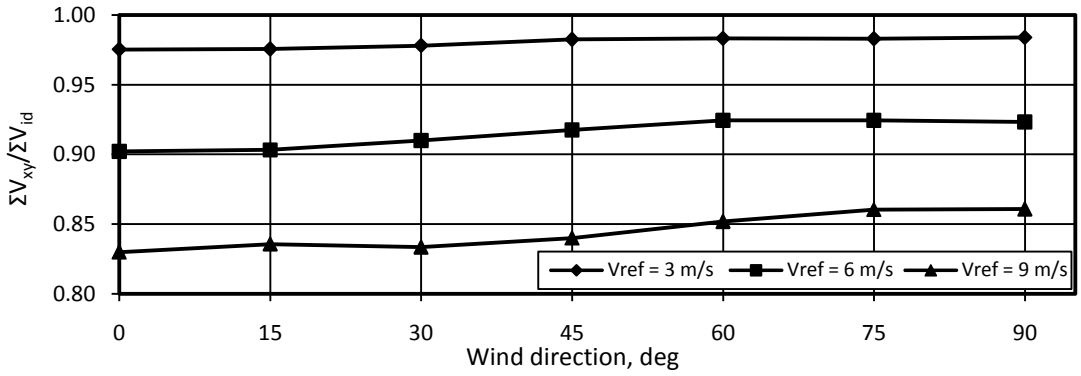

Figure 11. 2: System volumetric effectiveness as a function of wind direction and wind speed.

The system thermal effectiveness is shown in figure 11.3 and follows the same trends as the volumetric effectiveness. The thermal effectiveness is also calculated by setting the fan inlet temperature, T_{Fxy} in equation 3.4, equal to the ambient temperature T_a thereby excluding the effects of recirculation, thus the thermal performance is solely a function of reduced volumetric effectiveness. This is also shown in figure 11.3 and it can be seen that the 45° wind represents the wind direction resulting in the least recirculation whereas the wind directions aligned with the principal axis of the ACSC, namely the 0° and 90° wind, results in the most significant recirculation effects with the 90° wind resulting in slightly greater recirculation than the 0° wind. Section 3.3 showed that recirculation affects the downwind fans located on the sides of the ACSC parallel to the wind direction and for the case of the 90° wind there is one more fan in this direction per side of the ACSC, which increases the potential for recirculation as compared to the case of the 0° wind. This effect is more noticeable at high wind speeds as shown in figure 11.3.

It can also be seen that recirculation is not a factor at the low wind speed case (v_{ref} = 3m/s) and even at higher wind speeds it can be seen that wind induced fan performance reductions contribute considerably more to reduced ACSC thermal performance as compared to both hot plume air recirculation and wind direction effects.

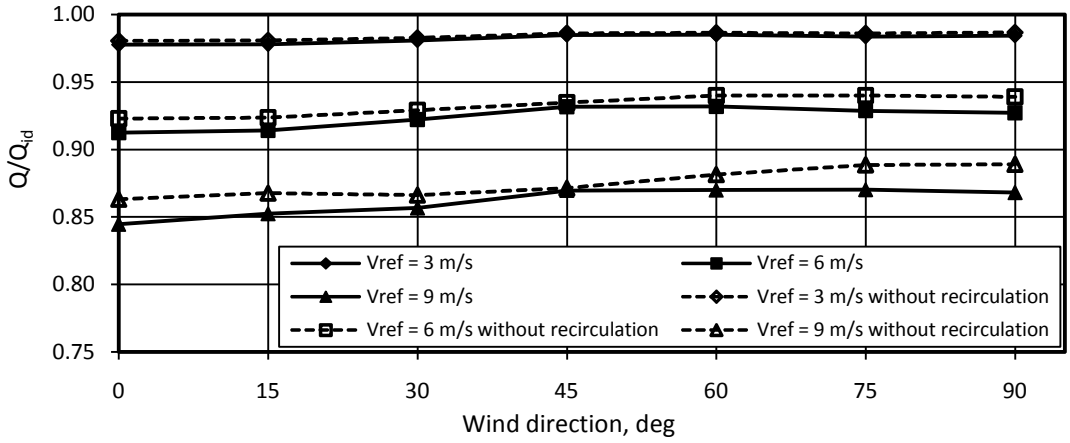

Figure 11. 3: System thermal effectiveness as a function of wind direction and wind speed.

12. Improved generic ACSC

This study examined the effect of a number of parameters on the performance of a generic ACSC and also explored methods of improving ACSC performance under windy conditions. The study would not be complete without selecting the most appropriate modifications and examining the combined improved effect on ACSC performance. One possibility to accomplish this improvement would be to select the best configuration from each previous section and incorporate these changes into the generic ACSC, however this would neither be practical or cost effective. With these considerations in mind the most practical and cost effective methods of improving ACSC performance are deemed to be the addition of wind screens and walkways as shown in figure 12.1.

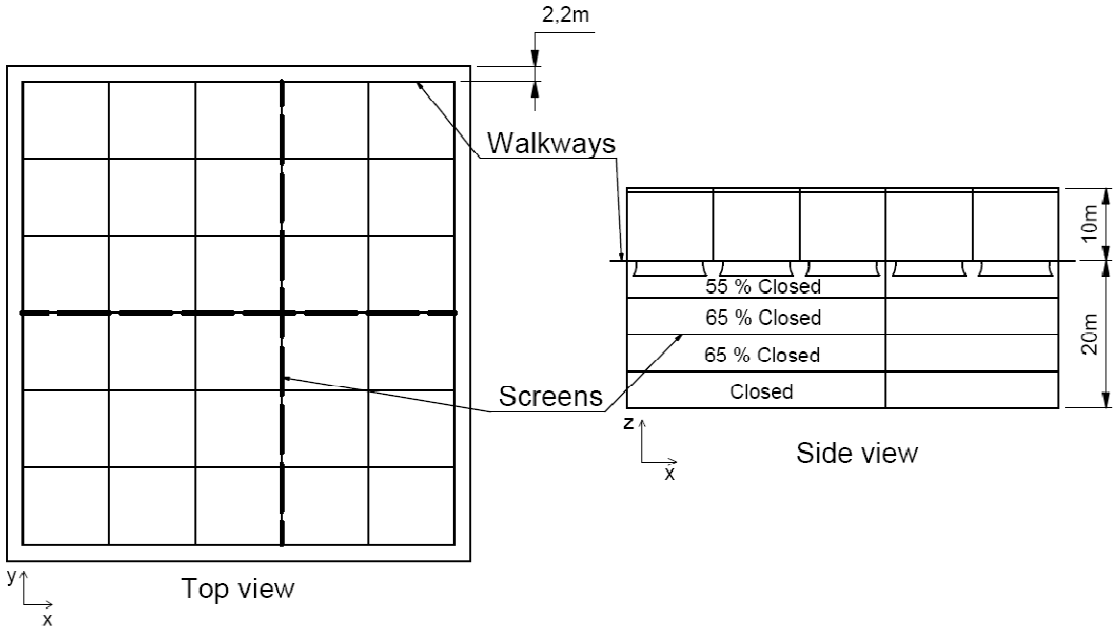

Figure 12. 1: Details of the generic ACSC with additional performance improvements.

The walkways are specified around the periphery of the ACSC with a width of W_w = 2.2 m. The screens are located parallel to the x-axis along the middle of the ACSC and parallel with the y-axis between the third and fourth fan row and configured according to Case A (Section 7) and shown in figure 12.1. Both the platform height and windwall height are kept as per the generic ACSC specifications (namely H_i = 20 m and H_w = 10m respectively) as these values are considered to provide suitable all round results. The B-fan is specified for all 30 fans with no power adjustments and all the fans are fitted with bellmouth inlets. The improved ACSC is modeled for three reference wind speeds (v_{ref} = 3 m/s, 6 m/s and 9 m/s as per equation (2.3)) for both the x- and xy-wind direction.

The system volumetric effectiveness is shown in figure 12.2 and it can be seen that at v_{ref} = 3 m/s the improvements result in the system operating at the design point. At v_{ref} = 9 m/s the systems shows an improvement in volumetric effectiveness of 0.12 for the x-wind and 0.07 for the xy-wind and it is due to the addition of the screens that the volumetric effectiveness is considerably improved for the x-wind.

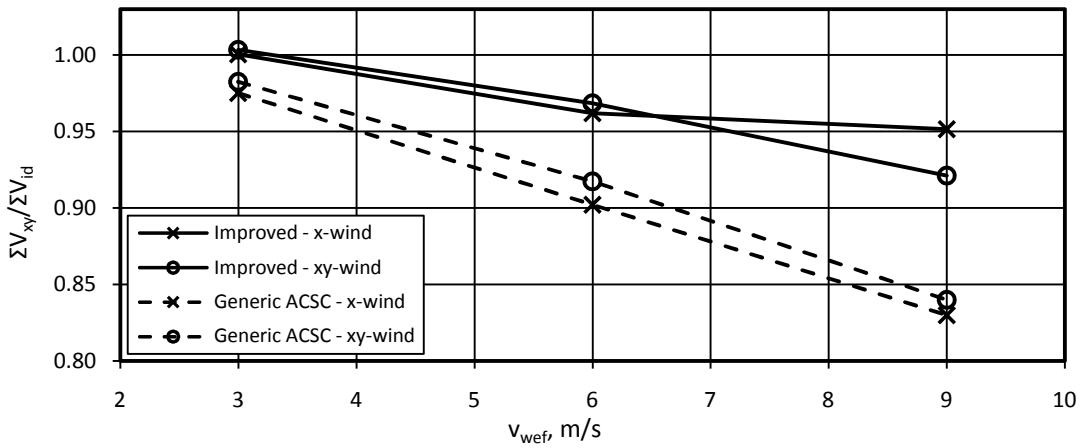

Figure 12. 2: System volumetric effectiveness showing the ACSC performance improvements resulting from the addition of walkways and screens.

The system thermal effectiveness is shown in figure 12.3 and as opposed to the system volumetric effectiveness the results are seen to be largely insensitive to wind direction. This is due to recirculation effects eroding the gains resulting from improvements in volumetric effectiveness for the x-wind. The performance at high wind speeds (v_{ref} = 9 m/s) is seen to have improved considerably and the flatter performance trends indicate that the performance is less sensitive to the detrimental wind effects.

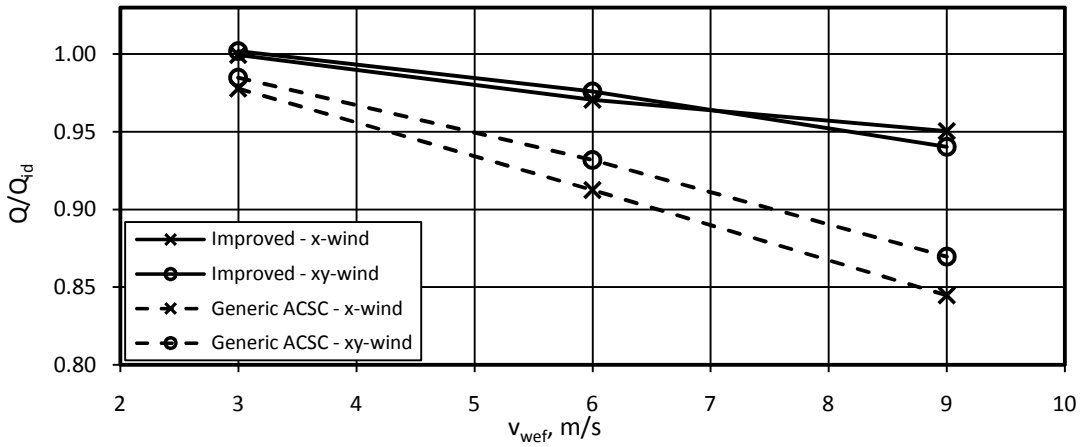

Figure 12. 3: System thermal effectiveness showing the ACSC performance improvements resulting from the addition of walkways and screens.

13. Conclusion.

13.1 Importance of study

The global power generation industry is confronted with growing constraints regarding the use of water. Not only has the cost of water increased drastically in some areas but the increasing stringent terms of water usage lead to additional costs. Traditionally wet cooling systems are responsible for the largest fraction of the water consumption. These systems rely on heat and mass transfer to indirectly (via a secondary cooling loop) condense the turbine exhaust steam. An alternative solution is direct cooling where forced draft air-cooled steam condensers (ACSCs) are used to condense the turbine exhaust steam. Due to very low water consumption such systems have found widespread application in arid areas where insufficient water resources eliminated the possibility of using wet cooling systems. However the global adoption of ACSCs is set to increase due to the previously mentioned rising water costs. Limitations imposed by current and proposed legislation regulating water use will also result in plant designers specifying ACSCs to provide the cooling requirements at many of the world's future power plants.

ACSCs use large axial flow fans to force ambient air through A-frame heat exchanger bundles comprising of a number of externally fined tubes through which the turbine exhaust steam is ducted and consequently condensed during the heat transfer process to the air. The heat rejection rate of an ACSC is proportional to the air mass flow rate and the temperature difference between the finned tubes and the air. Therefore ACSC performance is very sensitive to ambient (e.g. dry bulb temperature, wind etc.) and other (e.g. flow obstructions and distortions) conditions. Steam conditions in the ACSC, determined by ACSC performance, dictates steam conditions at the turbine exhaust resulting in ACSC performance directly impacting power plant output. This requires a fundamental understanding of the factors affecting ACSC performance to ensure adequate heat rejection across a wide range of operating conditions.

13.2 Research findings

The flow through a 30 fan ACSC (termed the generic ACSC) operating under windy conditions was solved using the commercial computational fluid dynamics (CFD) code FLUENT and the required data was extracted from the solution to calculate performance trends. The generic ACSC was then modified to investigate the influence of certain parameters aimed at obtaining optimal ACSC performance.

13.2.1 Generic ACSC performance

The results of the generic ACSC were used to investigate the mechanisms of reduced ACSC performance and these can be separated into factors affecting the air mass flow rate through the fan, or fan performance, and factors affecting fan inlet air temperatures.

Due to the fact that the plane of rotation of the fans of an ACSC is parallel to the ground it is unavoidable to have a degree of cross flow at the fan inlets. The cross flow conditions reduce fan performance by a combination of the following factors:

a) Increased flow losses caused by flow separation at the upstream edge of the ACSC and at the bellmouth fan inlets. It was found that the degree of separation is influenced by both the flow velocity and flow angle.

b) Off axial or distorted flow conditions at the fan face reduce the fan pressure rise.

These factors are closely linked to one another and it is difficult to isolate the one from the other and as a result the relative contribution of each factor to reduced fan performance could not be calculated.

Fan inlet air temperature is found to be affected by the recirculation of hot plume air, especially on the downwind fans located on the sides of the ACSC parallel to the wind.

It is found that reduced fan performance is the greater contributing factor to reduced ACSC performance as compared to recirculation affects.

13.2.2 Results of generic ACSC parameter variation

The fan platform height and the walkway height are two important ACSC design stage parameters. The height of the fan platform determines the open frontal area beneath the ACSC and is therefore inversely proportionate to the degree of cross flow underneath the ACSC and as a result impacts fan performance. Windwalls increase ACSC performance by mitigating recirculation effects. It is found that both the generic ACSC platform height (H_i = 20m) and windwall height (10m) produced acceptable performance.

13.2.3 Results of generic ACSC additions and modifications

A number of additions and modifications were introduced to the generic ACSC to increase performance under windy conditions by primarily aiming at improving fan performance.

The addition of external walkways or skirts improved fan performance by shifting the area of separation away from the periphery fans and reducing the flow distortion at the fan face. It was found that that the greatest performance gain per unit walkway width is achieved with a narrow walkway and the performance gain decreases with increasingly wider walkways to a point where wider walkways resulted in no further gain in performance, however this point is wind speed dependant. It was also found that a periphery walkway is superior to walkways located at just the up -and downstream ACSC edges.

Windscreens were added beneath the ACSC to recover the kinetic energy in the wind driven flow. The screens block the wind and create a stagnation effect underneath the fan platform leading to improved fan performance. The screens can also be configured to reduce distorted flow conditions by deflecting the flow into the fan inlets, accomplished by locating denser screens towards the ground and less dense screens towards the fan platform. As expected it was found that considerable system improvements resulted at high wind speeds perpendicular

to the wind screens which maximised the stagnation and flow deflection effect. Ten screen combinations were examined and both the best screen configuration and a screen configuration deemed to be a cost effective option were then used to determine the optimum screen location beneath the fan platform. The best ACSC performance was obtained by locating the screens between the two most downwind fan rows and the worst performance was obtained by locating the screens between the two most upwind fan rows. This indicated the importance of wind direction on screen location since a reversal in wind direction will result in the best screen location becoming the worst screen location and as a result the screen should be located centrally underneath the fan platform to account for all wind directions. On sites with strong prevailing winds it could be considered to slightly offset the screen location in the downwind direction but this should be done with care.

To eliminate wind induced flow separation upstream of the fans the bellmouth fan inlets were removed, in the first case for only the periphery fans and in the second case for all the fans in the generic ACSC. The removal of the inlet results in fan performance being reduced predominantly by distorted flow conditions. Although removing the bellmouths did not result in increased performance it was found that removing the periphery bellmouths at high wind speeds resulted in the same performance as the generic case. Considering that the performance of the ACSC fitted with bellmouths (hence additional flow losses is present because of separation in the bellmouth) is better than the case without bellmouths (hence negligible additional flow losses but considerably more distorted flow conditions at the fan inlet) indicates that the additional flow losses caused by the presence of the bellmouth are justified by the reduction in flow distortion affected by the bellmouths.

The generic ACSC was modeled in addition to the B-fan with two other fans, namely the L-fan with a steeper static pressure curve compared to the B-fan and the N-fan with a flatter static pressure curve. Due to its steeper fan curve the L-fan is shown to be less susceptible to reduced performance caused by additional losses. This highlights the fact that fans with steeper static pressure curves are better suited to ACSC applications where distorted flow conditions are expected. However this study did not consider fan power requirements which would be an essential step in selecting an appropriate fan.

The effects of increasing the fan power, resulting in increased fan rotational speed and hence air mass flow rates, was investigated. Although ACSC performance improved as expected, a more detailed study would be required to conclude if the improvements are justified.

An expanded and refined examination of wind direction effects on generic ACSC performance confirmed earlier results which showed that the xy-wind resulted in the least reduction in performance and that recirculation effects are most pronounced for wind directions aligned to the principal axis of the ACSC. From this section it can be concluded that there is a performance trade-off between recirculation effects, which are more pronounced for long ACSCs with wind parallel to the longitudinal axis, and fan performance reductions experienced by the upstream periphery fans which could be reduced with a long ACSC parallel to the wind.

Considering all the various ACSC additions and modifications it was decided that the addition of walkways and windscreens presents the most practical and cost effective method of increasing the performance of the generic ACSC under windy conditions. Consequently a periphery walkway of 2.2 m and screen configuration A located as per figure 7.1 is added to the generic ACSC. A measurable improvement was obtained with the systems thermal effectiveness being above 0.94 for all wind speeds and wind directions.

13.3 Future research and general conclusions

This study has successfully shown the applicability of CFD to calculate the performance trends of a generic ACSC subjected to windy conditions. The effect of varying geometrical parameters and the effect of various additions and modifications aimed at improving ACSC performance were also successfully modeled.

During the course of the study it was found that the results of the numerical model are the most sensitive to fan model variations. Therefore the study can be improved by refining the fan model, especially at low flow rates through the fan. The study can also be expanded to include turbine output as the most important parameter when evaluating the performance of the ACSC.

The merits of all the ACSC modifications examined in this study can ultimately only be evaluated by performing a complete life cycle assessment where the financial benefits of improved ACSC performance must be weighed up against the additional costs unique to each modification.

As stated in section 1.3 the performance trends results can be used to optimise the specifications of an ACSC similar to the generic ACSC as well as being used as a starting point for detailed performance improvement studies on specific ACSCs with different geometries. The results from the investigation into ACSC modifications and additions could be used to modify existing ACSCs suffering from wind induced performance reductions, ensuring adequate performance and in extreme cases reducing the possibility of turbine trips.

References

Bredell, J.R., Kröger, D.G., Thiart., G.D., 2005. Numerical investigation of fan performance in a forced draft air-cooled steam condenser, M.Sc. Eng thesis, Department of Mechanical Engineering, University of Stellenbosch.

Bredell, J.R., Kröger, D.G., Thiart, G.D., 2006. Numerical investigation of fan performance in a forced draft air-cooled steam condenser, Applied Thermal Engineering 26, 846-852.

Du Toit, C.G., Kröger, D.G., 1993. Modelling of the recirculation in mechanical-draught heat exchangers, Journal of the South African Institution of Mechanical Engineers 9 (1), 2-8.

Du Toit, C.G., Thiart, G.D., Kröger, D.G., 1993. Analysis of recirculation in mechanical-draught heat exchangers, in: Proceedings of the 3rd World Conference on Experimental Heat Transfer, Fluid Mechanics and Thermodynamics, Honolulu, Hawai.

Duvenhage, K., Kröger, D.G., 1996. The influence of wind on the performance of forced draught air-cooled heat exchangers, Journal of Wind Engineering and Industrial Aerodynamics 62, 259-277

Duvenhage, K., Vermeulen, J.A., Meyer, C.J., Kröger, D.G., 1996. Flow distrortions at the fan inlet of forced draught air-cooled heat exchangers, Applied Thermal Engineering 16 (8/9), 741-752.

EPRI, 2005. Air-cooled condenser design, specification and operation guidelines, Report number 1007688, Palo Alto.

FLUENT 6 User's Guide, 2006. Chapter 12. Fluent Inc., Lebanon.

FLUENT 6.3 Getting Started Guide, 2006. Fluent Inc., Lebanon.

Goldschagg, H.B., 1993. Lessons learned from the world's largest air-cooled condenser, in: Proceedings of the EPRI International Symposium on Improved Technology for Fossil Power Plants - New and Retrofit Applications, Washington D.C.

Goldschagg, H.B., Vogt, F., du Toit, C.G., Thiart, G.D., Kröger, D.G., 1997. Air-cooled steam condenser performance in the presence of crosswinds, in: Proceedings of the Cooling Tower Technology Conference, EPRI Report TR-108483, 1-61 to 1-77, Palo Alto.

Liu, P., Duan, H., Zhao, W., 2009. Numerical investigation of hot air recirculation of air-cooled condensers at a large power plant, Applied Thermal Engineering 29, 1927-1934.

Kröger, D.G., 1989. Reduction in performance due to recirculation in mechanical-draft cooling towers, Heat Transfer Engineering 10 (4), 37-43.

Kröger, D.G., 2004. Air-cooled heat exchanges and cooling towers. Pennwell Corporation, Tulsa.

Maulbetsch, J.S., DiFilippo M.N., 2007. Effects of wind on air-cooled condenser performance, Cooling Technology Institute, Paper no. TP07-04.

Meyer, C.J., 2005. Numerical investigation of the effect of inlet flow distortions on forced draught air-cooled heat exchanger performance, Applied Thermal Enginering 25, 1634-1649.

Monroe, R. C., 1979. Improving cooling tower efficiencies, Combustion Magazine 50 (11), 20-26.

Nagel, P., Wurtz, W., 2006. Dry cooling for power plants - An innovative modularization concept, Presented at PowerGen Europe, Cologne.

Owen, M.T.F., 2010, A numerical investigation of air-cooled steam condenser performance under windy conditions, MSc Eng Thesis, Department of Mechanical Engineering, University of Stellenbosch.

Salta, C.A., Kröger, D.G., 1995. Effect of inlet flow distortions on fan performance in forced draught air-cooled heat exchangers, Heat Recovery Systems & CHP 15 (6), 555-561.

Shih, T.H., Liou, W.W., Shabbir, A., Yang, Z., Zhu, J., 1995. A new k-ε eddy-viscosity model for high Reynolds number turbulent flows - Model development and validation, Computer Fluids 24 (3), 227-238

Stinnes, W.H., Von Backström, T.W., 2002. Effect of cross-flow on the performance of air-cooled heat exchanger fans, Applied Thermal Engineering 22, 1403-1415.

Thiart, G.D., Von Backström, T.W., 1993. Numerical simulation of the flow field near an axial flow fan operating under distorted inflow conditions, Journal of Wind Engineering and Industrial Aerodynamics 45, 189 -214.

Van Aarde, D. J., 1990. Vloeiverliese deur 'n A-raam vinbuisbundel in 'n lugverkoelde kondensator. University of Stellenbosch, M.Sc.Eng thesis, Department of Mechanical Engineering, University of Stelenbosch.

Van Rooyen, J.A., 2007, Performance trends of an air-cooled steam condenser under windy conditions, MSc Eng Thesis, Department of Mechanical Engineering, University of Stellenbosch.

Van Rooyen, J.A., Kröger, D.G., 2008. Performance trends of an air-cooled steam condenser under windy conditions, Journal of Engineering for Gas Turbines and Power 130 (2), 023006-1 to 023006-7.

Appendix A - Generic ACSC Specifications

The specifications (Bredell, 2005) of a typical A-frame fan unit, as shown in figure A.1, contained in the generic ACSC are detailed in this section.

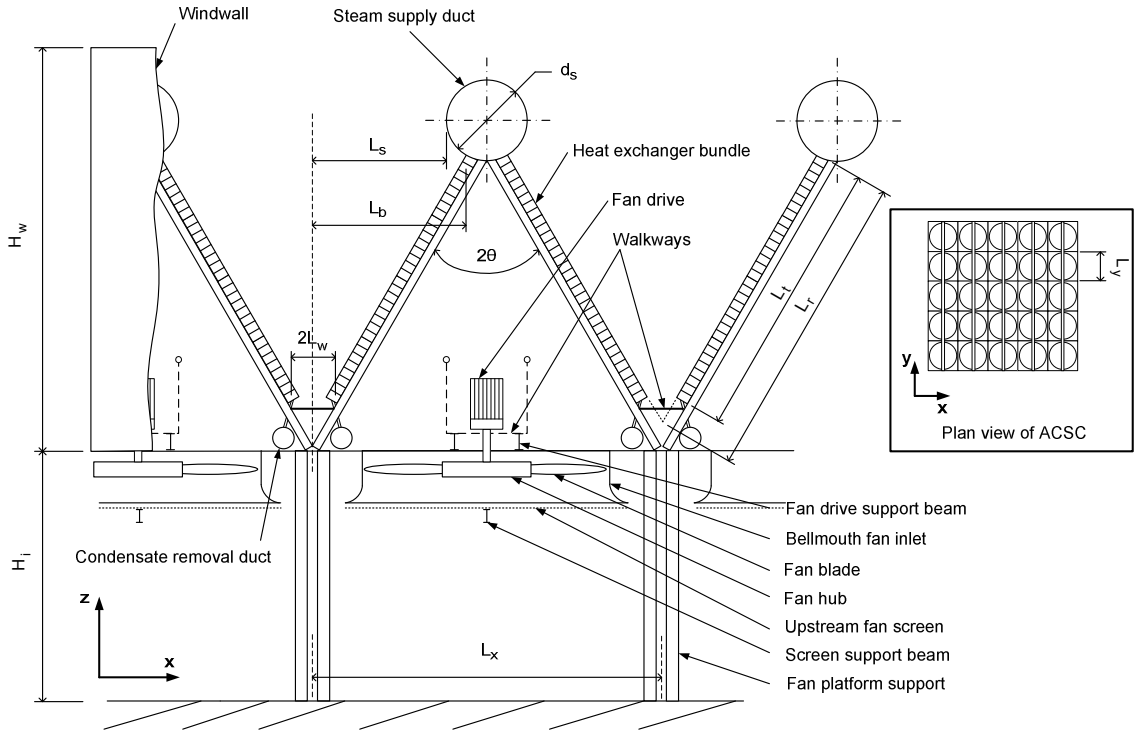

Figure A. 1: ACSC fan unit dimensions.

A.1. Atmospheric and steam design conditions

Air temperature at ground level	T_a = 15.6 °C
Barometric pressure at ground level	p_a = 90000 N/m^2
Saturated steam supply temperature	T_v = 60 °C

A.2. Air properties

The thermo-physical properties of air, evaluated at ambient temperature and pressure:

Density	ρ_a = 1.0857 kg/m^3
Thermal conductivity	k_a = 0.02535 W/mK
Specific heat	c_p = 1006.609 W/kgK
Molecular viscosity	μ_a = 1.7948x10^{-5} g/ms
Prandtl number	Pr = 0.71274

A.3. Finned tube bundle specifications

Number of heat exchanger bundles above one fan	n_b = 8
Frontal area of one bundle	A_{fr} = 27.434 m^2
Effective finned tube length	L_t = 9.55 m

Heat exchanger apex angle	$2\theta = 56°$
Number of finned tubes tube rows	$n_r = 2$
Number of finned tubes per bundle in the first row	$n_{tb1} = 57$
Number of finned tubes per bundle in the second row	$n_{tb2} = 58$
Ratio of minimum to free stream flow area through finned tube bundle	$\sigma = 0.41$
Ratio of minimum to free stream flow area at inlet of finned tube bundle	$\sigma_{21} = 0.86$

The characteristic heat transfer parameter, Ny, is experimentally determined for the first row of finned tubes as

$$Ny_1 = 583.8307Ry^{0.4031} \quad \text{(A.1)}$$

and for the second row

$$Ny_2 = 1277.726Ry^{0.3806} \quad \text{(A.2)}$$

The loss coefficient for both rows under normal flow conditions is

$$K_{he} = 4464.831Ry^{-0.43927} \quad \text{(A.3)}$$

where Ny and Ry are respectively defined by equation A.4 and A.5 below

$$Ny = \frac{hA}{k_a A_{fr} Pr^{0.333}} \quad \text{(A.4)}$$

and

$$Ry = \frac{m_a}{\mu_a A_{fr}} \quad \text{(A.5)}$$

Note that in equation A.4 and A.5 A_{fr} and m_a refer to the total frontal area and the corresponding mass flow rate.

A.4. Upstream and downstream obstacles

The following dimensions refer to obstacles upstream and downstream of the fan, as shown in figure A.1.

Inlet screen distance from fan blade (upstream)	$x_{sci} = 1.29$ m
Support beam distance from fan blade (upstream)	$x_{bi} = 1.336$ m
Support beam distance from fan blade (downstream)	$x_{bo} = 0.5345$ m
Walkway distance from fan blade (downstream)	$x_{wo} = 0.995$ m
Ratio of inlet screen area to fan casing area	$\sigma_{sci} = 0.109$
Ratio of support beam area to fan casing area (upstream)	$\sigma_{bi} = 0.154$
Ratio of support beam area to fan casing area (downstream)	$\sigma_{bo} = 0.0523$
Ratio of walkway area to fan casing area	$\sigma_{wo} = 0.0912$

A.5. Platform dimensions

The following dimensions are given with reference to figure A.1

Average steam header diameter	d_s = 2.34 m
Half-width of walkway between A-frames	L_w = 0.397 m
Height of windwall	H_w = 10 m
Dimension shown in figure A.1.	L_x = 10.56 m
Dimension shown in figure A.1.	L_y = 11.8 m
Dimension shown in figure A.1.	L_r = 10.6 m
Dimension shown in figure A.1.	L_b = 4.924 m
Dimension shown in figure A.1.	L_s = 4.102 m

A.6 Effective system resistance

The effective air-side flow system resistance, Δp_e, is given by Kröger (2004) as

$$\Delta p_e = -\left[K_{ts}\frac{1}{2\rho_{a1}}\left(\frac{m_a}{n_b A_{fr}}\right)^2 + K_{up}\frac{1}{2\rho_{a3}}\left(\frac{m_a}{A_e}\right)^2 + K_{do}\frac{1}{2\rho_{a3}}\left(\frac{m_a}{A_e}\right)^2 + K_{\theta t}\frac{1}{2\rho_{a56}}\left(\frac{m_a}{n_b A_{fr}}\right)^2\right] \quad \text{(A.6)}$$

To calculate the various loss coefficients in equation A.6 the flow is assumed to be isothermal and variation in thermo-physical properties is neglected.

A.6.1 Definition of loss coefficients

This section defines the loss coefficients in equation A.6. $K_{\theta t}$ is the flow losses for an A-frame heat exchanger, incorporating process fluid ducts and walkways and includes kinetic energy losses at the outlet of the A-frame array. For isothermal flow $K_{\theta t}$ is defined as:

$$K_{\theta t} = K_{he} + \left(\frac{1}{sin\theta_m} - 1\right)\left[\left(\frac{1}{sin\theta_m} - 1\right) + 2K_{ci}^{0.5}\right] + K_{dj} + K_o \quad \text{(A.7)}$$

The isothermal heat exchanger loss coefficient, K_{he} is given by equation A.3. θ_m is the mean flow incidence angle that has been adjusted to account for flow distortion downstream of the bundle and is given as a function of the semi apex angle by the following empirical equation:

$$\theta_m = 0.0019\theta^2 + 0.9133\theta - 3.1558 \quad \text{(A.8)}$$

K_{ci} is the entrance contraction loss coefficient for normal flow and is based on the normal approach free stream velocity:

$$K_{ci} = \left[\frac{1 - 1/\sigma_c}{\sigma}\right]^2 \quad \text{(A.9)}$$

where σ_c is a function of σ_{21} as given by the following empirical equation

$$\sigma_c = 0.6155417 + 0.04566493\sigma_{21} - 0.336651{\sigma_{21}}^2 + 0.4082743{\sigma_{21}}^3 + 2.672041{\sigma_{21}}^4 - 5.963169{\sigma_{21}}^5 + 3.558944{\sigma_{21}}^6 \quad \text{(A.10)}$$

K_{dj} is the jetting loss coefficient and is expressed by the following correlation:

$$K_{dj} = \left[\left\{-2.89188\left(\frac{L_w}{L_t}\right) + 2.93291\left(\frac{L_w}{L_t}\right)^2\right\}\left(\frac{L_t}{L_s}\right)\left(\frac{L_b}{L_s}\right)\left(\frac{28}{\sigma}\right)^{0.4} + \left\{\left(\frac{\mathrm{L_s}}{\mathrm{L_b}}\right)\exp\left(2.36987 + 5.80601\times10^{-2}\theta - 3.3797\times10^{-3}\theta^2\right)\right\}^{0.5}\left(\frac{\mathrm{L_t}}{\mathrm{L_r}}\right)\right]^2 \quad \text{(A.11)}$$

where θ is in degrees and the length dimensions denoted by L and an appropriate subscript are defined in figure A.1.

The outlet loss coefficient is defined as

$$K_o = \left[\left\{-2.89188\left(\frac{L_w}{L_t}\right) + 2.93291\left(\frac{L_w}{L_t}\right)^2\right\}\left(\frac{L_s}{L_b}\right)^3 + 1.9874 - 3.03783\left(\frac{d_s}{2L_b}\right) + 2.0187\left(\frac{d_s}{2L_b}\right)^2\right]\left(\frac{L_t}{L_s}\right)^2 \quad \text{(A.12)}$$

Upstream losses result from the inlet screen and the screen support beam whilst downstream losses result from the fan drive and system support and walkway. The up- and downstream loss coefficients, K_{up} and K_{do}, are based on the mean velocity through the fan. Kröger (2004) provides empirical relations for these loss coefficients as a function of the projected area of the obstacle and the distance from the fan. The pressure loss caused by the fan platform support structures is accounted for by the loss coefficient K_{ts}.

A.6.2 Evaluation of loss coefficients

The air properties defined in section A.2 are used to evaluate the loss coefficients.

From equation A.3 K_{he} is evaluated as

$$K_{he} = 4464.831Ry^{-0.43927} = 4464.831\left(\frac{m_a}{\mu_a\eta_b A_{fr}}\right)^{-0.43927} = 397.3837{m_a}^{-0.43927}$$

θ_m is calculated from equation A.8

$$\theta_m = 0.0019\cdot 28^2 + 0.9133\cdot 28 - 3.1558 = 23.91°$$

From equation A.10 σ_c is evaluated as

$$\sigma_c = 0.6155417 + 0.04566493 \cdot 0.86 - 0.336651 \cdot 0.86^2 + 0.4082743 \cdot 0.86^3$$
$$+ 2.672041 \cdot 0.86^4 - 5.963169 \cdot 0.86^5 + 3.558944 \cdot 0.86^6 = 0.761$$

and entrance contraction loss coefficient, K_{ci} is

$$K_{ci} = \left[\frac{1 - 1/0.761}{0.41}\right]^2 = 0.587$$

The jetting loss coefficient is calculated according to equation A.11

$$K_{dj} = \left[\left\{-2.89188\left(\frac{0.397}{9.55}\right) + 2.93291\left(\frac{0.397}{9.55}\right)^2\right\}\left(\frac{9.55}{4.102}\right)\left(\frac{4.924}{4.102}\right)\left(\frac{28}{0.41}\right)^{0.4}\right.$$
$$\left. + \left\{\left(\frac{4.102}{4.924}\right)\exp\left(2.36987 + 5.80601 \times 10^{-2} \cdot 28 - 3.3797 \times 10^{-3} \cdot 28^2\right)\right\}^{0.5}\left(\frac{9.55}{10.6}\right)\right]^2$$
$$= 1.696$$

The outlet loss coefficient is calculated according to equation A.12

$$K_o = \left[\left\{-2.89188\left(\frac{0.397}{9.55}\right) + 2.93291\left(\frac{0.397}{9.55}\right)^2\right\}\left(\frac{4.102}{4.924}\right)^3 + 1.9874 - 3.03783\left(\frac{2.34}{2 \cdot 4.924}\right)\right.$$
$$\left. + 2.0187\left(\frac{2.34}{2 \cdot 4.924}\right)^2\right]\left(\frac{9.55}{4.102}\right)^2 = 7.129$$

The A-frame loss coefficient from equation A.7 can now be evaluated in terms of m_a:

$$K_{\theta t} = 397.3837{m_a}^{-0.43927} + \left(\frac{1}{sin23.91} - 1\right)\left[\left(\frac{1}{sin23.91} - 1\right) + 20.587^{0.5}\right]$$
$$+ 1.696 + 7.129$$

$$K_{\theta t} = 397.3837{m_a}^{-0.43927} + 13.232$$

The upstream and downstream loss coefficients are given below (Kröger, 2004):

Table A. 1 : Upstream and downstream loss coefficients.

Obstacle	x_{ob}/d_c	A_{ob}/A_c	Loss coefficient
Upstream Obstacles			
Screen	0.140	0.109	0.11
Support Beam	0.145	0.154	0.17
		K_{up} =	**0.28**

Downstream Obstacles			
Support Beam	0.058	0.0523	0.16
Walkway	0.108	0.0912	0.19
		K_{do} =	**0.35**

In terms of mass flow rate equation A.6 now becomes

$$\Delta p_e = -\left[\frac{1.6033}{2 \cdot 1.0857}\left(\frac{m_a}{8 \cdot 27.434}\right)^2 + \frac{0.281}{2 \cdot 1.0857}\left(\frac{m_a}{\pi/4\,(9.216^2 - 1.4^2)}\right)^2 + \frac{0.35}{2 \cdot 1.0857}\left(\frac{m_a}{\pi/4\,(9.216^2 - 1.4^2)}\right)^2 + \frac{397.3837 {m_a}^{-0.43927} + 13.232}{2 \cdot 1.0857}\left(\frac{m_a}{8 \cdot 27.434}\right)^2\right]$$

$$= -(2.1029 \times 10^{-4}\, {m_a}^2 + 3.8018 \times 10^{-3}\, {m_a}^{1.56073}) \quad , \quad N/m^2$$

or in terms of volume flow rate V_a

$$\Delta p_e = -\left(2.4756 \times 10^{-4}\, {V_a}^2 + 4.31807 \times 10^{-3}\, {V_a}^{1.56073}\right) \quad , \quad N/m^2 \qquad \text{(A.13)}$$

Appendix B - Fan Specification

The specifications of the B-fan (Bredell, 2005), used in the generic model of the ACSC examined in this study, are given in this section.

B.1 Fan dimensions

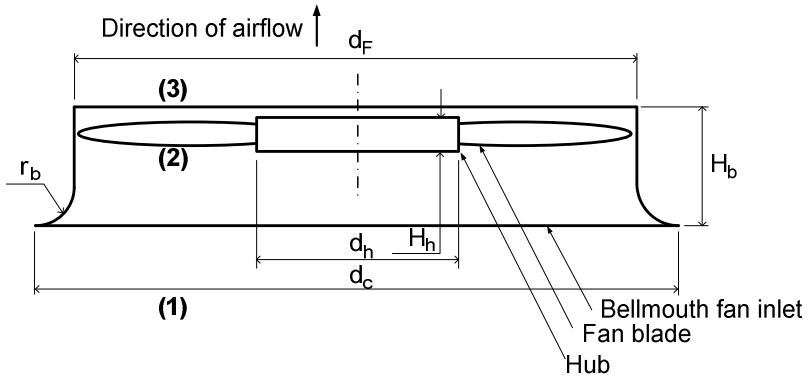

Figure B. 1: B-fan dimensions

Fan diameter	d_F = 9.145 m
Hub-tip ratio of B-fan	d_h/d_F= 0.4
Ratio of hub thickness to fan diameter of B-fan	H_h/d_h = 0.1
Bellmouth diameter	d_c = 10.134 m
Height of bellmouth fan inlet from fan platform	H_b = 1.92 m
Bellmouth inlet radius	r_b = 1.16 m
Number of fan blades	n_F = 8
Rotational speed	N = 125 rpm
Blade reference angle based on chord line	ζ_{cr} = 34.5°

B.2 Fan performance curve

The fan performance curves are given in figure B.2.

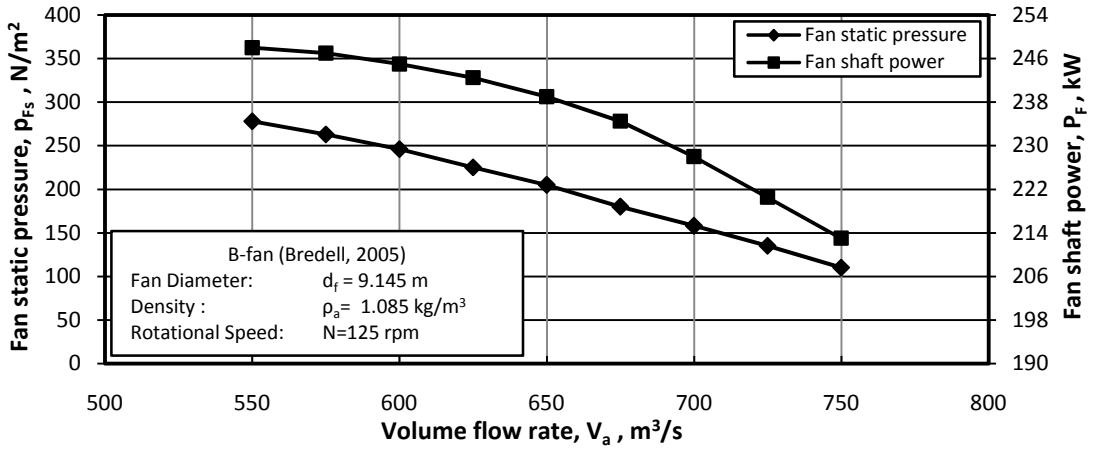

Figure B. 2: Fan static pressure, p_{Fs}, and shaft power, P_F, for B-fan (Bredell, 2005).

B.3 Derivation of fan curve used by FLUENT's fan pressure jump model

In figure B.1 point 1 is sufficiently far away from the fan inlet such that the air velocity at 1 is zero. Points 2 and 3 are upstream and downstream respectively of the fan blades. Stagnation, or total pressure, p_t, is defined as the sum of the static, p_s and dynamic, p_d, i.e.

$$p_t = p_s + p_d \tag{B.1}$$

where the dynamic pressure is defined as

$$p_d = \frac{1}{2}\rho {v_a}^2 \tag{B.2}$$

and the air velocity in this case is defined as

$$v_a = \frac{V_a}{\frac{\pi}{4}({d_F}^2 - {d_h}^2)} \tag{B.3}$$

where V_a is the volumetric flow rate through the fan. The fan static pressure rise is defined as

$$\Delta p_{Fs} = p_{s3} - p_{t1} \tag{B.4}$$

and is obtained in test setups as described by Kröger (2004). This pressure rise is plotted as a function of volumetric flow rate through the fan as shown in figure B.2 for the B-fan. However the velocity at 1 is essentially zero, thus according to equation (B.2), p_{d1} is also zero and from equation (B.1) it can be seen that

$$p_{t1} \approx p_{s1} \tag{B.5}$$

Under ideal conditions there are no flow losses and the small loss due to the rounded inlet can be ignored. As a result the total pressure at point 1 and 2 are equal and by introducing equation (B.5) the following is obtained:

$$p_{t2} = p_{t1} = p_{s1} \tag{B.6}$$

Combining (B.6) and (B.1) and rearranging the following is obtained:

$$p_{2s} = p_{1s} - p_{2d} \tag{B.7}$$

The pressure jump fan model employed by FLUENT introduces a static-to-static pressure jump across a face as follows:

$$\Delta p_F = p_{3s} - p_{2s} \tag{B.8}$$

Substituting equation (B.7) into (B.8) yields:

$$\Delta p_F = p_{3s} - p_{1s} + p_{2d} \tag{B.9}$$

and using the definition of the fan pressure rise as given by equation (B.4), equation (B.9) can be rewritten as:

$$\Delta p_F = \Delta p_{Fs} + p_{2d} \quad \text{(B.10)}$$

which can be rewritten using the definition of dynamic pressure from equation (B.2) as

$$\Delta p_F = \Delta p_{Fs} + \frac{1}{2}\rho {v_a}^2 \quad \text{(B.11)}$$

Thus it can be seen that the fan curve required by FLUENT is simply the fan static pressure curve to which the dynamic pressure component is added. A second order polynomial is fitted through the data and the dynamic pressure is added to produce

$$\Delta p_F = 323.2303 + 0.4938 V_a - 0.001 {V_a}^2 \ , \ N/m^2 \quad \text{(B.12)}$$

FLUENT requires the pressure jump to be expressed in terms of normal velocity:

$$\Delta p_F = 323.2303 + 27.2461 v_a - 2.6305 {v_a}^2 \ , \ N/m^2 \quad \text{(B.13)}$$

Appendix C - Heat exchanger models

This section details the two sub models of the heat exchanger model, as shown in figure C.1. The first model accounts for the pressure loss as described by the effective system resistance and the second model accounts for the thermal effects of the heat exchanger.

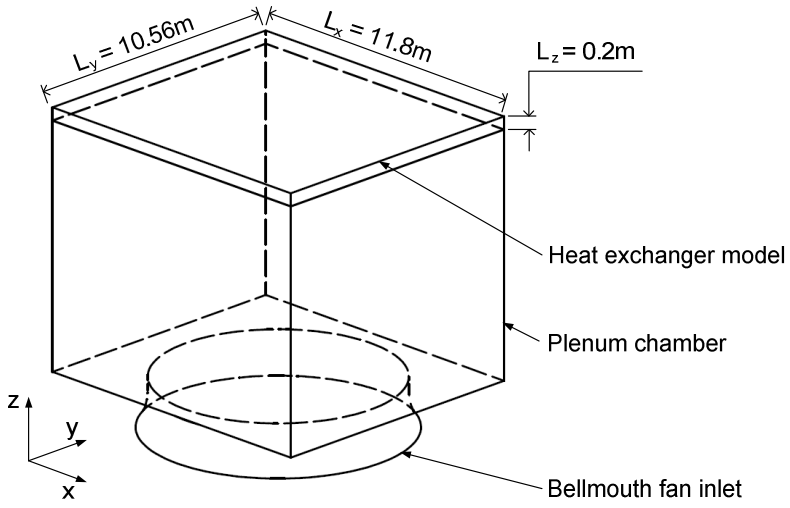

Figure C. 1: Numerical heat exchanger model

C.1 Pressure loss model - derivation of loss coefficients

As previously stated the components of the ACSC such as supports, screens, fan drives and ducting are not modeled explicitly, however their influences on the flow field are modeled as momentum sink terms as part of FLUENT's porous zone model representing the heat exchanger. This requires the calculation of the viscous and inertial loss coefficients, $1/\alpha_z$ and C_z respectively.

The effective system resistance given by equation (A.13) can be approximated as a second order polynomial as:

$$\Delta p_e \approx -\left(4.132315 \times 10^{-4} {V_a}^2 + 5.629484 \times 10^{-2} V_a\right) \ , \ N/m^2 \qquad \text{(C. 1)}$$

The volume flow rate can be written in terms of the average velocity in the z-direction, w, as

$$V_a = |w|\left(L_x \times L_y\right) \qquad \text{(C. 2)}$$

Equation (C.1) can then be written in terms w as

$$\Delta p_e = -\left(4.132315 \times 10^{-4} |w| w \left(L_x \times L_y\right)^2 + 5.629484 \times 10^{-2} w \left(L_x \times L_y\right)\right)$$

$$= 6.4163|w|w + 7.1048w \ , \ N/m^2 \qquad \text{(C. 3)}$$

The body forces acting in the z-direction in each cell of the numerical heat exchanger model, shown in figure C.1, is given by

$$F_z = \frac{\Delta p_e}{L_z} = 32.082|w|w + 35.074w \ , \ N/m^2 \qquad \text{(C. 4)}$$

Due to the fact that flow is restricted in the x and y-directions, $|v| \approx |w|$ so that the body force in the z-direction becomes

$$F_z = \left(C_z \frac{1}{2}\rho|w|w + \frac{\mu}{\alpha_z}w\right) \qquad \text{(C. 5)}$$

By comparing equations (C.4) and equation (C.5), the viscous and inertial loss coefficients, $1/\alpha_z$ and C_z, can now be calculated

$$C_z \frac{1}{2}\rho = 32.082$$

$$C_z = 59.1364$$

and

$$\frac{\mu}{\alpha_z} = 35.074$$

$$\frac{1}{\alpha_z} = 1.897 \times 10^6$$

C.2 Heat transfer model

To model the heat transfer from the heat exchanger to the air a user defined function (UDF) was written that extracts the air mass flow rate, m_a, and the air inlet temperature, T_{ai}, from the solver for each cell in the porous zone. These values are then used to calculate the heat source terms in the heat exchanger with each iteration as detailed below.

The characteristic flow parameter for the first tube row is adapted from equation (A.5) to account for the reduction in effective frontal area due to having one less row of tubes

$$Ry_1 = \frac{m_a}{\mu_a n_b A_{fr} \frac{n_{tb1}}{n_{tb2}}} \qquad \text{(C.6)}$$

From equation (A.4) the effective air-side heat transfer coefficient is

$$hA_1 = k_a n_b A_{fr} Pr^{0.333} Ny_1 \frac{n_{tb1}}{n_{tb2}} \qquad \text{(C.6)}$$

where Ny_1 is the characteristic heat transfer parameter given by equation (A.1). The heat transfer rate for the first tube row is

$$Q_1 = m_a c_{pa}(T_{ao1} - T_{ai1}) = e_1 m_a c_{pa}(T_s - T_{ai1}) \qquad \text{(C.7)}$$

Rearranging equation (C.7) to calculate the air outlet temperature:

$$T_{ao1} = e_1 T_s + (1 - e_1) T_{ai1} \quad \text{(C.8)}$$

where e_1 is the effectiveness of the first tube i.e.

$$e_1 = 1 - exp\left(\frac{-UA_1}{m_a c_{pa}}\right) \quad \text{(C.9)}$$

The thermal resistance caused by the condensate film, typically in the order of 2% of the total thermal resistance, is neglected and as a result $UA_1=hA_1$. The air outlet temperature of the first row, T_{ao1} is equal to the inlet temperature of the second tube row, T_{ai2}, and the heat transfer from the second tube row, Q_2, can be calculated in a similar fashion as described for the first row. The air outlet temperature for the second is thus calculated from

$$T_{ao2} = e_2 T_s + (1 - e_1) T_{ai2} = e_2 T_s + (1 - e_1)[e_1 T_s + (1 - e_1) T_{ai1}] \quad \text{(C.10)}$$

The total heat transfer rate per fan unit is then

$$Q_{tot} = Q_1 + Q_2 = m_a c_{pa}(T_{ao2} - T_{ai1}) \quad \text{(C.11)}$$

The heat transfer is modeled by adding heat source terms, F_E, to the relevant energy equations:

$$F_E = \frac{\delta Q}{\delta V} = \frac{\delta m_a c_{pa}}{\delta V}(T_{ao2} - T_{ai1}) = \frac{\rho |w| c_{pa}}{L_z}(T_{ao2} - T_{ai1}) \quad {}^{W}/_{m^3} \quad \text{(C.12)}$$

where δm_a and δV are the mass flow rate through a cell and the volume of a cell, respectively.

Appendix D - Comparison to previous work

This section compares the performance of the generic ACSC to the results obtained by Van Rooyen (2007) who studied the identical ACSC. Due to limited computational resources Van Rooyen did not model the airflow through all the fans simultaneously, but instead the solution of a global flow field was used as an input to a number of smaller more detailed models that solved the flow through a particular fan. Furthermore the flow through all 30 fans was not modeled but instead symmetry planes and a number of interpolation schemes were used to estimate the flow through the fans that were not modeled and the results were used to calculate the system performance. Figure D.1 shows the layout of the generic ACSC including the fan numbers and wind directions, modeled with three reference wind speeds (v_{ref} = 3 m/s, 6 m/s and 9 m/s as per equation (2.3)) and the results are presented thereafter.

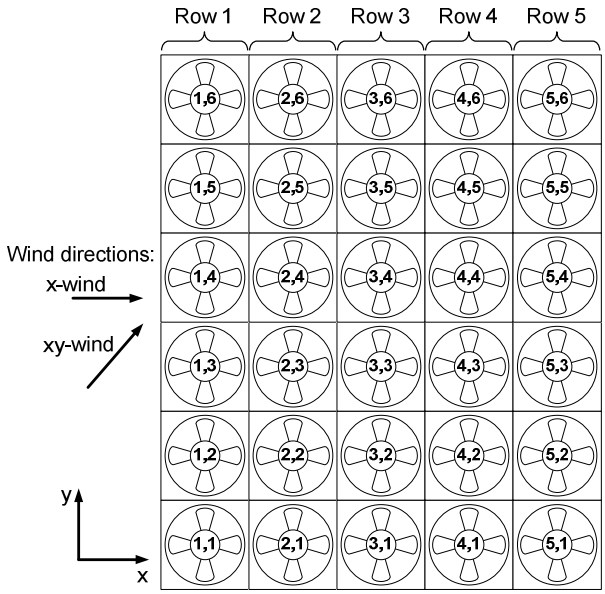

Figure D. 1: Details of fan numbers and wind direction of the generic ACSC.

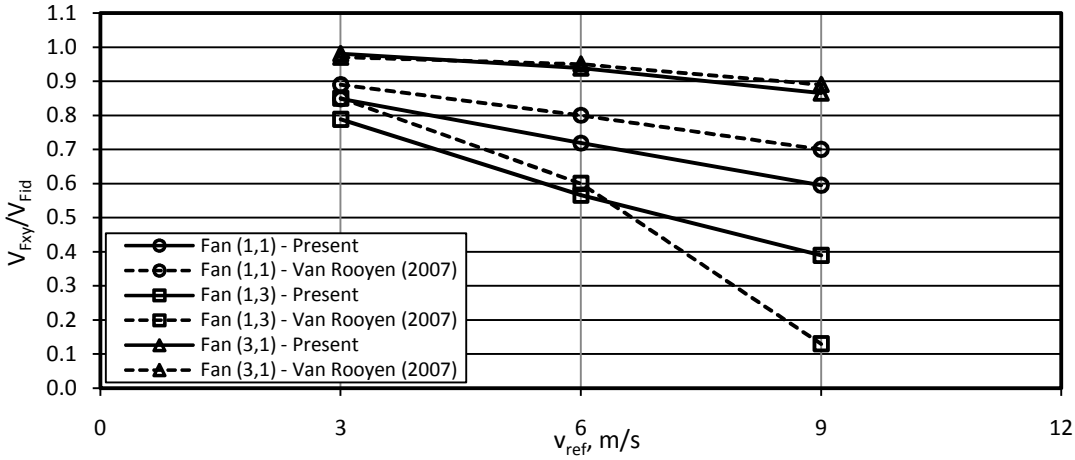

Figure D. 2: Comparison of the volumetric effectiveness of fan (1,1), (1,3) and (3,1) for an x-wind.

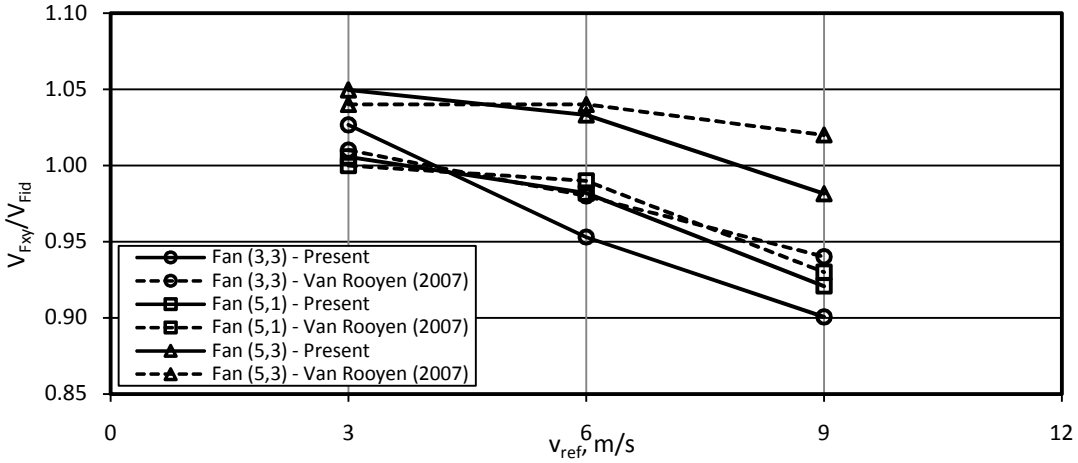

Figure D. 3: Comparison of the volumetric effectiveness of fan (3,3), (5,1) and (5,3) for an x-wind.

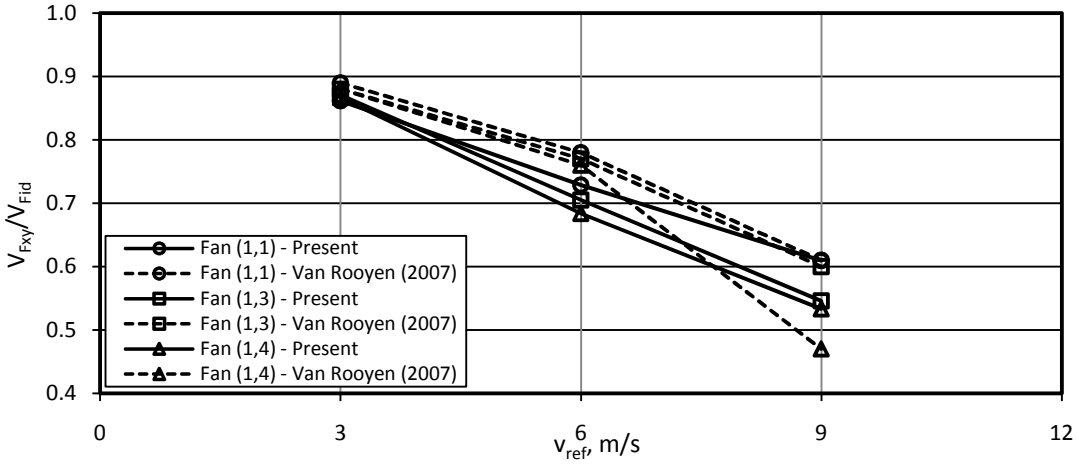

Figure D. 4: Comparison of the volumetric effectiveness of fan (1,1), (1,3) and (1,4) for an xy-wind.

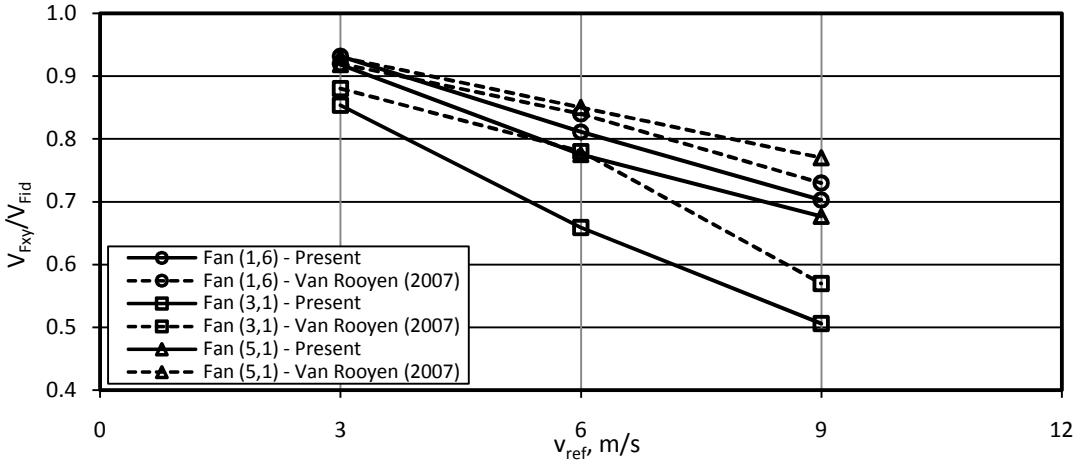

Figure D. 5: Comparison of the volumetric effectiveness of fan (1,6), (3,1) and (5,1) for an xy-wind.

It can be seen that the results of the individual fan volumetric effectiveness from this study are generally lower compared to the results of Van Rooyen (2007) however the trends between the studies are seen to be similar. Possible reasons for the differences at high wind speeds could be attributed to non-convergence between the global and detailed model used by Van Rooyen (2009), whereby the global model was not updated with the results from the detailed model which would then require another iteration of the solution. Van Rooyen (2007) used the actuator disk fan model which is known to be unreliable at high wind speeds and flow distortion. However, the system results shown in figures D.6 to D.9 show very close agreement between the respective studies.

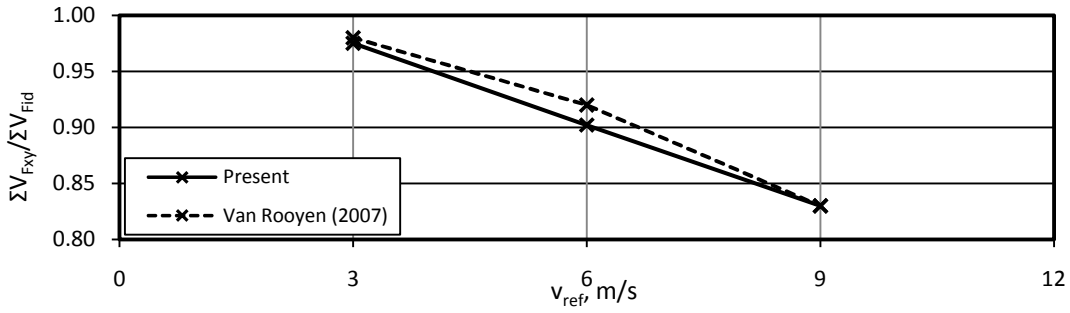

Figure D. 6: Comparison of system volumetric effectiveness, x-wind.

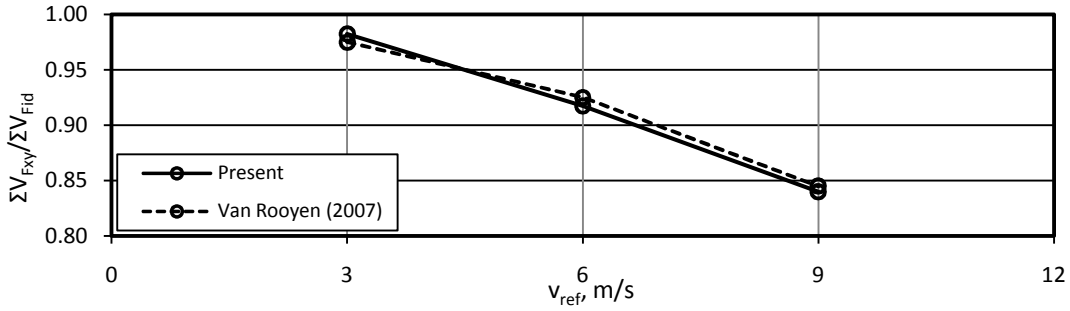

Figure D. 7: Comparison of system volumetric effectiveness, xy-wind.

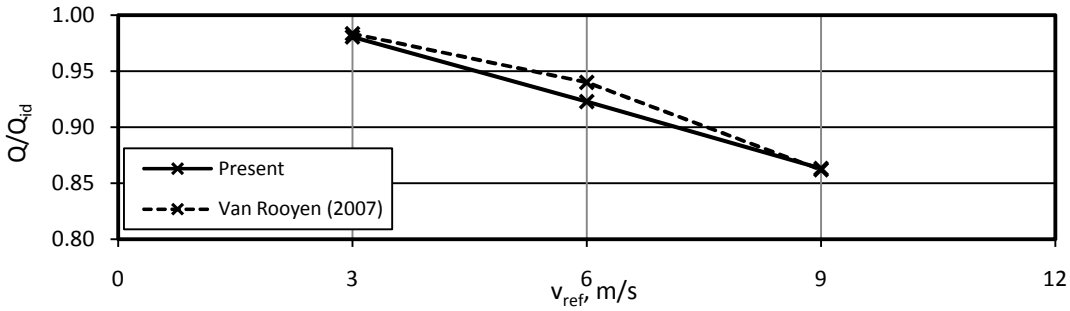

Figure D. 8: Comparison of system thermal effectiveness, x-wind.

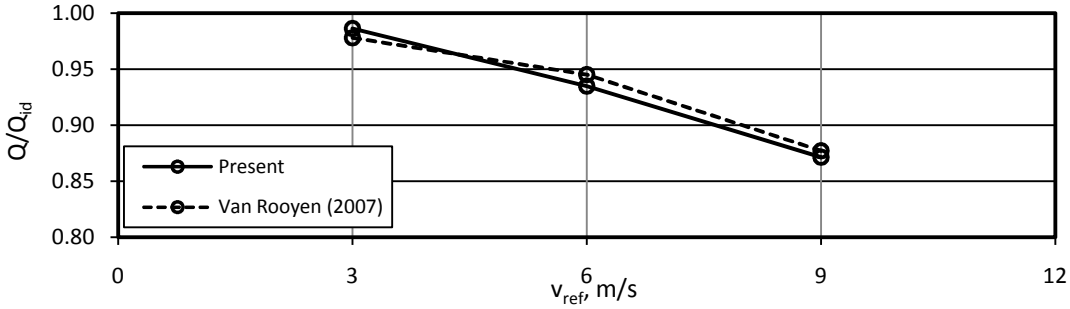

Figure D. 9: Comparison of system thermal effectiveness, xy-wind.

Appendix E - Complete detailed results.

This section presents the complete set of system performance parameters for each ACSC configuration examined in this study.

E.1. Effect of platform height variation - section 4

	H_i = 25 m x-wind			H_i = 20 m x-wind (generic ACSC)			H_i = 15 m x-wind			H_i = 10 m x-wind		
v_{ref}	3 m/s	6 m/s	9 m/s	3 m/s	6 m/s	9 m/s	3 m/s	6 m/s	9 m/s	3 m/s	6 m/s	9 m/s
$\Sigma V/\Sigma V_{id}$	0.99	0.92	0.84	0.98	0.90	0.83	0.95	0.87	0.81	0.89	0.81	0.75
Q/Q_{id}	0.99	0.93	0.86	0.98	0.91	0.84	0.96	0.88	0.82	0.90	0.82	0.76
T_v, K	333.7	336.6	340.3	334.2	337.4	341.1	335.1	339.0	342.7	337.9	342.7	346.6
p_v, N/m^2	20304	23139	27279	20737	23970	28329	21635	25797	30278	24508	30367	35719
	H_i = 25 m xy-wind			H_i = 20 m xy-wind (generic ACSC)			H_i = 15 m xy-wind			H_i = 10 m xy-wind		
v_{ref}	3 m/s	6 m/s	9 m/s	3 m/s	6 m/s	9 m/s	3 m/s	6 m/s	9 m/s	3 m/s	6 m/s	9 m/s
$\Sigma V/\Sigma V_{id}$	0.99	0.93	0.85	0.98	0.92	0.84	0.96	0.90	0.82	0.91	0.85	0.77
Q/Q_{id}	0.99	0.94	0.88	0.98	0.93	0.87	0.97	0.92	0.85	0.93	0.87	0.81
T_v, K	333.6	335.9	339.3	333.8	336.4	339.8	334.5	337.2	340.8	336.7	339.6	343.4
p_v, N/m^2	20177	22431	26150	20429	22948	26707	21031	23831	27929	23256	26422	31276

E.2. Effect of windwall height variation - section 5

	H_w = 10 m x-wind (generic ACSC)			H_w = 7.5 m x-wind			H_w = 5 m x-wind			H_w = 2.5 m x-wind		
v_{ref}	3 m/s	6 m/s	9 m/s	3 m/s	6 m/s	9 m/s	3 m/s	6 m/s	9 m/s	3 m/s	6 m/s	9 m/s
$\Sigma V/\Sigma V_{id}$	0.98	0.90	0.83	0.98	0.91	0.84	0.97	0.91	0.85	0.97	0.92	0.86
Q/Q_{id}	0.98	0.91	0.84	0.97	0.91	0.84	0.96	0.89	0.82	0.93	0.85	0.79
T_v, K	334.2	336.9	341.1	334.3	337.7	341.4	334.9	338.6	342.1	336.3	340.4	343.6
p_v, N/m^2	20737	23501	28329	20857	24336	28696	21436	25349	29511	22852	27413	31444
	H_w = 10 m xy-wind (generic ACSC)			H_w = 7.5 m xy-wind			H_w = 5 m xy-wind			H_w = 2.5 m xy-wind		
v_{ref}	3 m/s	6 m/s	9 m/s	3 m/s	6 m/s	9 m/s	3 m/s	6 m/s	9 m/s	3 m/s	6 m/s	9 m/s
$\Sigma V/\Sigma V_{id}$	0.98	0.92	0.84	0.98	0.92	0.85	0.98	0.92	0.85	0.97	0.92	0.86
Q/Q_{id}	0.98	0.93	0.87	0.98	0.93	0.87	0.98	0.92	0.87	0.95	0.90	0.85
T_v, K	333.8	336.4	339.8	333.9	336.4	339.6	334.0	336.8	339.7	335.2	337.9	340.6
p_v, N/m^2	20429	22948	26707	20460	22969	26497	20612	23424	26581	21793	24532	27698

E.3. Effect of walkways - section 6

	No walkways x-wind (generic ACSC)			UD W_w = 1.2m x-wind			UD W_w = 1.7m x-wind			UD W_w = 2.2m x-wind		
v_{ref}	3 m/s	6 m/s	9 m/s	3 m/s	6 m/s	9 m/s	3 m/s	6 m/s	9 m/s	3 m/s	6 m/s	9 m/s
$\Sigma V/\Sigma V_{id}$	0.98	0.90	0.83	0.99	0.92	0.85	0.99	0.94	0.86	1.00	0.94	0.87
Q/Q_{id}	0.98	0.91	0.84	0.99	0.93	0.86	0.99	0.94	0.87	1.00	0.95	0.88
T_v, K	334.2	337.4	341.1	333.7	336.5	340.1	333.5	336.0	339.4	333.4	335.6	338.9
p_v, N/m^2	20737	23970	28329	20273	23047	27022	20133	22503	26254	19997	22174	25729
	UD W_w = 3.0m x-wind			UD W_w = 4.0 m x-wind			UD W_w = 6.0 m x-wind			UD W_w = 8.0 m x-wind		
v_{ref}	3 m/s	6 m/s	9 m/s	3 m/s	6 m/s	9 m/s	3 m/s	6 m/s	9 m/s	3 m/s	6 m/s	9 m/s
$\Sigma V/\Sigma V_{id}$	1.00	0.95	0.89	1.01	0.96	0.90	1.01	0.97	0.92	1.01	0.98	0.93
Q/Q_{id}	1.00	0.95	0.89	1.00	0.96	0.90	1.00	0.97	0.91	1.01	0.97	0.92
T_v, K	333.2	335.3	338.4	333.1	335	337.9	333	334.6	337.2	332.9	334.4	336.9
p_v, N/m^2	19866	21833	25081	19737	21513	24524	19631	21153	23806	19589	20991	23441

	No walkways x-wind (generic ACSC)			P W_w = 1.2m x-wind			P W_w = 1.7m x-wind			P W_w = 2.2m x-wind		
v_{ref}	3 m/s	6 m/s	9 m/s	3 m/s	6 m/s	9 m/s	3 m/s	6 m/s	9 m/s	3 m/s	6 m/s	9 m/s
$\Sigma V/\Sigma V_{id}$	0.98	0.90	0.83	0.99	0.93	0.86	1.00	0.94	0.87	1.00	0.95	0.88
Q/Q_{id}	0.98	0.91	0.84	0.99	0.94	0.88	1.00	0.95	0.89	1.00	0.95	0.90
T_v, K	334.2	337.4	341.1	333.5	336.0	339.3	333.3	335.6	338.7	333.1	335.2	338.2
p_v, N/m^2	20737	23970	28329	20101	22519	26120	19917	22124	25440	19743	21777	24886
	P W_w = 3.0m x-wind			P W_w = 4.0 m x-wind			P W_w = 6.0 m x-wind			P W_w = 8.0 m x-wind		
v_{ref}	3 m/s	6 m/s	9 m/s	3 m/s	6 m/s	9 m/s	3 m/s	6 m/s	9 m/s	3 m/s	6 m/s	9 m/s
$\Sigma V/\Sigma V_{id}$	1.01	0.96	0.90	1.01	0.97	0.91	1.02	0.98	0.92	1.02	0.99	0.93
Q/Q_{id}	1.01	0.97	0.91	1.01	0.97	0.92	1.01	0.98	0.94	1.01	0.99	0.95
T_v, K	332.9	334.7	337.6	332.7	334.3	336.9	332.6	333.9	336.1	332.5	333.6	335.7
p_v, N/m^2	19575	21287	24222	19402	20864	23444	19292	20462	22637	19234	20226	22274

	No walkways xy-wind (generic ACSC)			UD W_w = 1.2m xy-wind			UD W_w = 1.7m xy-wind			UD W_w = 2.2m xy-wind		
v_{ref}	3 m/s	6 m/s	9 m/s	3 m/s	6 m/s	9 m/s	3 m/s	6 m/s	9 m/s	3 m/s	6 m/s	9 m/s
$\Sigma V/\Sigma V_{id}$	0.98	0.92	0.84	0.99	0.93	0.86	0.99	0.94	0.87	0.99	0.94	0.87
Q/Q_{id}	0.98	0.93	0.87	0.99	0.94	0.89	0.99	0.95	0.89	0.99	0.95	0.89
T_v, K	333.8	336.4	339.8	333.6	335.8	338.9	333.5	335.6	338.6	333.4	335.4	338.3
p_v, N/m^2	20429	22948	26707	20186	22330	25635	20098	22132	25289	20022	21970	25053
	UD W_w = 3.0m xy-wind			UD W_w = 4.0 m xy-wind			UD W_w = 6.0 m xy-wind			UD W_w = 8.0 m xy-wind		
v_{ref}	3 m/s	6 m/s	9 m/s	3 m/s	6 m/s	9 m/s	3 m/s	6 m/s	9 m/s	3 m/s	6 m/s	9 m/s
$\Sigma V/\Sigma V_{id}$	1.00	0.95	0.87	1.00	0.95	0.88	1.00	0.96	0.89	1.00	0.96	0.89
Q/Q_{id}	1.00	0.95	0.90	1.00	0.96	0.91	1.00	0.96	0.91	1.00	0.96	0.91
T_v, K	333.3	335.2	338.2	333.3	335	337.8	333.2	334.9	337.5	333.3	334.9	337.5
p_v, N/m^2	19953	21786	24850	19893	21560	24398	19884	21429	24113	19895	21432	24112

	No walkways xy-wind (generic ACSC)			P W_w = 1.2m xy-wind			P W_w = 1.7m xy-wind			P W_w = 2.2m xy-wind		
v_{ref}	3 m/s	6 m/s	9 m/s	3 m/s	6 m/s	9 m/s	3 m/s	6 m/s	9 m/s	3 m/s	6 m/s	9 m/s
$\Sigma V/\Sigma V_{id}$	0.98	0.92	0.84	1.00	0.95	0.88	1.00	0.96	0.89	1.01	0.96	0.90
Q/Q_{id}	0.98	0.93	0.87	1.00	0.96	0.90	1.00	0.96	0.91	1.00	0.97	0.92
T_v, K	333.8	336.4	339.8	333.3	335.2	338	333.1	334.8	337.4	333	334.5	336.9
p_v, N/m^2	20429	22948	26707	19937	21741	24705	19752	21352	23988	19640	21051	23451
	P W_w = 3.0m xy-wind			P W_w = 4.0 m xy-wind			P W_w = 6.0 m xy-wind			P W_w = 8.0 m xy-wind		
v_{ref}	3 m/s	6 m/s	9 m/s	3 m/s	6 m/s	9 m/s	3 m/s	6 m/s	9 m/s	3 m/s	6 m/s	9 m/s
$\Sigma V/\Sigma V_{id}$	1.01	0.97	0.91	1.02	0.98	0.92	1.02	0.99	0.94	1.02	0.99	0.94
Q/Q_{id}	1.01	0.98	0.93	1.01	0.99	0.94	1.01	0.99	0.95	1.01	0.99	0.96
T_v, K	332.8	334.1	336.4	332.7	333.7	335.9	332.6	333.4	335.4	332.5	333.4	335.2
p_v, N/m^2	19499	20692	22909	19365	20324	22449	19280	20053	21971	19244	20014	21739

E.4. Effect of windscreens - section 7

E.4.1 Screen configuration study

	No screens x-wind (generic ACSC)			Case A x-wind			Case B x-wind			Case C x-wind		
v_{ref}	3 m/s	6 m/s	9 m/s	3 m/s	6 m/s	9 m/s	3 m/s	6 m/s	9 m/s	3 m/s	6 m/s	9 m/s
V/Vid	0.98	0.90	0.83	0.98	0.93	0.92	0.97	0.93	0.91	0.97	0.93	0.91
Q/Qid	0.98	0.91	0.84	0.98	0.95	0.92	0.98	0.94	0.90	0.98	0.94	0.91
Ts	334.2	337.4	341.1	333.9	335.6	336.9	334.1	336.0	337.7	334.1	336.0	337.7
ps	20737	23970	28329	20539	22150	23529	20714	22542	24377	20722	22523	24293

	Case D x-wind			Case E x-wind			Case F x-wind			Case G x-wind		
v_{ref}	3 m/s	6 m/s	9 m/s	3 m/s	6 m/s	9 m/s	3 m/s	6 m/s	9 m/s	3 m/s	6 m/s	9 m/s
V/Vid	0.98	0.93	0.91	0.97	0.93	0.91	0.98	0.93	0.90	0.97	0.93	0.91
Q/Qid	0.98	0.95	0.92	0.98	0.94	0.91	0.98	0.95	0.92	0.98	0.94	0.91
Ts	333.9	335.6	337	334.1	336	337.6	333.9	335.7	337.1	334.1	335.9	337.3
ps	20533	22150	23549	20723	22512	24180	20523	22250	23714	20679	22401	23918
	Case H x-wind			Case I x-wind			Case J x-wind					
v_{ref}	3 m/s	6 m/s	9 m/s	3 m/s	6 m/s	9 m/s	3 m/s	6 m/s	9 m/s			
V/Vid	0.98	0.92	0.88	0.98	0.93	0.91	0.98	0.93	0.89			
Q/Qid	0.98	0.94	0.90	0.98	0.94	0.93	0.98	0.94	0.91			
Ts	333.9	336.2	338.1	333.9	335.8	336.7	333.9	335.9	337.6			
ps	20537	22726	24791	20469	22328	23234	20500	22424	24233			

	No screens xy-wind (generic ACSC)			Case A xy-wind			Case B xy-wind			Case C xy-wind		
v_{ref}	3 m/s	6 m/s	9 m/s	3 m/s	6 m/s	9 m/s	3 m/s	6 m/s	9 m/s	3 m/s	6 m/s	9 m/s
V/Vid	0.98	0.92	0.84	0.98	0.94	0.88	0.98	0.93	0.87	0.98	0.93	0.87
Q/Qid	0.98	0.93	0.87	0.99	0.95	0.91	0.99	0.95	0.90	0.99	0.95	0.90
Ts	333.8	336.4	339.8	333.8	335.4	337.6	333.8	335.7	338.0	333.8	335.7	338.0
ps	20429	22948	26707	20370	21956	24177	20395	22212	24656	20409	22221	24664
	Case D xy-wind			Case E xy-wind			Case F xy-wind			Case G xy-wind		
v_{ref}	3 m/s	6 m/s	9 m/s	3 m/s	6 m/s	9 m/s	3 m/s	6 m/s	9 m/s	3 m/s	6 m/s	9 m/s
V/Vid	0.98	0.94	0.88	0.98	0.93	0.87	0.98	0.94	0.88	0.98	0.93	0.87
Q/Qid	0.99	0.95	0.91	0.99	0.95	0.90	0.99	0.95	0.90	0.99	0.95	0.90
Ts	333.8	335.4	337.6	333.8	335.7	338	333.8	335.5	337.8	333.8	335.6	337.9
ps	20355	21963	24234	20385	22225	24676	20421	22063	24483	20393	22134	24564
	Case H xy-wind			Case I xy-wind			Case J xy-wind					
v_{ref}	3 m/s	6 m/s	9 m/s	3 m/s	6 m/s	9 m/s	3 m/s	6 m/s	9 m/s			
V/Vid	0.98	0.94	0.88	0.98	0.94	0.89	0.98	0.93	0.88			
Q/Qid	0.99	0.95	0.90	0.99	0.95	0.91	0.99	0.95	0.90			
Ts	333.7	335.6	337.8	333.7	335.4	337.5	333.8	335.6	337.9			
ps	20331	22118	24492	20340	21986	24139	20357	22179	24598			

E.4.2 Screen location study

	No screens x-wind (generic ACSC)			Row 1 Case A x-wind			Row 1 Case G x-wind			Row 2 Case A x-wind		
v_{ref}	3 m/s	6 m/s	9 m/s	3 m/s	6 m/s	9 m/s	3 m/s	6 m/s	9 m/s	3 m/s	6 m/s	9 m/s
V/Vid	0.98	0.90	0.83	0.95	0.88	0.82	0.95	0.87	0.81	0.97	0.90	0.86
Q/Qid	0.98	0.91	0.84	0.96	0.89	0.83	0.96	0.88	0.81	0.97	0.92	0.88
Ts	334.2	337.4	341.1	334.8	338.6	342.1	335.1	339.2	343.0	334.3	336.9	339.0
ps	20737	23970	28329	21370	25329	29542	21652	26014	30646	20862	23517	25758
	Row 2 Case G x-wind			Row 3 Case A x-wind			Row 3 Case G x-wind			Row 4 Case A x-wind		
v_{ref}	3 m/s	6 m/s	9 m/s	3 m/s	6 m/s	9 m/s	3 m/s	6 m/s	9 m/s	3 m/s	6 m/s	9 m/s
V/Vid	0.96	0.89	0.84	0.98	0.93	0.92	0.97	0.93	0.91	0.99	0.96	0.92
Q/Qid	0.97	0.91	0.87	0.98	0.95	0.92	0.98	0.94	0.91	0.99	0.96	0.93
Ts	334.5	337.5	339.8	334	335.6	336.9	334.1	335.9	337.3	333.6	334.9	336.4
ps	21027	24079	26765	20545	22150	23529	20681	22405	23919	20248	21418	22926
	Row 4 Case G x-wind											
v_{ref}	3 m/s	6 m/s	9 m/s									
V/Vid	0.99	0.96	0.92									
Q/Qid	0.99	0.96	0.93									
Ts	333.6	334.9	336.5									
ps	20256	21406	23014									

E.4. Effect of bellmouth fan inlets - section 8

	Generic ACSC x-wind			Periphery bellmouths removed x-wind			All bellmouths removed x-wind		
v_{ref}	3 m/s	6 m/s	9 m/s	3 m/s	6 m/s	9 m/s	3 m/s	6 m/s	9 m/s
V/Vid	0.98	0.90	0.83	0.97	0.90	0.83	0.95	0.88	0.82
Q/Qid	0.98	0.91	0.84	0.97	0.91	0.84	0.96	0.90	0.84
Ts	334.2	337.4	341.1	334.5	337.6	341.1	335.1	338.1	341.6
ps	20737	23970	28329	21038	24219	28301	21673	24794	28908
	Generic ACSC xy wind			Periphery bellmouths removed xy-wind			All bellmouths removed xy-wind		
v_{ref}	3 m/s	6 m/s	9 m/s	3 m/s	6 m/s	9 m/s	3 m/s	6 m/s	9 m/s
V/Vid	0.98	0.92	0.84	0.97	0.91	0.84	0.95	0.90	0.83
Q/Qid	0.98	0.93	0.87	0.98	0.93	0.87	0.96	0.92	0.86
Ts	333.8	336.4	339.8	334.2	336.5	339.5	334.9	337.2	340.2
ps	20429	22948	26707	20794	23116	26405	21421	23775	27151

E.5. Effect of fan type - section 9

	B-fan x-wind (Generic ACSC)			L-fan x-wind			N-fan x-wind		
v_{ref}	3 m/s	6 m/s	9 m/s	3 m/s	6 m/s	9 m/s	3 m/s	6 m/s	9 m/s
V/Vid	0.98	0.90	0.83	0.99	0.92	0.85	0.90	0.79	0.71
Q/Qid	0.98	0.91	0.84	0.99	0.93	0.86	0.92	0.82	0.74
Ts	334.2	337.4	341.1	333.5	336.6	340.3	337.0	342.7	348.7
ps	20737	23970	28329	20138	23202	27299	23542	30365	38997
	B-fan xy-wind (Generic ACSC)			L-fan xy-wind			N-fan xy-wind		
v_{ref}	3 m/s	6 m/s	9 m/s	3 m/s	6 m/s	9 m/s	3 m/s	6 m/s	9 m/s
V/Vid	0.98	0.92	0.84	1.00	0.94	0.86	0.93	0.82	0.71
Q/Qid	0.98	0.93	0.87	1.00	0.94	0.89	0.94	0.85	0.75
Ts	333.8	336.4	339.8	333.2	335.8	338.9	335.9	341.1	347.6
ps	20429	22948	26707	19874	22299	25681	22491	28222	37319

E.5. Effect of fan power variation - section 10

	Generic ACSC x-wind			Periphery 5% x-wind			All 5% x-wind			Periphery 10% x-wind		
v_{ref}	3 m/s	6 m/s	9 m/s	3 m/s	6 m/s	9 m/s	3 m/s	6 m/s	9 m/s	3 m/s	6 m/s	9 m/s
$\Sigma V/\Sigma V_{id}$	0.98	0.90	0.83	0.98	0.91	0.84	0.99	0.91	0.84	0.99	0.92	0.85
Q/Q_{id}	0.98	0.91	0.84	0.98	0.92	0.85	0.99	0.92	0.85	0.99	0.92	0.86
T_v, K	334.2	337.4	341.1	333.9	337.1	340.9	333.7	337.0	340.7	333.5	336.7	340.4
p_v, N/m^2	20737	23970	28329	20479	23733	28045	20294	23567	27846	20158	23291	27431
	All 10% x-wind			Periphery 20% x-wind			All 20% x-wind					
v_{ref}	3 m/s	6 m/s	9 m/s	3 m/s	6 m/s	9 m/s	3 m/s	6 m/s	9 m/s			
$\Sigma V/\Sigma V_{id}$	1.01	0.93	0.86	1.01	0.94	0.87	1.04	0.96	0.89			
Q/Q_{id}	1.00	0.93	0.86	1.01	0.94	0.87	1.02	0.96	0.89			
T_v, K	333.1	336.3	340	332.9	336	339.4	332.2	335.2	338.5			
p_v, N/m^2	19795	22903	26942	19568	22518	26275	18909	21752	25277			

	Generic ACSC xy-wind			Periphery 5% xy-wind			All 5% xy-wind			Periphery 10% xy-wind		
v_{ref}	3 m/s	6 m/s	9 m/s	3 m/s	6 m/s	9 m/s	3 m/s	6 m/s	9 m/s	3 m/s	6 m/s	9 m/s
$\Sigma V/\Sigma V_{id}$	0.98	0.92	0.84	0.99	0.92	0.85	1.00	0.93	0.85	1.00	0.93	0.86
Q/Q_{id}	0.98	0.93	0.87	0.99	0.94	0.87	1.00	0.94	0.88	1.00	0.94	0.88
T_v, K	333.8	336.4	339.8	333.6	336.2	339.6	333.4	336	339.4	333.2	335.7	339.1
p_v, N/m^2	20429	22948	26707	20179	22705	26437	19984	22536	26246	19861	22292	25851

	All 10% xy-wind			Periphery 20% xy-wind			All 20% xy-wind		
v_{ref}	3 m/s	6 m/s	9 m/s	3 m/s	6 m/s	9 m/s	3 m/s	6 m/s	9 m/s
$\Sigma V/\Sigma V_{id}$	1.01	0.95	0.87	1.01	0.95	0.87	1.05	0.98	0.90
Q/Q_{id}	1.01	0.95	0.89	1.01	0.95	0.89	1.03	0.98	0.91
T_v, K	332.8	335.4	338.6	332.8	335.4	338.6	331.9	334.2	337.3
p_v, N/m^2	19492	21920	25380	19492	21918	25374	18646	20825	23895

E.6. Effect of wind direction - section 11

	0° (Generic ACSC x-wind)			15°			30°			45° (Generic ACSC xy-wind)		
v_{ref}	3 m/s	6 m/s	9 m/s	3 m/s	6 m/s	9 m/s	3 m/s	6 m/s	9 m/s	3 m/s	6 m/s	9 m/s
$\Sigma V/\Sigma V_{id}$	0.98	0.90	0.83	0.98	0.90	0.84	0.98	0.91	0.83	0.98	0.92	0.84
Q/Q_{id}	0.98	0.91	0.84	0.98	0.91	0.85	0.98	0.92	0.86	0.98	0.93	0.87
T_v, K	334.2	337.4	341.1	334.1	337.3	340.7	334.0	336.9	340.5	333.8	336.4	339.8
p_v, N/m^2	20737	23970	28329	20723	23886	27796	20600	23441	27541	20429	22948	26707

	60°			75°			90°		
v_{ref}	3 m/s	6 m/s	9 m/s	3 m/s	6 m/s	9 m/s	3 m/s	6 m/s	9 m/s
$\Sigma V/\Sigma V_{id}$	0.98	0.92	0.85	0.98	0.92	0.86	0.98	0.96	0.89
Q/Q_{id}	0.99	0.93	0.87	0.98	0.93	0.87	1.02	0.96	0.89
T_v, K	333.8	336.4	339.7	333.9	336.5	339.6	332.2	335.2	338.5
p_v, N/m^2	20414	22919	26599	20477	23078	26520	18909	21752	25277

E.6. Improved generic ACSC - section 12

	Generic ACSC x-wind			Improved ACSC x-wind			Generic ACSC xy-wind			Improved ACSC xy-wind		
v_{ref}	3 m/s	6 m/s	9 m/s	3 m/s	6 m/s	9 m/s	3 m/s	6 m/s	9 m/s	3 m/s	6 m/s	9 m/s
$\Sigma V/\Sigma V_{id}$	0.98	0.90	0.83	1.00	0.96	0.95	0.98	0.92	0.84	1.00	0.97	0.92
Q/Q_{id}	0.98	0.91	0.84	1.00	0.97	0.95	0.98	0.93	0.87	1.00	0.98	0.94
T_v, K	334.2	337.4	341.1	333.2	334.5	335.4	333.8	336.4	339.8	333.1	334.2	336.0
p_v, N/m^2	20737	23970	28329	19820	21060	21986	20429	22948	26707	19719	20815	22517